DIVALENT CATION–INDUCED REGULATION OF ALPHA 5 BETA 1–FIBRONECTIN INTERACTION FORCE ASSESSED USING ATOMIC FORCE MICROSCOPY

by

Nicolas A. Perrusquia

B.S. Physics, Delaware State University, 1996

M.S., Bioengineering, University of Pittsburgh, 1999

Submitted to the Graduate Faculty of

School of Engineering in partial fulfillment

of the requirements for the degree of

Doctor of Philosophy

University of Pittsburgh

2007

UNIVERSITY OF PITTSBURGH

SCHOOL OF ENGINEERING

This dissertation was presented

by

Nicolas A. Perrusquia

It was defended on

July 23, 2007

and approved by

Harvey S. Borovetz, Ph.D., Professor, Departments of Bioengineering and Surgery

Co-Director: Hai Lin, Ph.D., Assistant Professor, Department of Bioengineering

Scott X. Mao, Ph.D., Professor, Department of Mechanical Engineering

Dissertation Director: Sanjeev G. Shroff, Ph.D., Professor, Department of Bioengineering

DIVALENT CATION–INDUCED REGULATION OF ALPHA 5 BETA 1–FIBRONECTIN INTERACTION FORCE ASSESSED USING ATOMIC FORCE MICROSCOPY

Nicolas Andres Perrusquia, Ph.D.

University of Pittsburgh, 2007

Cellular attachment to the extracellular matrix (ECM) via integrin cell surface receptors is essential for signaling of the most basic of biological function such as apoptosis, differentiation and motility (Hynes, 1992).

Divalent cations play a critical role in the α5β1–fibronectin interaction as evidenced by (1) regulation of the affinity of interaction by cations [e.g., Ca^{2+} down regulates and Mg^{2+} or Mn^{2+} up regulates α5β1 binding affinity (Gailit, 1988; Mould, 1995)] and (2) loss of molecular interaction between α5β1 and fibronectin upon chelation using EDTA (Mould, 1995; Li, 2003).

The primary goal of the present study was to investigate the mechanisms underlying the cation-induced changes in α5β1–fibronectin interaction. We used atomic force microscopy (AFM) to directly examine the α5β1-fibronectin interaction in the presence of affinity regulating cations (i.e. Ca^{2+}, Mg^{2+}, Mn^{2+}, CaMg or CaMn) and at load rates commensurate with known cellular motility speeds.

The rupture force was linearly proportional to load rate and plotted data for this relationship corresponded to a single line resulting from limited bond separation resistance for down regulated α5β1 (Ca^{2+}, CaMg); or two lines (the second showing

rapidly increasing rupture force) resulting from up regulated α5β1 (CaMn, Mg^{2+}, Mn^{2+}). A sole 'outer barrier' dominated bond separation resistance for down regulation and low load rates (< 10,000 pN/s) while up regulation produced the additional, second barrier (inner barrier), which dominated resistance at high load rates (> 10,000 pN/s).

No significant difference in bond rupture force (*P = 0.68)* existed at low load rates between down and up regulated α5β1, since each encountered the same resistance (outer barrier). However, only the up regulated form of α5β1 encountered the additional energy barrier at high load rates, resulting in sharply increasing forces.

Although both Mg^{2+} and Mn^{2+} up regulated α5β1, the addition of Ca^{2+} down regulated α5β1, resulting in the elimination of the second (inner barrier) only for Mg^{2+}; it was unable to do so for Mn^{2+}.

Overall, these results support the premise that a cation related mechanism is responsible for affinity regulation of α5β1 leading to different bond separation resistance at low and high load rates.

TABLE OF CONTENTS

NOMENCLATURE XIII

PREFACE XV

1.0 INTRODUCTION AND SPECIFIC AIMS 1

1.1 INTRODUCTION 1

1.2 SPECIFIC AIMS 3

2.0 BACKGROUND 5

2.1 INTEGRINS 6

2.2 FIBRONECTIN 11

2.3 THE ALPHA 5 BETA 1-FIBRONECTIN INTERACTION 14

2.4 METHODS IN FORCED SEPARATION OF ALPHA 5 BETA 1 AND FIBRONECTIN 16

3.0 RESULTS 20

3.1 CALIBRATION OF CANTILEVER SPRING CONSTANTS 21

3.2 MODIFICATION OF SILICON NITRIDE AFM PROBES 24

3.2.1 Attachment of Microspheres to AFM Probes 25

3.2.2 Surface Modification of Microsphere to Attach α5β1 27

3.3 IMMOBILIZATION OF FIBRONECTIN ON MICA SUBSTRATES 31

3.4 ASSAY FOR THE MEASUREMENT OF ALPHA 5 BETA 1–FIBRONECTIN BOND RUPTURE FORCE 32

3.5 CONTROL EXPERIMENTS TO ESTABLISH THE VALIDITY OF THE ALPHA 5 BETA 1–FIBRONECTIN ASSAY 35

3.6 EFFECTS OF DIVALENT CATIONS ON ALPHA 5 BETA 1–FIBRONECTIN INTERACTION: SINGLE LOAD RATE 39

3.7 EFFECTS OF DIVALENT CATIONS ON ALPHA 5 BETA 1–FIBRONECTIN INTERACTION: MULTIPLE LOAD RATES 46

3.7.1 Determining and Fitting Distinct Linear Regions for Force – Load Rate Data 53

3.7.2 Statistical Comparison of Low and High Load Regions Using ANCOVA. 55

3.7.3 Calculation of Bell Model Parameters 59

3.8 BIOCHEMICAL ANALYSIS OF CATION BINDING TO ALPHA 5 BETA 1 AND FIBRONECTIN 63

3.8.1 Analyisis of Competitive Binding of Divalent Cation to α5β1 63

3.8.2 Analyisis of Competitive Binding of Divalent Cation to Fibronectin 69

3.9 CD ANALYSIS OF MOLECULES IN THE PRESENCE OF DIVALENT CATIONS 73

3.9.1 CD ANALYSIS PFN IN THE PRESENCE OF DIVALENT CATION.. 73

3.9.2 CD Analysis α5β1–Fibronectin Complexation in the Presence of Divalent Cation..... 77

4.0 DISCUSSION 80

4.1 BINDING ASSAY TO MEASURE ALPHA 5 BETA 1–FIBRONECTIN RUPTURE FORCE 81

4.1.1 Tip Modification..... 81

4.1.2 Initial Test Measurement of the α5β1–Fibronectin Interaction 82

4.2 EFFECTS OF DIVALENT CATIONS ON THE ALPHA 5 BETA 1–FIBRONECTIN INTERACTION: SINGLE LOAD RATE 83

4.2.1 Effects of Divalent Cations on Rupture Force Magnitude 84

4.2.2 Effects of Divalent Cations on Interaction Frequency 86

4.3 EFFECTS OF DIVALENT CATIONS ON THE ALPHA 5 BETA 1–FIBRONECTIN INTERACTION: MULTIPLE LOAD RATES 93

4.3.1 Energy Barriers Along the Dissociation Path Effect Rupture Force Data Patterns 93

4.3.2 Influence of Cation Regulated α5β1 Binding Affinity on Rupture Force Magnitude 103

4.4 BIOCHEMICAL ANALYSIS OF CATION BINDING TO ALPHA 5 BETA 1 115

4.5 CONCLUSIONS 119

APPENDIX A: METHODS 122

APPENDIX B: SCRIPT TO ANALYZE RUPTURE FORCE DATA 127

APPENDIX C: SCRIPT TO LOCATE TRANSITION POINT BETWEEN LOW AND HIGH LOAD REGIONS 129

APPENDIX D: ERROR PROPAGATION FOR BELL MODEL PARAMETERS 131

BIBLIOGRAPHY 135

LIST OF TABLES

Table 3.1 Estimated Cantilever Spring Constants (Single Load Rate) 23

Table 3.2 Estimated Cantilever Spring Constants (Multiple Load Rates) 23

Table 3.3 Frequency of Binding Counts at 4800 pN/s 43

Table 3.4 Mean Rupture Force at 4800 pN/s 44

Table 3.5 Divalent Cation Treatment Dosage for Experiments 46

Table 3.6 Tip – Substrate Retraction Rates for Plasma Fibronectin and Fnf120 47

Table 3.7 Estimated Transition Point between Low and High Load Rate Regions 54

Table 3.8 Determining Probability of Distinction between Low and High Load Regimes: Calculation of F-ratio 55

Table 3.9 Comparison to Investigate if Different Ligands (pFn and Fnf120) Have Effect on Low Load Rupture Force Per Cation Treatment 57

Table 3.10 Lack of Cation Effect on Low and High Load Rupture Force for Grouped Data 58

Table 3.11 Calculated Bell Parameters for Plasma Fibronectin (pFn) Data 61

Table 3.12 Calculated Bell Parameters for 120 kDa Fibronectin Fragment (Fnf120) Data 61

Table 3.13 Combined Bell Parameters for pFn and Fibronectin Fragment (Fnf120) Data Lack of Cation Effect on Low and High Load Rupture Force for Grouped Data 62

Table 3.14 Ratio of Densitometry Measurements ($^{45}Ca^{2+}$/ PVDF) for α5β1 69

Table 3.15 Ratio of Densitometry Measurements for pFn & Fnf120 ($^{45}Ca^{2+}$/ Amido Stain) 73

Table 4.1 Atomic Properties of Divalent Cation Used in Study. 89

LIST OF FIGURES

Figure 2.1 The 24 known vertebrate integrins 7

Figure 2.2 General integrin structure 8

Figure 2.3 Cartoon depicting down regulated and up regulated integrin states 9

Figure 2.4 Cartoon depicting integrin regulation pathways 10

Figure 2.5 Fibronectin Dimer 12

Figure 2.6 Fibronectin typeIII domains 12

Figure 2.7 Schematic illustrating AFM tip – sample separation maintenance by means of feedback 17

Figure 3.1 Thermal Resonance Peak Measurement 22

Figure 3.2 AFM Probe Modified with Silica Microsphere 26

Figure 3.3 Examination of SPDP Cross-linker Reactivity Using UV Absorbance 28

Figure 3.4 Modification of AFM Tips with α5β1 29

Figure 3.5 Fluorescence Label Detection of α5β1 on Modified Si_3N_4 AFM Tips 30

Figure 3.6 AFM tapping mode image of pFn 31

Figure 3.7 Illustration of α5β1-Fibronectin Binding 33

Figure 3.8 Force Curve Anatomy 34

Figure 3.9 Determination of Background Adhesion Force Between the Modified AFM Tip and Fibronectin Coated Substrate for Relevant Tip Modification Steps 37

Figure 3.10 Reduction of Multiple α5β1-Fibronectin Interactions Using Antibody. 38

Figure 3.11 Typical Rupture Force Measurements for α5β1-Fibronectin Interaction at 4800 pN/s. 41

Figure 3.12 Divalent Cation Effects on α5β1-pFn Rupture Force at a Single Load Rate 42

Figure 3.13 Specificity of α5β1-Fibronectin Interaction 45

Figure 3.14 Effects of Divalent Cation on α5β1 - pFn Rupture Force at Multiple Load Rates..... 49

Figure 3.15 Effects of Divalent Cation on α5β1 - Fnf120 Rupture Force at Multiple Load Rates 50

Figure 3.16 SDS-PAGE Gel of α5β1 and Fibronectin: Electrophoretic..... 65

Figure 3.17 Competition Between Mg^{2+}, Mn^{2+} and $^{45}Ca^{2+}$ for Integrin Cation Binding Sites for Separated α5 and β1 Dimers..... 67

Figure 3.18 Amido Black Staining of α5 and β1 Dimers Transferred to PVDF 68

Figure 3.19 $^{45}Ca^{2+}$ Labeling of pFn, Fnf120 and N-Terminus Fragments..... 71

Figure 3.20 $^{45}Ca^{2+}$ Only Binds the 120 kDa Cell Attachment Fragment..... 72

Figure 3.21 CD Spectrographs of pFn for Various Divalent Cation 75

Figure 3.22 CD Spectra for Bound α5β1 and pFn 77

Figure 4.1 Cantilever Deflection Versus Time for Bare AFM Tip on Mica at 0.5 Hz. 90

Figure 4.2 Probability of Bond Rupture Time for CaMg and Mn^{2+}.. 91

Figure 4.3 Idealized Energy Barriers Which Impede α5β1–Fibronectin Dissociation... 95

Figure 4.4 Reduction of Prominent Outer Energy Barrier as α5β1–Fibronectin Rupture Force Increases.. 98

Figure 4.5 Molecular Bond Energy Calculations , $\Delta G(0)$, for Inner and Outer Barriers..... 100

Figure 4.6 Crystal Structure of αVβ3 with Bound RGD Peptide... 108

Figure 4.7 Ratio of Bond Rupture Pull Time and Natural Dissociation Time for all Tip Speeds... 112

Figure 4.8 Divalent Cation Regulated Pathways for α5β1 Binding Affinity..... 118

NOMENCLATURE

Abbreviations

SPDP	*N*-succinimidyl3-(2-pyridyldithio) propionate.
RGD	Cell binding sequence; Arg – Gly - Asp.
PHSRN	Synergy binding sequence; Pro – His – Ser – Arg – Asn.
pFn	Human plasma fibronectin (~ 500 kDa whole molecule dimer).
Fnf120	120 kDa cell binding fragment digest from pFn.
α5β1	Glycoprotein cell surface receptor (a.k.a. fibronectin receptor).
αVβ3	Glycoprotein cell surface receptor (a.k.a. vitronectin receptor).
k_B	Boltzmann's constant;
h	Planck's constant;
γ	Reaction coordinate along force path (bond extension to rupture), m.
Ca^{2+}	Calcium Ion.
Mg^{2+}	Magnesium Ion.
Mn^{2+}	Manganese Ion.
CaMg	Calcium + Magnesium mixture.
CaMn	Calcium + Manganese mixture.
Hepes	buffer
mM	Milli moles, 10^{-3} moles.

k_s	Cantilever spring constant, pN/nm.
k^0	Dissociation rate of molecular bond in absence of applied force, s^{-1}.
k(f)	Dissociation rate of molecular bond (Bell's model) for applied force, s^{-1}.
AFM	Atomic Force Microscopy.
N_{peak}	Number of force curves displaying a single, molecular interaction.
N_{Total}	Total number of force curves collected during an experiment.
EDTA	
JBS5	Anti –α5, function blocking antibody.
P1D6	Anti –α2, function blocking antibody.
t_c	Time duration of molecular bond rupture, s.
r_f	Load rate (k_s* tip – substrate separation speed), pN/s.
C	Transition point between low and high load regions, pN/s.
k_0, k_1, k_2	Multiple linear regression model coefficients (k_0 = intercept).
z	Binary parameter for regression model, (z = 0 before C, z = 1 after C).
GLM	Generalized Linear Model (multi - regression model used for ANCOVA).
NL	Number of data points for linear fit low load region (r_f < ~10,000 pN/s).
NH	Number of data points for linear fit high load region (r_f >~10,000 pN/s).

PREFACE

I would simply like to thank all my committee members for allowing me to graduate. I could not have finished had Dr. Borovetz not allowed me to stay around despite all the difficulty I had. Dr. Mao gave me the opportunity to begin learning to use the AFM back in 2000 and Dr. Shroff got me back on track when I got lost trying to figure out how to perform some of my critical experiments. Dr. Lin is awesome with an AFM and quite technically gifted at performing experiments and helped get me through some difficult experimental quagmires. All in all, every one of my committee members has contributed to the successful completion of this work.

I had this great opportunity to be here because of the people that have guided me while I was an undergraduate; those people are Dr. Fatma Helmy and her sister, Dr. Esham Helmy. These two individuals are dictionary examples of what a mentor should be. They are two of the most dedicated academic advisors I have ever met. Then there was this math instructor that I had, Mr. H. Allen Hamilton. He was a great inspiration to me because he came from a family of ten or more, was poor and still made it against all odds. It's the heart and soul of people like this that have made a lasting impression on me.

Last but not least, I would like to offer gratitude for the support I received from my sister, Shirley and my brothers, Marc and Max. I wish my mom could be here to see

this because she wouldn't believe it otherwise. A special thanks to all my friends in Delaware, the Office of Engineering Administration, and all Bioengineering Staff. The NIH (and the Povost's fund) for financial support while I had it. Also, I would like to dedicate this work to the many guys and girls in my old neighborhood who never had the educational opportunities I was lucky to get and my Chinese family, the Lin's.

1.0 INTRODUCTION AND SPECIFIC AIMS

1.1 INTRODUCTION

Cellular binding to the ECM at the molecular level provides both anchoring and bi-directional signaling pathways that are crucial for normal cell function and survival. Integrins are cell surface receptors that facilitate ECM binding and provide signaling linkage to the cyto-skeleton. Expressed by all multi-cellular organisms, integrins make up a family of non-covalently linked α, β heterodimers that consists of more than 20 individual members (Hynes:2002).

Processes such as differentiation, proliferation and motility, as well as the progression of many diseases such as atherosclerosis, tumor metastasis, and neurological disorders are rooted in the cells ability or inability to properly attach to the ECM (Hynes, 1995; Baillari, 1999; Blindt, 2002; Tan, 2004).

Unlike most integrins, α5β1 has a sole ligand Fn; making the pair well suited to study cellular receptor-ligand interactions. The glycoprotein Fn is a 550 kDa dimer that circulates as a soluble molecule in blood and is transformed into an insoluble matrix upon cellular binding (Hynes, 1985; Ruoslahti, 1988). Each dimer is contains an RGD and PHSRN synergy sequence that binds α5β1. Further, α5β1 (along with αVβ3) have been implicated as the primary receptors involved in cellular traction during motility (Hynes, 1992; Zamir 2001).

Integrins have been predicted to exist in multiple states of ligand binding affinity. These states range from ‘low’ to ‘high’ and correspond to the level of attraction of the receptor for the

ligand. Cells regulate binding affinity through so called 'inside-out' signaling. The binding affinity of integrins can be externally regulated (i.e. 'outside- in' signaling) using either divalent cation or stimulatory antibody. The binding affinity of α5β1 is down regulated by Ca^{2+} and up regulated by Mg^{2+}, Mn^{2+} and anti-bodies such TS2/16 and AG89 (Arroyo, 1993; Mould, 1995; Tsuchida, 1998). Mn^{2+} has been shown to produce at least a two – fold increase in binding of purified α5β1 or cells to Fn with respect to Mg^{2+}, whereas Ca^{2+} supported low levels of binding (Gailit, 1988; Mould 1995; Mould 1998).

Upon binding cation, the α5 and β1 dimers undergo a change in conformation that is attributed to changes in binding affinity state (Baneres, 2000; Bazzoni, 1995). Further, it has been reported that integrin binding affinity state affects the molecular rupture force magnitude between α5β1 and Fn; where an increase in rupture force was correlated to an increase in receptor binding affinity (Li, 2004; Garcia, 1998).

In this study, the dynamic rupture force characteristics between α5β1 and Fn are measured over a range of speeds for each treatment of divalent cation using AFM. Divalent cation treatments are used to regulate integrin binding affinity in a system where an AFM tip is coated with purified α5β1 and Fn coats the substrate. The range of tip-sample separation speeds includes those of previous studies and known ranges for keratinocyte motility on fibronectin. The measurements are aimed at providing physical insight into the interfacial strength between α5β1 and Fn with regard to divalent cation induced regulation of binding affinity. Biophysical measurements compliment knowledge of biochemical signaling for integrins to establish a more complete understanding of the integrin binding process.

1.2 SPECIFIC AIMS

The primary focus of this study is to characterize the physical attributes of divalent cation stimulated α5β1-fibronectin binding, and then determine a mechanism associated with α5β1 that contributes to its heightened affinity for fibronectin in the presence of Mn^{2+}. In this study, the phenomena of up regulated binding affinity in the presence of Mn^{2+} (and Mg^{2+}) and its affect on α5β1-fibronectin rupture force is examined using Atomic Force Microscopy (AFM), Circular Dichroism Spectroscopy (CD), and competitive binding of divalent cation with radio-labeled calcium ($^{45}Ca^{2+}$) as presented in the following aims.

The aims in this study are based on the following observations: 1) In the presence of Mn^{2+}, α5β1 has been shown to promote a two-fold increase in the binding of pFn (or RGD peptides) in binding assay studies as compared to Mg^{2+} (Gailit and Ruoshslahti,1988; Altieri, 1991; Bazzoni, 1998; Mould,1995; Yamada, 1995). 2) Mn^{2+} has been shown to bind α5β1 competitively in the presence of Ca^{2+} but not Mg^{2+}, suggesting a common binding site with Ca^{2+} (Gailit and Ruoshslahti, 1988; Springer, 2004). 3) Increases in AFM measured rupture force between α5β1 and fibronectin following up regulation with TS2/16 (Li, 2004).

A. *Develop an assay to measure the single molecule rupture force magnitude between α5β1 and human plasma fibronectin (pFn) using Atomic Force Microscopy (AFM).* In order to mimic actual cellular binding to the ECM, standard AFM probes coated with α5β1 and substratum coated with either full molecule pFn or a pFn fragment containing the cell binding domain are used for these experiments.

B. *Determine the effect of divalent cation and/or tip-substrate separation speed on bond rupture force.* The affinity state (i.e up regulated or down regulated) of integrin for its ligand has been reported to affect bond rupture force magnitude.The measurements of rupture force are made at varying tip – substrate separation speeds and in buffer containing divalent cation (i.e. either Ca^{2+}, Mg^{2+}, Mn^{2+}, CaMg or CaMn) to determine if cation and/or load rate has an affect on rupture force. chiral analysis of α5β1-Fn complex by Circular Dichroism Spectroscopy.

C. *Determine a mechanism for cation governed changes for integrin affinity.* It has been reported that changes in integrin conformation occur following cation binding. Further, Mn^{2+} up regulates α5β1 binding affinity for fibronectin, while Ca^{2+} down regulates it. In this study, we will employ competitive cation binding between divalent cation with radio-labeled calcium ($^{45}Ca^{2+}$) and monitor changes in conformation using circular dichroism spectroscopy.

D. *Develop a model describing the mechanism for down and up regulation of α5β1 binding affinity for fibronectin;* following treatment with individual or mixed divalent cation (i.e. Ca^{2+}, Mg^{2+}, Mn^{2+}, CaMg or CaMn) and its relationship to bond rupture force at different separation speeds.

2.0 BACKGROUND

Cellular attachment to the extra cellular matrix (ECM) is necessary for the establishment of signaling pathways that regulate physiological functions such as apoptosis and differentiation (Hynes, 1992; McDonald, 1987). The attachment process is complex and involves a variety of cell adhesion molecules (CAMs) on the cell surface and ligand molecules that are meshed together in the ECM. The integrin class of (CAMs) is primarily responsible for anchorage to the ECM and cellular motility. During motility the integrin – ligand interface is dynamically loaded by cellular traction forces applied to the ECM. These forces are tensile in nature and result in the eventual rupture of the integrin – ligand bond. The examination of integrin – ligand bond rupture forces, similar in magnitude and load rate to those experienced during cellular motility is essential in gaining a more thorough picture of interfacial binding during movement.

In this background, a general description of the integrin – ligand interaction is explained with an eventual emphasis on the interaction between the integrin α5β1 and its sole ligand, fibronectin. The α5β1-fibronectin molecular pair was used in this study to investigate the dynamic loading of the bond interface at varying speeds and when α5β1 binding affinity was externally down or up regulated.

The structure of integrins and regulation of binding affinity is described in *Section 2.1* followed by a description of fibronectin in *Section 2.2*. The interaction between α5β1 and

fibronectin is depicted in *Section 2.3*. An overview of the techniques used to physically measure the bond rupture forces between α5β1 and fibronectin is briefly summarized in *Section 2.4*.

2.1 INTEGRINS

Integrins are glycoproteins composed of α, β hetero-dimers that are non-covalently associated. Integrins fold into a globular shape with the majority of the α and β dimers exposed outside the cytoplasm, while the remaining tail region is enclosed in the cytoplasm (Takagi, 2001; Xiong, 2001). There are currently 24 known distinct integrins in vertebrates (Figure 2.1) generated from 18 α dimers and 8 β dimers (Hynes, 2002; Shimaoka, 2003). Integrins are limited to the metazoan kingdom and no homologs are found elsewhere (Whittaker, 2002). The entire set associated with vertebrates evolved from a single set found in primitive bilateria (Hynes, 2000).

Integrins function by changing shape as directed through extra or intra cellular stimulus (Mould, 2004; Kamata, 2005). Thus a cursory description of the various means by which changes in conformation occurs; which coincidently accompanies changes in integrin binding affinity is covered. The recent crystal structure solution for integrin αVβ3 has given insight into the tertiary organization and conformational changes that occur upon binding cation and RGD peptide (Xiong, 2001).

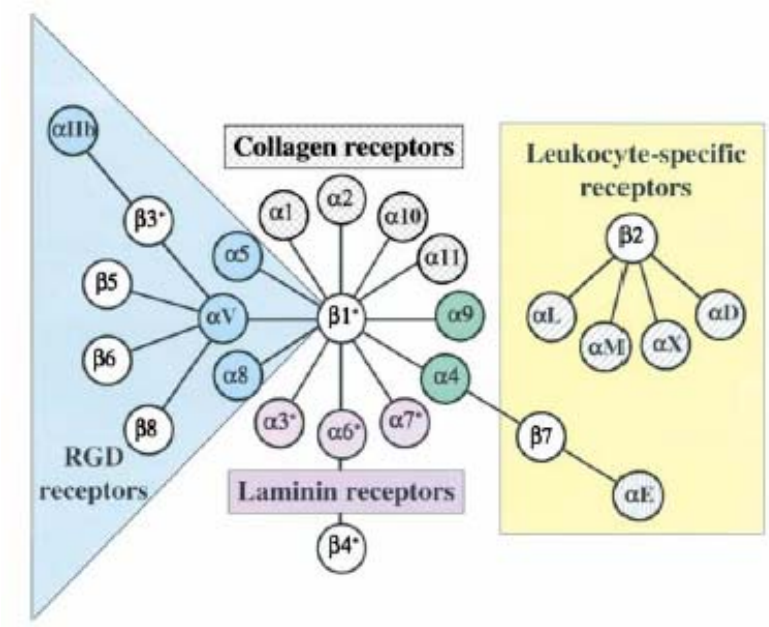

Figure 2.1 The 24 known vertebrate integrins comprised from 18 α and 8 β dimers (Hynes, 2002).

Further, the structure of integrins can be separated into those with α subunits that contain an αA (or I - domain) and those without one. Half of all α - subunits for vertebrate integrins have the αA domain. This domain contains cation binding sites which are adequate for ligand binding and is homologous with the structure of von wilebrand factor (vWF) (Colombatti, 1993; Tuckwell, 1997). All β subunits contain an αA –like domain that is similar in homology to the αA domain (Lee, 1995; Humphries, 2000). Additionally, the αA – like domain also binds ligand in divalent cation dependent manner (Michishita, 1993; Humphries, 2000).

The αA structure has a β pleated sheet center surrounded by α-helixes that adopts a Rossman fold with the metal ion dependent adhesion site (MIDAS) on top (Lee, 1995; Huang, 2000). The β - dimer αA – like domain contains 3 cation binding sites; the MIDAS site, an adjacent to MIDAS binding site known as (ADMIDAS) and a ligand induced metal binding site known as (LIMBS) (Xiong, 2001; Xiong, 2002). Further structural features of the α dimer are the

thigh region and two calf domains located below the β propeller structure and composed of β sheet, while the β dimer contains a hybrid domain just beneath the αA – like domain followed by a plexin/semaphoring/integrin (PSI) domain and 4 EGF - like domains (Figure 2.2). The junction between the thigh and calf domains of the α dimer is a flexible joint like - knee and contains a cation binding site. When the site is occupied by divalent cation, the integrin assumes an up-right position, representing an activated structure (Figure 2.2 & 2.3).

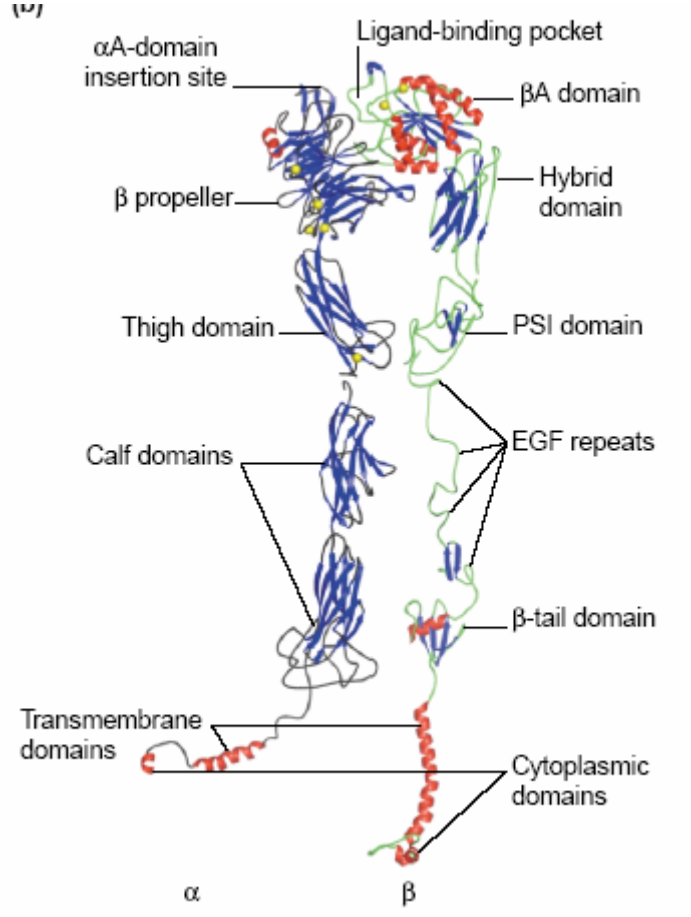

Figure 2.2 General integrin structure (Mould, 2004).

Integrin α5β1 does not contain an αA domain; instead the α dimer only contains a β - propeller structure which has seven α -helix and β sheet structural repeats. Repeats (4 – 7)

contain four divalent cation binding sites and the 2nd and 3rd repeats form a portion of the fibronectin binding pocket with the αA - like domain of the β dimer (Mould; 1998; Bazzoni, 1995; Xiong, 2001). The structural model of α5β1 is based on the αVβ3 crystal structure of Xiong, et al. (Coe, 2001). The amino acid sequence of α5β1 was accomplished which established an α dimer containing 1008 residues while the β dimer contained 778 residues (Argraves, 1987).

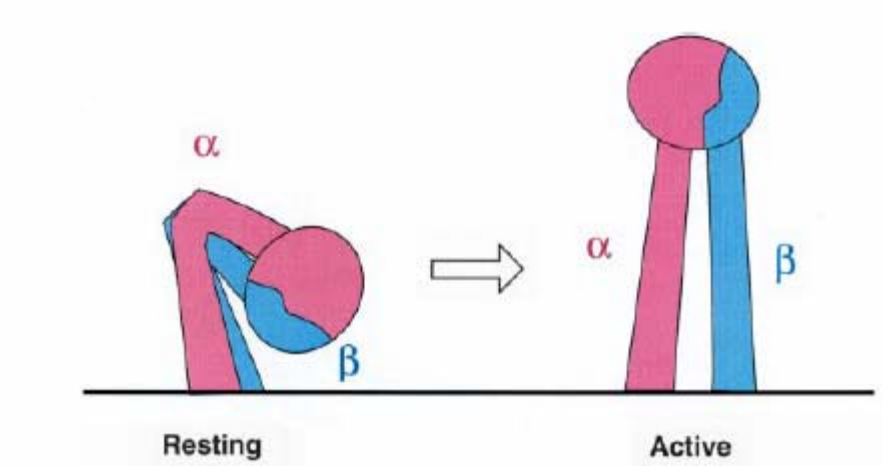

Figure 2.3 Cartoon depicting 'down regulated' (left) and 'up regulated' (right) integrin states (Takagi, 2002).

Integrins have been reported to exist in different states of affinity for ligands; where down regulated states have a lower probability of binding than up regulated states. As previously mentioned, intracellular signaling controls the receptor-ligand binding affinity by regulating conformational changes in integrin shape. However, external probes such as divalent cation and stimulatory antibodies can also regulate integrin binding affinity; thus either 'inside – out' or 'outside – in' pathways lead to down regulated or up regulated of binding affinity (Figure 2.4) (Mould, 1995; Gailit, 1988; Kamata, 2005). The conformational changes accompanying the binding of divalent

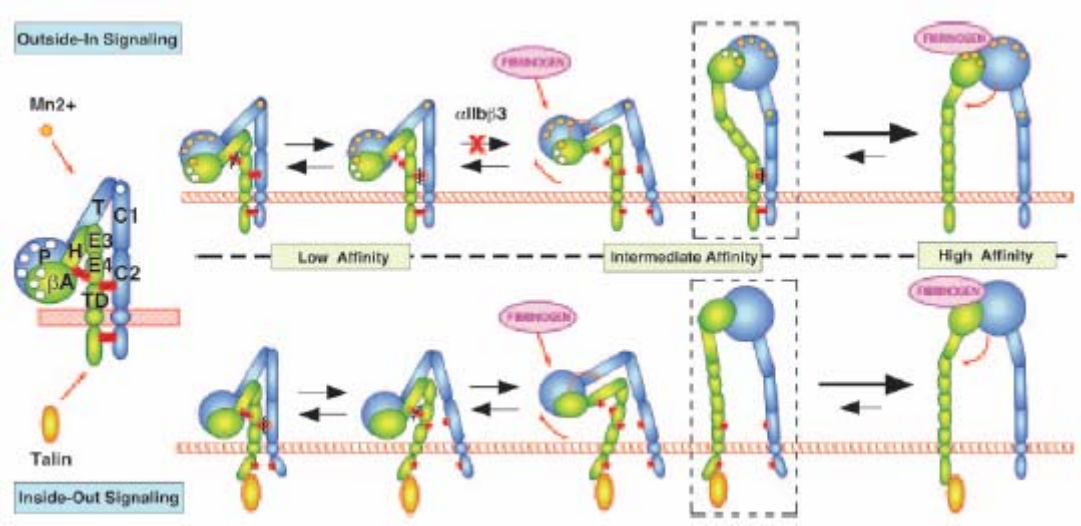

Figure 2.4 Cartoon depicting integrin regulation pathways (Kamata, 2004).

cation and/or stimulatory antibodies by integrin α5β1 dimers has been reported. The uptake of Mn^{2+} or Mg^{2+} results in an up regulated (upright) conformation, while Ca^{2+} results in a down regulated (bent) conformation (Takagi, 2002; Mould, 2004). The mapping of antibody epitopes using both inhibitory and stimulatory antibodies after subsequent binding of divalent cation showed that conformational changes in α5β1 led to the exposure of mAb epitopes near ligand binding site (Mould, 1998); while the use of circular dichroism spectroscopy (CD) showed changes in absorbance of UV spectra corresponding to the binding of divalent cation by the α5 and β1 dimers (Baneres, 2000).

Upon ligation, integrins cluster and form focal adhesions following an 'outside in' pathway. Integrin ligation also signals the linking of integrin cytoplasmic tail domains to the cytoskeleton via intracellular structural proteins such as paxillin, talin and vinculin (Schaller, 1995; Tanaka, 1996). The integrin binding affinity is regulated by the binding of these structural

proteins, as well as regulatory proteins such as focal adhesion kinase (FAK), calcineurin and calcium integrin binding protein (CIB) that adhere to the α, β dimer integrin tail regions. The binding of the regulatory and structural proteins follows the 'inside out' pathway of affinity regulation. Additionally, there exists homologous domains universally present in the a and b cytoplasmic tail domains which are believed to maintain a binding affinity state in integrins. Mutations of these highly conserved amino acid residues of the α and β integrin cytoplasmic tail regions results in a chronic state of binding affinity up regulation (Hughes, 1996). The α subunit tail region has a highly conserved GFFKR region that inactivates the integrin. While replacement of the arginine residue leads to chronic activation state; mutation of the aspartate residue in the homologous KLLxxxHDR sequence of the β dimer also led to persistent activation (Briesewitz, 1995). This overview of integrin structure and affinity regulation is followed by a description of the sole ligand of α5β1, fibronectin, in the following section.

2.2 FIBRONECTIN

The ECM is an array of filamentous glycoproteins and proteoglycans that provides cells with a scaffold for anchorage, traction for movement, and positional recognition (Kato, 2004). Fibronectin is a 550 kDa dimer that exists as a soluble protein in plasma and an insoluble protein in matrix form (Akiyama, 1985). It is a multifunctional protein that interacts with many other ECM proteins as well as cell receptors (Figure 2.5). However, it is the sole ligand of integrin α5β1, which recognizes fibronectin through an RGD sequence and an adjacent 'synergy' sequence (PHSRN). The RGD and Synergy sequences are in the same dimensional plane and are

separated by 30 - 40 Å (Leahy, 1996; Krammer, 2002). The synergy region is thought to stabilize the α5β1 interaction with RGD an increase binding affinity compared to RGD peptides (Akiyama, 1985; Obara, 1988).

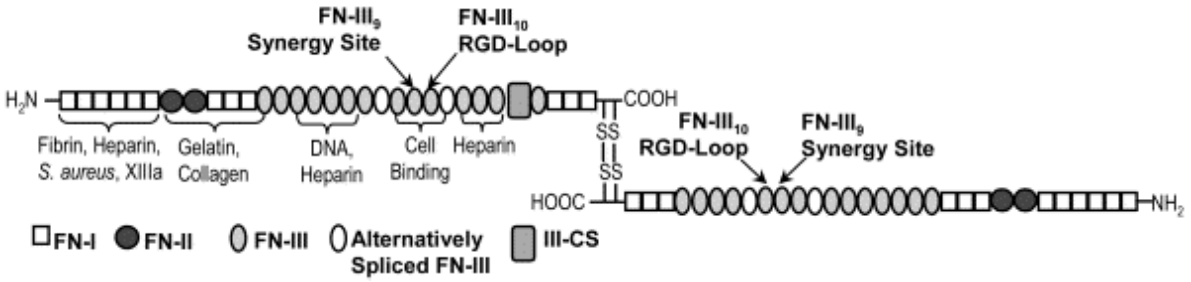

Figure 2.5 Fibronectin Dimer (Krammer, 2002).

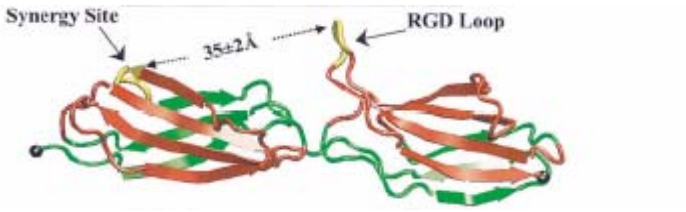

Figure 2.6 Fibronectin typeIII domains 9 (synergy) and 10 (RGD) (Krammer, 2002).

The structure of fibronectin consists of anti-parallel beta sheet structured repeats (or modules) whose overall assembly resembles a beaded necklace. The repeats differ by sequence length and the absence or presence of disulfide bonds between the anti-parallel pleated structures that affect the mechanical stability. The type I and type II repeats contain two disulfide bonds between the beta pleated structures resulting from four conserved cysteine residues; while type

III repeats contain no disulfide bonds (Isaacs, 1989). The type III modules are the largest at (90 a.a.) with the type II and type I modules at (60 a.a.) and (45 a.a.) respectively.

Fibronectin mRNA produces many variants or alternatively spliced dimer forms. The extra domain A (EDA) or extra domain B (EDB) spliced modules are incorporated into the sequence of type III modules following modules type III_{11} and type III_7 respectively. The (EDA) is a ligand for integrins α4β1 and α9β1 and is expressed primarily during embryogenesis or during wound healing (Liao, 2002). The variable domain (V) is also incorporated into the sequence of type III domains and is a ligand for integrin α4β7 (Pankov, 2002). Overall, the alternatively spliced domains assist in cellular adhesion.

The thermo stability of modules has been investigated. Fibronectin fragments and individual modules were thermally denatured and type III modules were found to be the most thermo-stabile, requiring higher temperatures to unfold (Litvinovich, 1995; Plaxco, 1997). However, mechanical extension and subsequent unfolding of fibronectin or engineered fragments containing copies of repeating modules using AFM showed that type III modules were the least mechanically stabile (Oberhauser, 2002). The extension of fibronectin occurs during cell motility which is thought to unfold type III modules, exposing cryptic sites necessary for matrix assembly (Zhong, 1998; Hocking, 1994). Observed extension of fibronectin shows bundles of individual dimers attached at focal adhesions on the cell and being extended up to four times their relaxed length and exposing cryptic sites labeled with green fluorescent protein (Ohashi, 1999). The structure of fibronectin allows a unique interaction with a5b1 whereas other fibronectin binding integrins only recognize the RGD sequence. This unique interaction is briefly covered in the following section.

2.3 THE ALPHA 5 BETA 1–FIBRONECTIN INTERACTION

Because many integrins have multiple ligands, the integrin α5β1 is often chosen to study receptor – ligand interactions as it has only a sole ligand, fibronectin (Pytela, 1985; Yamada, 1987). The binding between integrin α5β1 and fibronectin links the extra cellular environment to the cyto-skeleton, establishing bi-directional signaling pathways. It is well known that so called inside-out signaling controls integrin binding affinity and many important cellular functions such as apoptosis, differentiation and motility.

The use of either divalent cation or stimulatory antibodies to externally regulate binding affinity of α5β1 for fibronectin has been previously shown (Gailit, 1988; Mould, 1995). Gailit *et al.,* measured the α5β1–fibronectin interaction using receptor – liposome binding assays. The attachment of liposomes containing purified α5β1 to wells coated with the 110 kDa fibronectin cellular binding fragment was measured in the presence of Ca^{2+}, Mg^{2+} and Mn^{2+}. These assays showed a 2 – 3 fold increase in liposome binding in the presence of Mn^{2+} as compared to basal liposome adhesion in the presence of calcium + magnesium. Mould *et al.,* also showed that increased binding occurred in the presence of Mn^{2+} and to a lesser extent with Mg^{2+} for assays using purified α5β1 adsorbed to micro titer wells (or K562 cells) and fibronectin cell binding fragments. The resultant binding in the presence of Ca^{2+} produced greatly reduced binding as compared to Mn^{2+} or Mg^{2+}. In a later study, Mould, *et al.,* used inhibitory and stimulatory antibodies in the presence of varying concentrations of Ca^{2+}, Mg^{2+} and Mn^{2+} to map epitopes at the fibronectin binding site of α5β1. A change in affinity of α5β1 for both anti α5 and anti – β1 antibodies was observed and attributed to cation stimulated changes in integrin conformation at the binding site (Mould, 1998).

In single molecule interaction studies' involving α5β1 and fibronectin, increased integrin binding affinity has been correlated with increased bond rupture force during tensile loading of the bound molecular pair (Li, 2003, Garcia).

Both the α and β dimers participate in binding the RGD and 'synergy' sequences of fibronectin. The fibronectin binding site locality is the NH2 terminus of α5β1; a cleft shaped region formed by the fusion of the α and β dimers. A study mapping the fibronectin binding site of α5β1 with monoclonal antibodies determined that overlap between the dimers existed (Mould, 1997). The binding of fibronectin fragment containing the RGD and 'synergy' sequences blocked adhesion of anti – α5 antibodies with epitopes at the fibronectin binding site. However, RGD peptide did not inhibit anti – α5 antibody but inhibited anti β1 antibodies. Further, mutant fibronectin fragments lacking the synergy site failed to inhibit anti - α5 antibodies. A subsequent study also showed considerable overlap of epitopes for anti – α5 and anti – β1 antibodies existed (Mould, 1998). The epitopes for the anti- α5 antibodies JBS5 and mAb 16 (which are located in the fibronectin binding site of α5β1) showed overlap with the anti – β1 antibodies 12G10 and mAb13, indicating the close proximity of the epitopes and the overlap of the fibronectin binding site. Overall, these studies showed that the α5 dimer mainly interacts with the synergy sequence of module type III_9, while the RGD sequence of module type III_{10} interacts mainly with the β1 dimer.

In - vivo studies involving deleted alleles for expression of either (α5) dimer or (Fn) in mice reported embryonic maldevelopment; resulting in vascular, mesodermal and neural defects that subsequently lead to embryonic death after 10 days (Yang, 1993; George, 1993). George *et al.,* showed that fibronectin was essential to embryonic development in mice with inactivated fibronectin gene. Homozygous mice embryos primarily displayed mesodermal and vascular

defects at 8 days and died after 11 days. The heterozygous genotype appeared normal but had half the plasma fibronectin of wild type, while homozygous embryos totally lacked fibronectin. Yang, *et al.,* produced α5 null mouse embryos to examine the role of α5β1 in embryogenesis. Mesodermal defects were present (as in embryos lacking fibronectin) however the development of the mesoderm advanced further than fibronectin null embryos before lethality occurred around 10 days. The advanced development of the mesoderm was attributed to other integrins that target fibronectin as a ligand however; the essential role of both fibronectin and α5β1 in embryogenesis was established.

In summary, the interaction between α5β1 and fibronectin is essential to establish signaling pathways for normal cellular function which highlights the importance of integrin interaction with the ECM. This relationship is further emphasized during cellular motility which relies primarily on integrin α5β1. A few methods in which measurement of bond rupture force between α5β1 and fibronectin due to applied force are briefly covered in the following section.

2.4 METHODS IN FORCED SEPARATION OF ALPHA 5 BETA 1 AND FIBRONECTIN

The measurement of specific molecular interactions has been previously plagued by limitations in either force resolution or spatial resolution. Where as optical tweezers techniques have the necessary sensitivity they are limited in force to a few piconewtons; other techniques such as magnetic beads or pipette suction probes have limited spatial resolution (Florin, 1994). The implementation of AFM has for the most part remedied these problems by offering molecular

resolution under physiological conditions and piconewton sensitivity (Drake, 1989; Radmacher, 1992).

The AFM can manipulate live samples under physiological conditions, making it an idea tool for biophysical measurements between proteins. While operated in force - contact mode, the AFM maintains tip – sample separation via a feedback loop. Cantilever deflection from decreasing tip – sample separation results in feedback that maintains constant force on the sample (Figure 2.7). The Initial studies involving single molecule interactions with AFM measured the interaction between avidin – biotin or antigen – antibody pairs where the (Florin, 1994; Hinterdorfer, 1996).

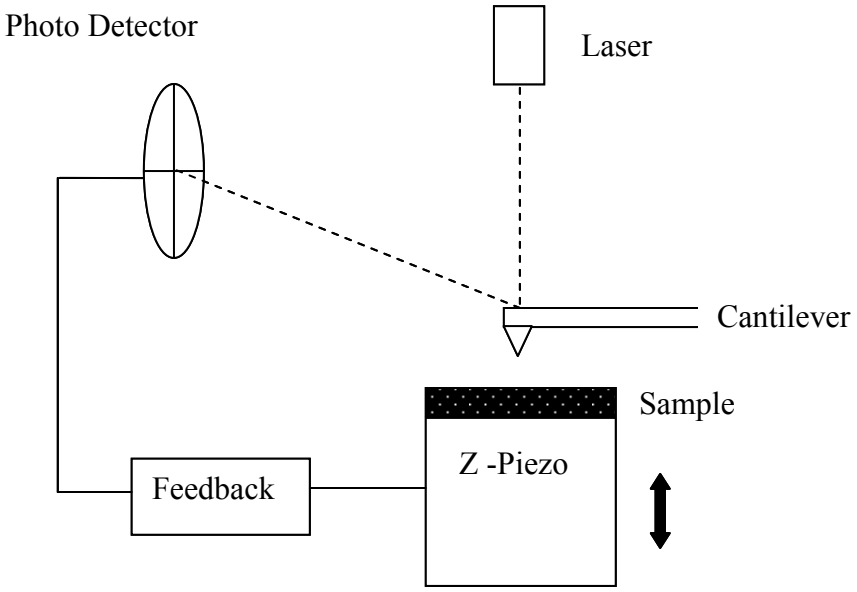

Figure 2.7 Schematic illustrating AFM tip – sample separation maintenance by means of. feedback.

The reported methods that have been used to measure the α5β1–fibronectin interaction applied either a direct tensile force to separate the pair (AFM) or hydrodynamic dynamic shear to adherent cells (Garcia, 1998, Sun, 2005). Garcia *et al.,* used a spinning disk in fluid and coated with varying fibronectin concentration to apply hydrodynamic forces to adherent K562 cells. The radial speed was used to determine how much shear stress (τ, Dyn/cm^2) was needed to detach cells. The rupture shear stress ($\tau = 0.8r\sqrt{\rho\mu\omega^3}$), r = radial distance, ρ, μ= density and viscosity respectively, ω= angular speed) reportedly increased with fibronectin concentration for cells treated with TS2/16 antibody as compared to untreated cells. However, assumptions regarding the location and density of bonds in the contact area must be made to arrive at single molecule force.

There are a few recent studies which measure the α5β1–fibronectin interaction using AFM (Li, 2003; Kokkoli, 2004). Li *et al.,* measured the rupture force between α5β1 and the cell binding fragment of fibronectin at different load rates using K562 cells attached to AFM tips. The integrin binding affinity was either upregulated using TS2/16 stimulatory antibody or left untreated and in the dormant affinity conformation. The bond rupture magnitude for forced molecular separation of the pair was reported to increase for upregulated α5β1 as was previously reported by Garcia *et al.,* however, it is unclear what role increased binding affinity plays in increasing interfacial strength between α5β1 and fibronectin.

In another AFM study, Kokkoli *et al.,* used purified α5β1 attached to the tip and GRGDSP / PHSRN mixed peptide substrate to measure the rupture force in the presence of divalent cation. The bond rupture force was measured at different load rates (100 – 300000 pN/s) and in the presence of either Mn^{2+} or Ca^{2+}. The rupture force versus load rate data showed that two load barriers exist in the presence of upregulated α5β1 due to Mn^{2+} uptake. A low and high

load barrier existed showing two linear regions of increasing rupture force as a function of increasing load rate. These two load regimes were also reported by Li *et al.,* for both the down and up regulated integrin affinity states. However, it was reported that the upregulated load regime had a higher rupture force (y- intercept) than the downregulated load regime.

Finally, steered molecular dynamics (SMD) can play a role in determining integrin – ligand behavior during rupture through direct comparisons with experimental AFM data. However, there exists a difference in time frames corresponding to bond rupture between the two methods with SMD simulations differing by as several orders of magnitude (Evans, 1997). The slowest SMD load rates are (10^{12} pN/s) while the highest AFM load rates are perhaps 10^{6} pN/s. The use of Monte Carlo simulation algorithms alleviates the time frame discrepancy and has been employed for the separation of the RGD peptide binding integrin αVβ3. The model used the integrin αVβ3 crystal structure with bound RGD with Mn^{2+} as the divalent cation (Xiong, 2002). The simulation predicted that the aspartic acid of the RGD peptide binds to Mn^{2+} at the β3 dimer MIDAS site and is stabilized by a single coordinating water molecule and resists disbonding.

Overall, the examination of the dynamic strength at the molecular interface between α5β1 and fibronectin adds a biophysical complement to current biochemical knowledge for interaction. The combination of biochemical and biophysical results regarding cellular binding gives a more complete picture of cellular adhesion (Orsello, 2001).

3.0 RESULTS

The interaction between α5β1 and fibronectin was quantified by examining the response of the bound molecules to externally applied force. This was accomplished using the Atomic Force Microscope (AFM) wherein α5β1 molecules were attached to the AFM cantilever probe and fibronectin molecules were immobilized on a mica substrate. The development of the AFM-based interaction force measurement assay is first described (*Sections* 3.1 - 3.4), followed by a discussion of the control experiments to establish the validity of this assay (*Section* 3.5). Next, the effects of divalent cation on the α5β1-fibronectin bond rupture force is examined at a single molecular separation speed (*Section 3.6*), followed by the examination at multiple molecular separation speeds (*Section 3.7*). The competitive binding of radio-labeled, divalent cation to either α5β1 or fibronectin is examined in *Section 3.8* as a complimentary study to the data presented in *Section 3.7*. Finally, circular dichroism spectroscopy (CD) is used to examine conformational changes in shape for either α5β1 or fibronectin upon binding divalent cation or upon forming a bound complex (*Section 3.9*).

3.1 CALIBRATION OF CANTILEVER SPRING CONSTANTS

Cantilevers oscillate when at thermal equilibrium with their environment. Thermal influences cause agitation of electrons in the cantilever resulting in high frequency oscillation. This thermal noise (due to oscillation) can be exploited to determine the cantilever spring constant, k_s.

The determination of the spring constant is important when the AFM is used for measuring minute forces such as protein – protein interactions. A portion of the cantilevers used in this study were manually calibrated by the thermal resonance method of (Bechhoefer and Hutter, 1993). Alternatively, the cantilevers were calibrated using an Asylum MFP 3D AFM with tip calibration software. The MFP uses a calibration algorithm similar to the method of Bechhoefer and Hutter. All calibrations were performed at room temperature (22 ˚C). The manual calibrations involved capturing the cantilever deflection signal and performing a power spectral analysis to determine its resonance frequency. The resonance peak was fitted with a Lorentz distribution and the area was converted to mean amplitude of oscillation for the cantilever (Figure 3.1).

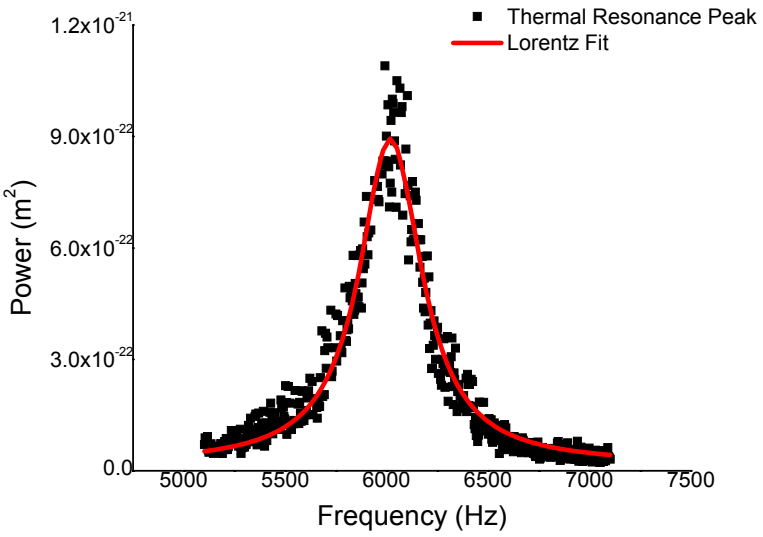

Figure 3.1 Thermal Resonance Peak Measurement. Resonance peak collected in air for the MLCT type of cantilever used in this study. The resonance peak was fit with a Lorentz distribution function and the area under calculated using equation (1). The calculated spring constant for this particular cantilever (k_s = 7.44 ± 1.01 pN/nm) differs by 25 % from the manufacturer's specified value (k_s = 10 pN/nm; Veeco Instruments, Santa Barbara, CA).

Because the cantilever was modeled as a simple harmonic oscillator (mass – spring) with one degree of freedom, the mean oscillation, $\langle x^2 \rangle$, was used to calculate the spring constant using (Equation 3.1).

$$k = \frac{k_B T}{\langle x^2 \rangle} \tag{3.1}$$

Both methods produced results that were within 25% of the manufacturers stated value for the spring constant for cantilever models MLCT (k_s = 10 pN/nm) and NPS (k_s = 60 pN/nm) (Veeco, Santa Barbara, CA). The mean cantilever displacement, $\langle x \rangle$, due to thermal noise was calculated and determined to be ~ 7.4 (Å) for the MLCT model and ~ 3.3 (Å) for NPS model.

The actual measurement of thermal noise in force curve measurements has averaged 1 nm of peak to peak deflection for MLCT types and 0.5 nm for NPS types at room temperature.

The spring constant for each cantilever was determined before any further modifications (i.e. attachment of microspheres or protein) which add weight and thus change the resonance properties of cantilever. The estimated spring constant values for all cantilevers are displayed in Table 3.1 and Table 3.2.

Table 3.1 Estimated Cantilever Spring Constants (pN/nm, single load rate experiments)

	Exp1, k_s	*Exp2, k_s*	*Exp3, k_s*	*Exp4, k_s*	*Exp5, k_s*
CaMg	41.1	65.7	32.8	56.0	67.3
Mn^{2+}	75.0	52.6	59.1	46.1	50.9

All spring constant values, k_s (pN/nm), were calculated using thermal noise method of Hutter & Bechhoefer, 1993. Nominal spring constant value (60 pN/nm) given by manufacturer, Veeco Instruments, Santa Barbara, CA.

Table 3.2 Estimated Cantilever Spring Constants (pN/nm, multiple load rate experiments)

Divalent Cation	*pFn: k_s (pN/nm)*	*Fnf120: k_s (pN/nm)*
Ca^{2+}	8.5	11.2
CaMg	9.9	12.5
Mg^{2+}	10.5	12.9
Mn^{2+}	13.2	12.0
CaMn	9.0	9.7

All table values calculated using Asylum MFP 3D AFM. ** Nominal spring constant value (10 pN/nm) given by manufacturer, Veeco Instruments, Santa Barbara, CA.

The calibration of cantilevers in this section using two different methods resulted in spring constant values that differed from the manufacturers reported values by up to 25%. This is consistent with the manufacturer's claim that the chemical etching process of silicon nitride

wafers results in batches of tips with varying thickness. Because of this varied thickness, individual tips need to be calibrated for the true spring constant value; especially when the tips will be used for force related studies.

3.2 MODIFICATION OF SILICON NITRIDE AFM PROBES

The pulling force experiments required the modification of standard silicon nitride AFM probes. The modification was broken into two parts; the attachment of a silica microsphere *Section 3.2.1* and crosslinking of integrin α5β1 to the microsphere *Section 3.2.2*.

The modification of AFM cantilevers for single molecule measurements is not new. The first cantilevers were functionalized with avidin or biotin (Florin, 1994) and the bond rupture force measured at a single bond separation speed. Today, bond separation measurements are conducted over a range of separation speeds to get a picture of the energy landscape surrounding forced molecular separation (Evans, 1997; Tees, 2001). To withstand such physical rigors, proteins are often covalently linked to the tip surface. Covalent linking results in a bond that exceeds the strength of non-covalent ligand - receptor interactions which is primarily the result of salt bridges or hydrogen bonds. Several single rupture force studies have even attached cells to AFM cantilevers to make use of *in - vivo* receptor interactions (Li, 2003).

The modification of AFM tips with purified α5β1 results in a system in which the dynamic binding properties of a single cellular receptor can be measured when contacted with a substrate modified with its sole ligand, fibronectin. However, this system which crosslinks α5β1 to the AFM tip, does not allow for natural factors such as lateral diffusion of integrin in the

cellular bilayer and hence the effects of integrin clustering are not observed. Further, covalent linking of proteins to the tip results in a bond that is stronger than most receptor –ligand interactions. Thus eliminating an effect in which receptors have been known to be extracted from the lipid membrane during receptor ligand loading such as during cell motility (Evans, 1991; Tees; 1996).

3.2.1 Attachment of Microspheres to AFM Probes

The process of cross-linking proteins to the AFM tip requires the availability of free SiO_x surface groups. Because silica possesses more SiO_x surface groups than typical AFM tip starting material, silicon nitride, silica microspheres were attached to the cantilevers to better facilitate this process. The cantilevers used were the ~ 320 μm Microlever Probes (k_s ~ 10 pN/nm) and the 200 μm (k_s ~ 60 pN/nm), NPS probes (Veeco; Santa Barbara, CA).

A low magnification SEM image of an assortment of Microlever® probes shows the 320 μm cantilever with an attached silica microsphere of diameter ~ 7 μm. The 320 μm cantilever was selected because of its ultra sensitivity and suitability in measuring pN forces (Figure 3.2).

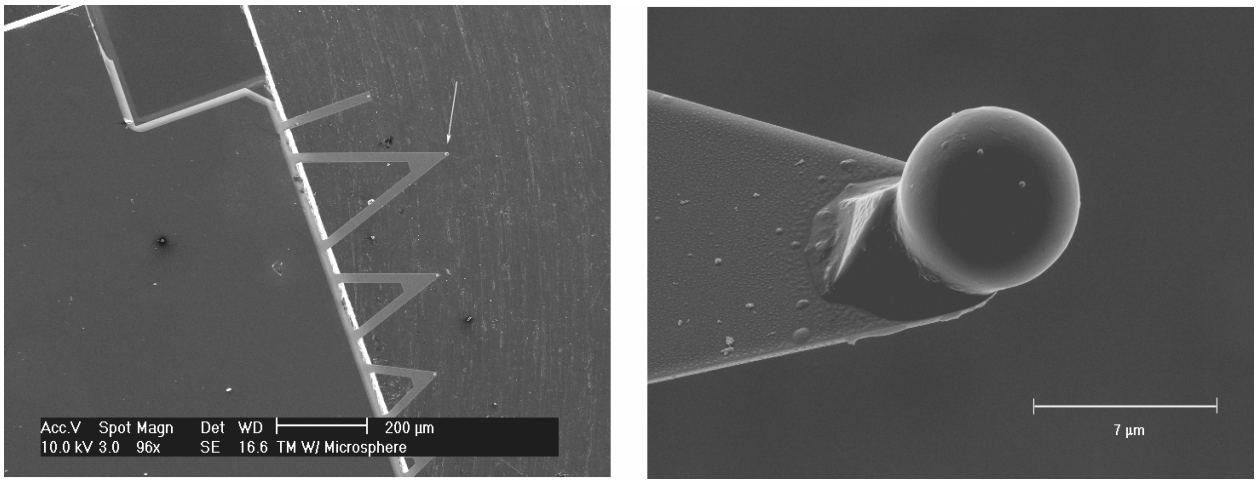

Figure 3.2 AFM Probe Modified with Silica Microsphere. (A) Low magnification SEM image (100 X) of type cantilever used in this study (Arrow). (B) High magnification image (6000 X) showing silica microsphere attached with epoxy cement. Note the pyramid tip (underlying microsphere) used for AFM imaging. The cantilever spring constant has a manufacturer's specification of (k_s = 10 pN/nm).

The attachment of the silica microspheres (Bangs Labs; Fishers, IN) was accomplished under high magnification, and using an x - y translation stage of a Digital Instruments LFM /AFM. Using a glass substrate with mono-dispersed microspheres, the tips were first dipped into epoxy and then positioned onto a microsphere for attachment. The high magnification SEM image of a cantilever with attached microsphere shows the available surface area for modification as compared to the native pyramid tip (adjacent to microsphere). The SEM micrographs also show that the microspheres are roughly centered on the tip of the cantilever. Higher magnification scans (not shown) show that the epoxy adhesive used to attach the microspheres does not cover the surface to be modified with crosslinker, but instead has a distinct boundary well below the target surface. The modification of the microsphere surface with crosslinker (to attach α5β1) is described in the next section.

3.2.2 Surface Modification of Microsphere to Attach α5β1

The microsphere modified tips were first cleaned with UV-ozone, then functionalized with sulfhydryl terminated chemistry (3'-mercaptopropyl-trimethoxysilane, sigma). The reaction between the tips and silane was performed under inert conditions (argon) to enhance polymerization of adjacent silane molecules in the formation of a self assembled monolayer.

The tips were then reacted with N-Succinimidyl 3-(2-pyridyldithio) propionate (SPDP) cross-linker and incubated in purified α5β1. Prior to attachment to the tip, the cross linker reactivity was tested over a period of one hour by absorbance measurements at 280 nm. The absorbance at 280 nm signifies the release of the *N*-hydroxysuccinimide (NHS) ester from the cross-linker due to either hydrolysis or protein conjugation (Figure 3.3).

The reactivity of a given concentration of the cross-linker at room temperature can be up to four hours at pH (7-8) but reduces exponentially with rising pH (> 8). The addition of strong base (1N, NaOH) to a 6.4 μM solution of SPDP caused a noticeable increase in absorbance which subsided after 25 minutes at a final pH of 9.2.

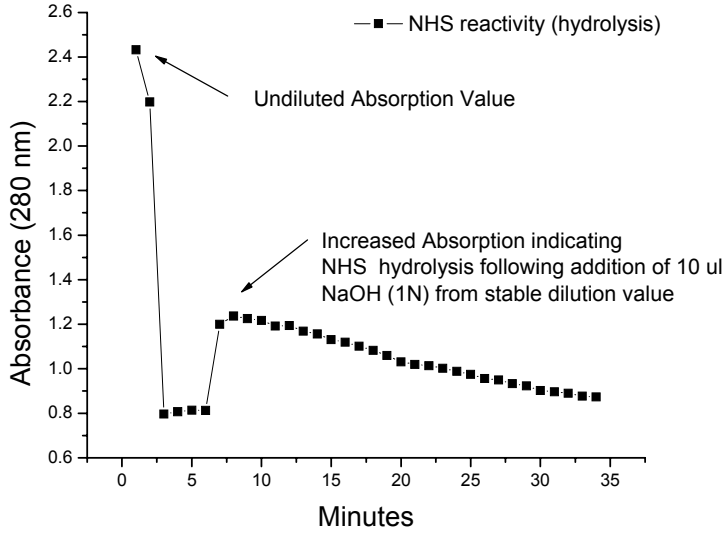

Figure 3.3 Examination of SPDP Cross-linker Reactivity Using UV Absorbance. SPDP cross-linker covalently attaches to proteins via the amine terminal through a nucleophilic reaction in which the NHS ester is a leaving group. Increased UV absorbance at 280 nm is an indicator of NHS ester release during protein linking reactions. The presence of the NHS ester group is essential for the protein binding reaction to occur. Because SPDP degrades very rapidly in aqueous solution due to hydrolysis of the NHS ester group, the absorbance was measured during NHS ester release. Complete molecular hydrolysis of NHS ester typically occurs after 4 hours at neutral pH. However, increasing pH considerably reduces the time necessary for complete hydrolysis. The absorbance was measured at a starting pH of 7(neutral) then after the addition of NaOH (1N). The peak shows a increase of absorbance immediately following the addition of NaOH that gradually returns to neutral pH absorbance levels over time coincident with molecular depletion of NHS ester.

The SPDP molecule is a heterobifunctional cross-linker in which the pyridyl disulfide residue reacts with the sulfhydryl terminated silane while the N-hydroxysuccimide residue bonds the protein's NH2 terminus (Figure 3.4).

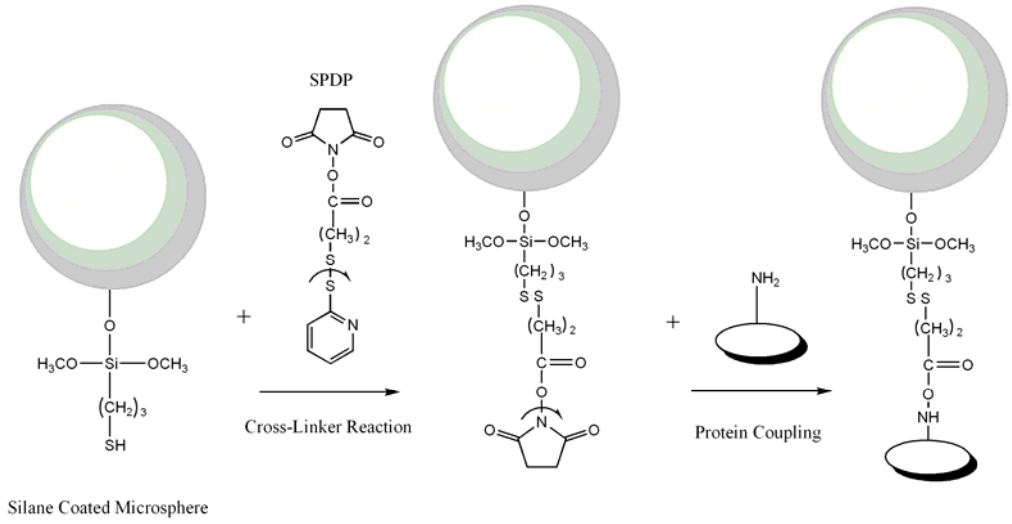

Figure 3.4 Modification of AFM Tips with α5β1. Schematic adapted from (Wangsa-Wirawan *et al.,* 2001) showing functionalization steps to cross-link protein (i.e. α5β1) via the amine terminal. AFM tips fitted with silica microspheres are coated with a mono-layer of silane coating, and then are subjected to a crosslinker (SPDP), which attaches at the silane thiol terminus. The protein is then bound via an amine group through nucleophilic reaction with NHS –ester terminus of the crosslinker.

The modified tips were tested for the presence of α5β1 using fluorescence microscopy. The labeling strategy used an initial treatment with a primary antibody followed by treatment with Cy3 labeled, secondary antibody. The primary antibodies used were: *1) a function blocking, monoclonal antibody* (JBS5 clone; Chemicon) that binds the fibronectin attachment site and *2) A polyclonal antibody that binds the amino acid sequence* 840-943 in the c-terminus region of the α5 dimer (H-104; Santa Cruz Biotech).

The fluorescence signal was measured in the blue, green and red signal channels for 30 seconds . Fluorescence emission signal was observed at 550 nm (typical of Cy3 labeling) and was localized to the microsphere region of the tip. The region was highly illuminated for both the monoclonal and polyclonal antibodies (Figure 3.5). A control tip not incubated in primary

antibody but incubated in secondary fluorescent antibody, only showed a faint signal at 550 nm most likely from auto - fluorescence of the silica microsphere.

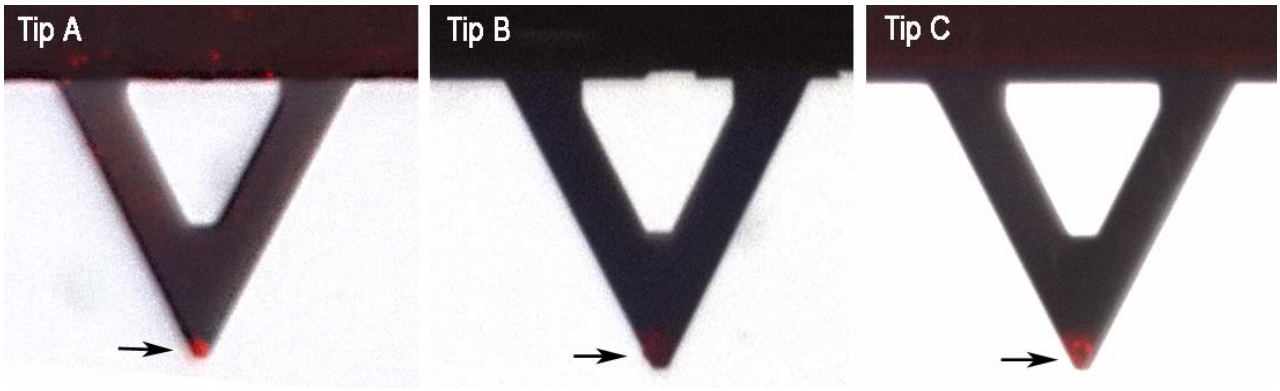

Figure 3.5 Fluorescence Label Detection of α5β1 on Modified Si_3N_4 AFM Tips. All tips were initially fitted with a silica microsphere (7 μm diameter) and cross-linked with purified integrin α5β1before incubated in BSA solution. Measurements; Tips A and C were first incubated in primary antibody, then a secondary antibody with fluorescent label at 550 nm. Tip B was a control incubated solely in secondary antibody with fluorescent label. Fluorescence measurements were made in the Red, Green and Blue wavelengths for 30 seconds. Results; Note that tip A and C display strong fluorescence at 550 nm in the region of the attached microsphere (see arrows) while tip B displays a faint signal most likely resulting from auto-fluorescence of the microsphere. A primary, monoclonal antibody against α5β1 (JBS5 clone, Chemicon) was used for tip A while a polyclonal antibody (H-104, SantaCruz Biotech) against the α5 dimer was used for tip C. The surrounding AFM tip material composed of Si3N4 shows far less fluorescence signal due to fewer SiO_2 groups needed for that attachment of silane groups and eventual protein crosslinking. Thus a silica microsphere was attached to each AFM tip which facilitated attachment of silane groups. A further control tip (not shown) was not modified with α5β1 but was incubated in BSA and secondary antibody with fluorescent label and displayed no fluorescence signal.

The tips incubated in primary antibody also showed sparse patches of fluorescence on the remainder of the cantilever surface, demonstrating that the Si_3N_4 surface was not functionalized uniformly. Measurement in the blue and green channels did not yield any fluorescence signal.

Additional tips not functionalized with α5β1 also showed no fluorescence signal. Non-specific absorption of antibody was controlled for by incubation of tips in BSA. The

modification of the microsphere surface with α5β1 was confirmed using fluorescence microscopy and now allows for testing of the α5β1-fibronectin interaction.

3.3 IMMOBILIZATION OF FIBRONECTIN ON MICA SUBSTRATES

Substrate for this study consisted of freshly cleaved mica onto which fibronectin was passively adsorbed. Hepes buffer (10 mM at pH 7.4, 150 mM NaCl) containing either pFn or Fnf120 at a concentration of 50 μg/ml was allowed to adsorb at room temperature for 10 minutes. To avoid background adhesion between the tip and bare spots on the substrate, 2% BSA was also adsorbed onto the mica. A tapping mode image (1 μm x 1 μm) in air of pFn at 50 μg/ml on mica was accomplished on a sample (Figure 3.6).

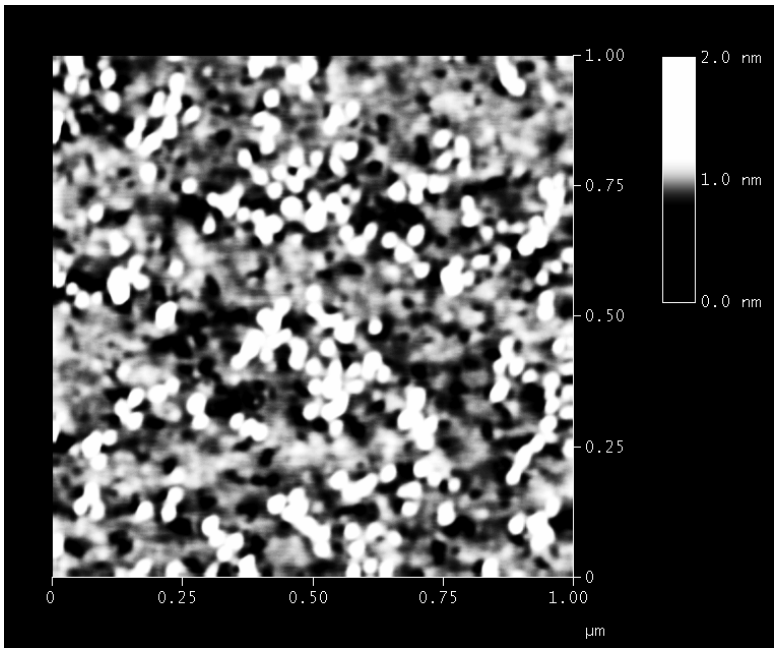

Figure 3.6 AFM tapping mode image of pFn. A (1μm x 1μm) image from 50 μg/ml sample of pFn adsorbed onto freshly cleaved mica. The sample was imaged in air after extensive rinsing of the sample with distilled H_20.

The image shows dense coverage of immobilized fibronectin on the mica substrate. The fibronectin coated substrates are the second component necessary to examine the α5β1 - fibronectin interaction along with α5β1 modified AFM tips.

3.4 ASSAY FOR THE MEASUREMENT OF ALPHA 5 BETA 1-FIBRONECTIN BOND RUPTURE FORCE

In this study, the bond rupture force between individual ligands and receptors was measured by separating bound α5β1-fibronectin through the application of tensile force. The tensile force is exerted by the AFM as a result of the retraction portion of the force curve's 'approach – retraction' cycle; during which the separation distance between the AFM tip and substrate increases. Brief contact (< 1.5 ms) between the tip-and substrate during the approach portion of the cycle allows for bond formation (Figure 3.7).

Because the receptor and ligand molecules are tethered to the tip and substrate respectively, the molecular interface experiences tensile loading during the retraction cycle. The loading increases until the tensile force equals the bond adhesion force and bond rupture occurs.

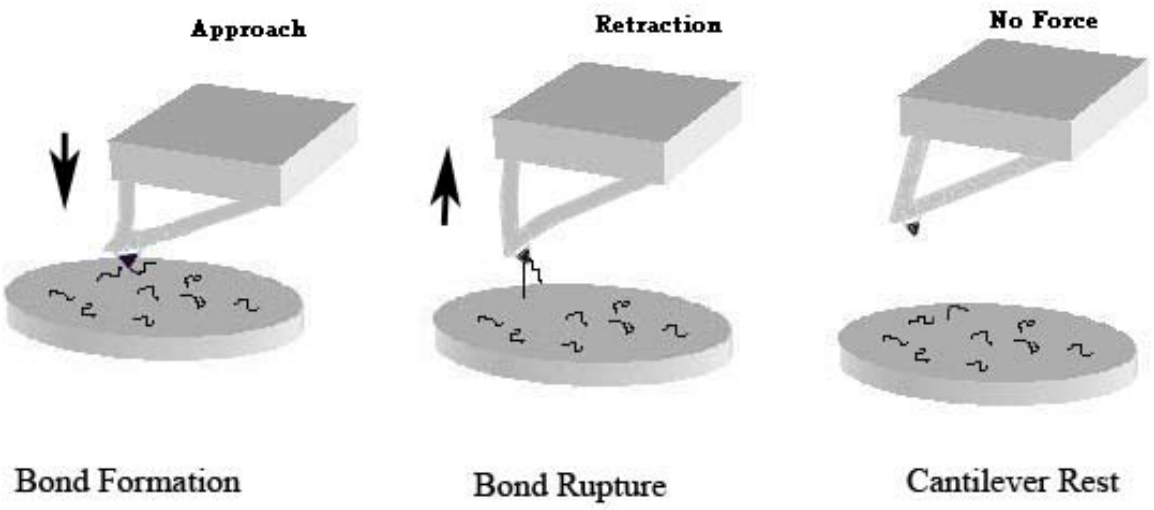

Figure 3.7 Illustration of α5β1-Fibronectin Binding. An α5β1 coated tip contacts the substrate (approach) coated with either pFn (or Fnf120) forming molecular bonds. As the tip and substrate are separated (retraction) at various speeds, the molecular interface is dynamically loaded until bond rupture occurs. Each adhesion event between α5β1 and fibronectin is collected in the form of a force curve which represents cantilever deflection plotted against sample/piezo travel.

The typical anatomy of the force curve is shown in Figure 3.8. The diagram shows the approach cycle (starting at A) then a retraction cycle (starting at C). At point A, the tip is not influenced by the substrate (i.e. attractive or repulsive forces) and thus no cantilever deflection occurs. At point B, the tip jumps onto the substrate due to an attractive force, causing the cantilever deflection downward below the zero deflection level.

The upward, linear slope (point C) represents the cantilever deflecting as a linear spring as the contact force with the substrate increases; showing a 1:1 correspondence between tip deflection and piezo travel. At a threshold value of deflection, the cycle reverses and the tip – substrate separation distance starts to increase. However, the tip is held onto the surface by an attractive force causing a downward deflection until point D, where the deflection of cantilever results in a force large enough to overcome the attractive force. The tip instantaneously returns its zero deflection level.

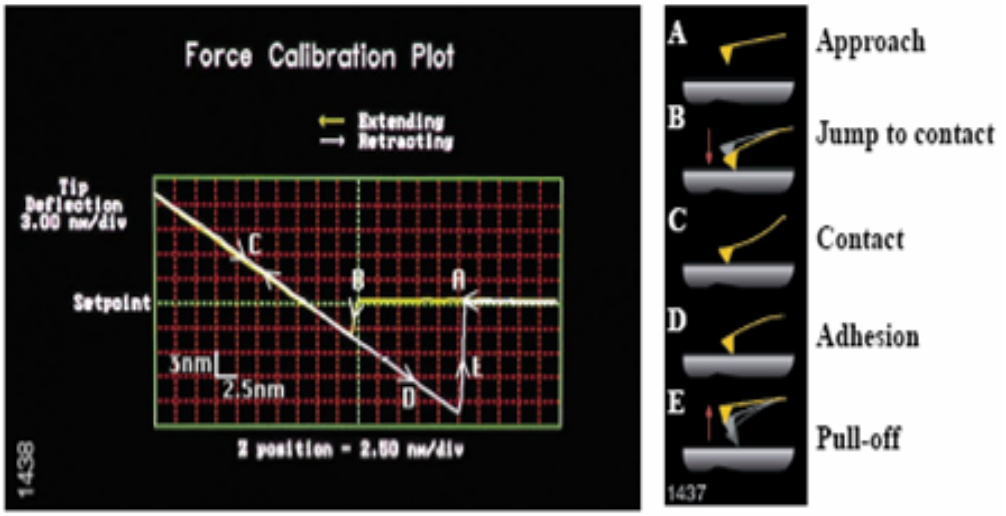

Figure 3.8 Force Curve Anatomy. Schematic of typical force curve features for approach of tip towards the substrate (labeled yellow). Tip retraction away from the substrate is labeled in white. As the tip nears the substrate, The tip senses long and short range attractive and repulsive forces. As the tip nears the surface (B), attractive Vander Waals interactions result in the tip jumping onto the substrate surface. Contact with the substrate results in a linear change in tip deflection with respect to piezo travel (C). As the tip retracts from the substrate after reaching a maximum deflection, the tip adheres to the substrate surface (D). As the separation distance between the tip and substrate increases, the bound cantilever increasingly deflects until the cantilever force equals the tip adhesion force and the tip instantaneously pulls free from the surface (E). The force required to separate the tip from the substrate is calculated as the cantilever deflection (peak height E to A) multiplied by the cantilever spring constant, k_s. *(Figure from Veeco Multimode Training manual).*

The actual bond rupture magnitudes were determined by analyzing the rupture peak feature of the 'force curve'. The rupture peak's vertical height is shown as steps E to A in Figure 3.8. The force curves' vertical features result from cantilever deflection while horizontal features result from translation of the piezo-electric crystal that holds the sample.

It should be noted that Figure 3.8 represents a typical example of a force curve in which the tip interacts with the substrate in a non-specific manner and does not represent a biological interaction. Never the less, the diagram illustrates the basic features of a force curve. The biological interaction examined in this study features a pair of molecules in which one

recognizes a specific amino acid sequence in the other. A further feature from figure 3.8 that is not native to biological interactions is the initial non-specific tip attraction at point B of the approach.

For the AFM used in this study, the cantilever is fixed and is the system's force sensor. The substrate is fixed to the piezo – electric ceramic that expands and contracts when voltage is applied - resulting in vertical, linear translation precise to nm dimension.

Previous studies have shown that molecular separation force increases with increased tip-substrate separation speed. An accumulation of these measurements are most frequently analyzed in a histogram to determine the modal separation force for a particular ligand – receptor pair at the single molecule level. However, a method using the 'average' rupture force of a symmetrical distribution of values has been used in the place of the modal value (Tees, 1997).

In this section, the concept of α5β1-fibronectin bond formation and rupture has been presented. Also, the 'force curve', which is generated by the AFM during the α5β1-fibronectin rupture force measurement was introduced. The general anatomy of the force curve was described for future reference.

3.5 CONTROL EXPERIMENTS TO ESTABLISH THE VALIDITY OF THE ALPHA 5 BETA 1–FIBRONECTIN ASSAY

Initial testing of modified tips involved measuring the adhesion force between the tip and a pFn coated mica substrate after each tip modification step. Because of the specificity of the α5β1–fibronectin interaction, the tests were necessary to determine specific from non – specific

adhesion. The background adhesion for each sequential modification step was measured on a fibronectin coated substrate and is shown in (Figure 3.9). The measurements were made in hepes buffer containing 0.5 mM Mn^{2+}. The tip modification steps were previously described in *section 3.2.2*.

The modification steps involving silane coating alone or with silane + crosslinker resulted in no detectable background interaction between the tip and fibronectin coated substrate except for occasional interactions presumably at areas that lacked fibronectin coating (See figure 3.9, A-D). The modification step involving the addition of α5β1 shows interaction with fibronectin as expected. The interactions are in the form of multiple adhesion peaks (See figure 3.9, E-F). The peaks represent cantilever deflection due to bond rupture forces between α5β1 and fibronectin.

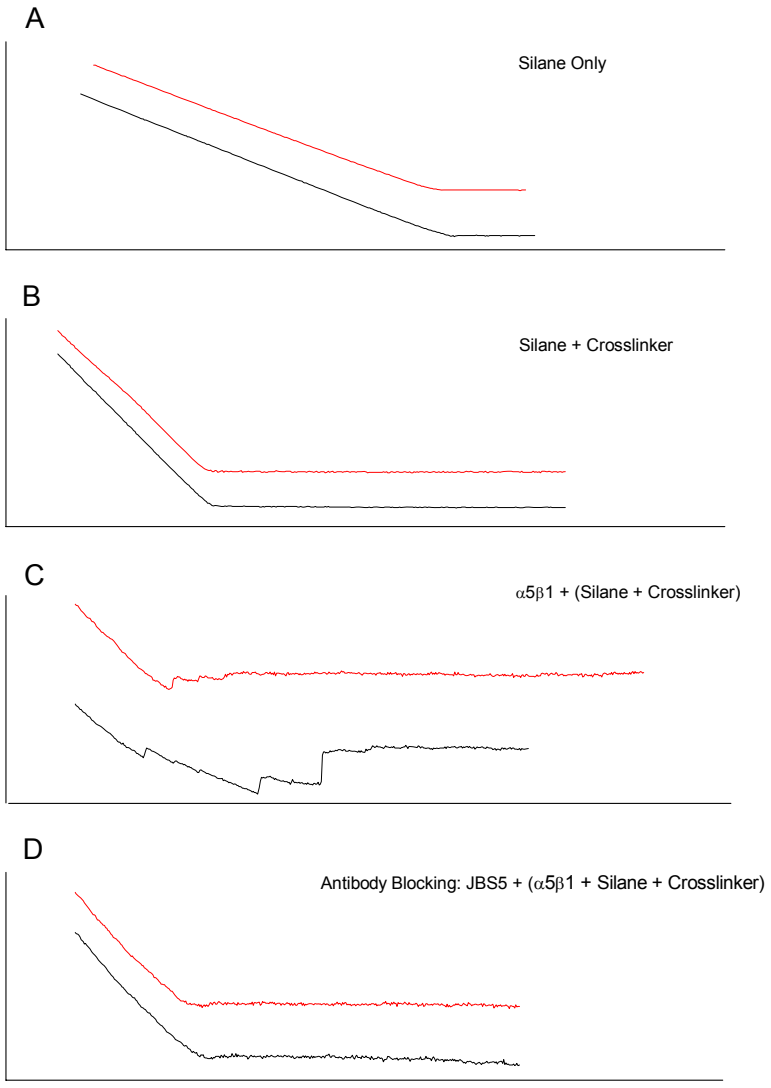

Figure 3.9 Determination of Background Adhesion Force Between the Modified AFM Tip and Fibronectin Coated Substrate for Relevant Tip Modification Steps. The force curves contain only the tip - substrate retraction data for clarity and were collected in buffer with 0.5 mM Mn^{2+}. (Panel A) shows no background adhesion for silane coating of AFM tips and for modification with crosslinker (Panel B). Modification with α5β1, following the silane and crosslinker steps, results in multiple bond rupture peaks between α5β1 and pFn (Panels C). The multiple α5β1 – fibronectin interactions can be blocked following the addition of a (1:200) dilution of JBS5 antibody, which inhibits the attachment of fibronectin to α5β1 (Panel D). The addition of the non-function disrupting antibody, P1E6 had no effect on binding (data not shown).

Due to the relatively large tip - substrate contact force (> 150 pN), multiple adhesion peaks were observed. In the following section, and in previous studies, it has been shown that limiting the tip - substrate contact force results in reduced probability of receptor - ligand binding and single (rather than multiple) bond rupture peaks. Control of tip – substrate contact force is important for analysis of single molecule rupture force behavior.

The blocking of this interaction with the anti - α5 antibody, JBS5, resulted in the loss of bond rupture peaks and a noticeable reduction in the frequency in which any peaks occurred (See Figures 3.9 E - F and Figure 3.10).

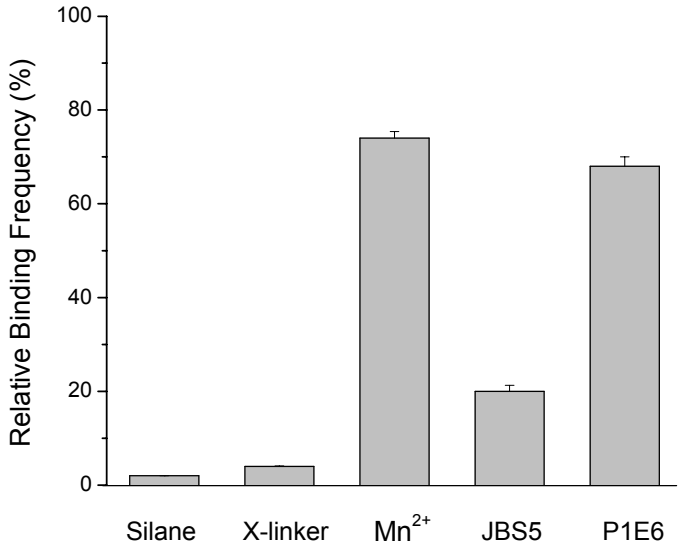

Figure 3.10 Reduction of Multiple α5β1-Fibronectin Interactions Using Antibody. The frequency of multiple peak interactions (figure 3.9 above) as determined by the number of measurements (force curves) displaying multiple interaction peaks normalized by the total number of measurements collected. All measurements were collected in 10 mM hepes buffer (pH 7.4) with 0.5 mM Mn^{2+} at room temperature. The addition of JBS5, which disrupts the α5β1 - fibronectin interaction, reduced the frequency of occurrence of measurements containing bond rupture peaks. While P1E6, which binds integrin α2 dimer and does not disrupt the interaction was used as a control with no loss of binding frequency when compared to basal measurements in Mn^{2+} buffer containing no antibody. The silane or silane + crosslinker modification steps resulted in little or no background adhesion noise. Data is presented as Mean ± S.E.M.

The monoclonal antibody P1E6 (Chemicon International) was used as a control as it solely binds to α2 integrin dimers, which was not present in our study. The addition of P1E6 resulted in no loss in interaction frequency (not shown) between α5β1 and fibronectin which was observed following JBS5 treatment (See Figure 3.10).

These preliminary results establish that JBS5 disrupts the α5β1-fibronectin interaction and shows the specificity of JBS5 compared to the control antibody P1E6.These initial experiments show that the silane coating and crosslinker do not contribute background adhesion to the α5β1-fibronectin interaction.

Further, the α5β1-fibronectin interaction can be disrupted by function blocking antibody, JBS5, but not by control antibody such as P1E6, which is an anti - α2 antibody. The validation of the assay for the initial bond rupture force measurements showed the functionality of the α5β1 modified tips when binding fibronectin. This allowed the progression (in the following sections) to experiments that measure rupture force magnitude and frequency of binding for α5β1and fibronectin under conditions of divalent cation regulated binding affinity.

3.6 EFFECTS OF DIVALENT CATIONS ON ALPHA 5 BETA 1-FIBRONECTIN INTERACTION: SINGLE LOAD RATE

The influence of divalent cation on the binding affinity of α5β1 is well documented (Gailit, 1988; Mould, 1995). In this section, the separation force between α5β1 and fibronectin is measured at a single tip – substrate separation speed and in the presence of divalent cation. These

experiments seek to examine the affects of divalent cation regulated binding affinity on rupture force magnitude as well as the effects of tip – substrate separation speed.

The effect of Ca^{2+} is the down regulation of α5β1 binding affinity while Mg^{2+} and Mn^{2+} are known to up regulate its binding affinity. Down regulation refers to the 'inactive' or folded conformation of α5β1 that less readily interacts with fibronectin due to hindered access to the integrin binding site. While up regulation refers the 'activated' or up right conformation of α5β1 in which the integrin binding site is not obstructed (Figure 2.3). The physiological levels of Ca^{2+} and Mg^{2+}used in this experiment refer to amounts found in wound healing experiments (Grzesiak, 1995). The physiological levels of serum Ca^{2+} and Mg^{2+} have been reported as 2 mM/L and 1 mM/L respectively (Kratz, 1998). The concentrations of Ca^{2+} and Mg^{2+} in wound tissue are both 1 mM each, however in non-wound tissue, Ca^{2+} concentration remains at 1 mM while Mg^{2+} decreases to 0.5 mM

Although Mn^{2+} is a trace element, it is often used in cellular or binding assays using purified integrin because of its phenomenal ability to increase binding interactions as compared to physiological Ca^{2+} and Mg^{2+} (Mould, 1995; Gailit, 1988). However, the reason for this increased activity is unknown. Further, the levels of Mn^{2+} reported in experiments citing increased binding activity are levels that are far higher than physiological amounts of Mn^{2+} found in the human body. Such is the case in this study with treatment levels of 0.5 mM Mn^{2+}, which is 14 times higher than known physiological levels in blood (36 μM/L human blood; ~ 0.04 μM in liver tissue).

The bond rupture force measurements were conducted in Hepes buffer with the addition of divalent cation. The number of interactions (i.e. rupture peaks) per force curve depends on the *amount of force* with which the cantilever was engaged onto the substrate as well as the *tip* –

substrate contact time (Li, 2004). Thus, the substrate contact force was limited between 20 and 150 pN in order that mostly single bond rupture peaks occurred (Figure 3.11). Force curves involving multiple interaction peaks (Figure 3.9, panel E) were not included in the analysis.

Prior to the measurement of α5β1-fibronectin rupture force, extensive measurements for the control of background adhesion between the tip and substrate were conducted (Figure 3.9).

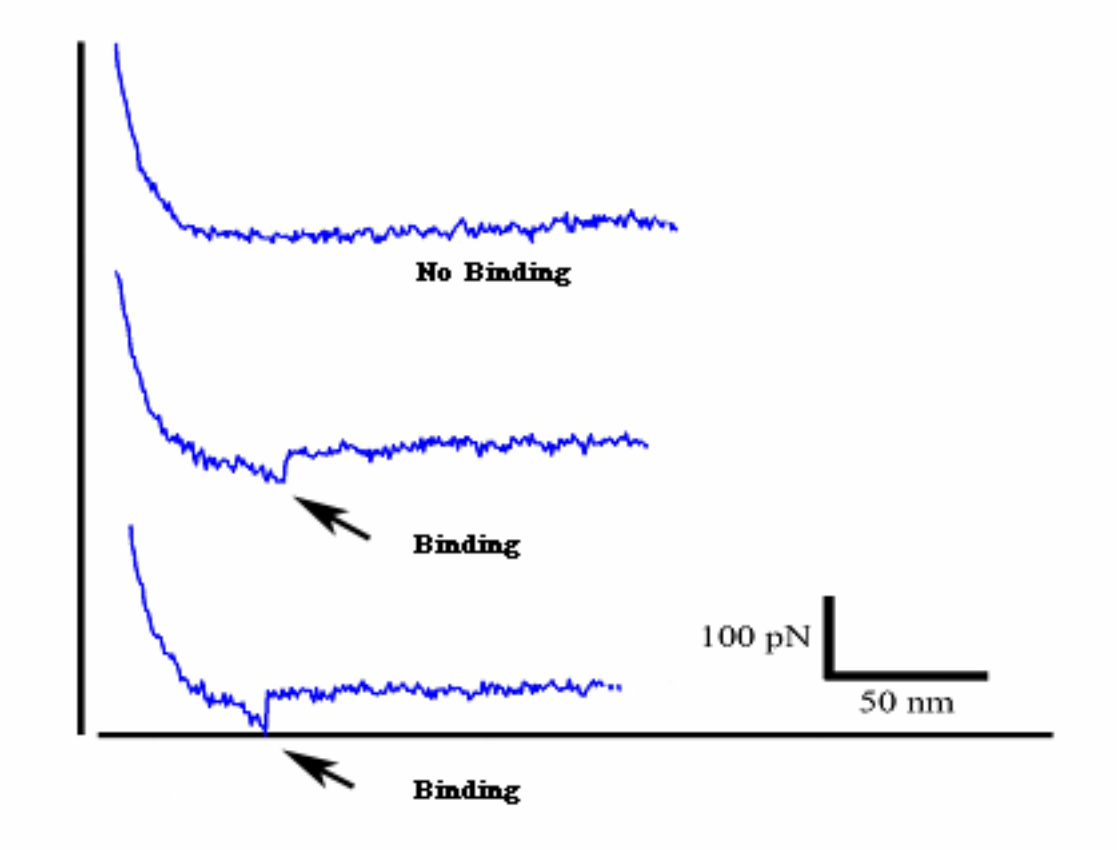

Figure 3.11 Typical Rupture Force Measurements for α5β1-Fibronectin Interaction at 4800 pN/s. The inset shows retraction only traces of the rupture force (ordinate). The tip-substrate separation (piezo translation) is on the abscissa. The top retraction trace shows that no molecular interaction occurred. The remaining traces show a single bond rupture peak, which was interpreted to be a single molecular interaction. The tip-substrate contact force was minimized (~20 – 150 pN) in order that a frequency of single peak interactions occurred 30 – 45 % of the time. The measurements were conducted in buffer containing 0.5 mM Mn^{2+}. Force curves containing more that one peak (i.e. multiple molecular interactions) were not counted in this study.

Our results indicated that coating a bare mica substrate with BSA eliminated background adhesion for AFM tips functionalized with α5β1 (not shown). The measurements at 4800 pN/s were collected and analyzed in histograms. The histogram vertical axis display frequency of rupture force events while the horizontal axis displays rupture force magnitude (Figure 3.12).

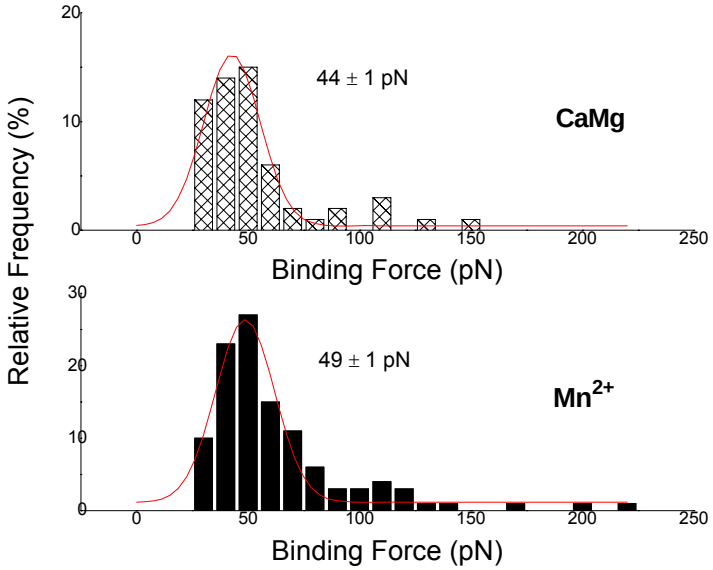

Figure 3.12 Divalent Cation Effects on α5β1-pFn Rupture Force at a Single Load Rate. Binding force measurement results for α5β1 activated with 1 mM $CaMg^{2+}$ (TOP) and 0.5 mM Mn^{2+} (Bottom) compiled into a histogram showing relative frequency versus binding separation force. The curves were fit with a Gaussian function and show the increased binding frequency increased for Mn^{2+} as compared to CaMg. The unbinding force shown is the magnitude plus the S.E.M. The histograms were generated using the data for (n=100) force curves each for both CaMg and Mn^{2+}.

The frequency in which binding interactions occurred for treatments of 1 mM CaMg or 0.5 mM Mn^{2+} showed that Mn^{2+} supported a higher frequency of binding in five experiments (Table 3.3; $P < 0.05$). A single modified tip was used for each experiment (i.e. cation treatment) in this study and no tips were reused.

Table 3.3 Frequency of Binding Counts at 4800 pN/s

	Exp 1 (%)	*Exp 2 (%)*	*Exp 3 (%)*	*Exp 4 (%)*	*Exp 5 (%)*	*Average(%)*
CaMg	26	15	18	11	16	17 ± 2.5
Mn^{2+}	35	26	35	30	25	30 ± 2.1

Data Average: Mean ± S.E.M.; Statistical difference of average frequency according to t-test, *P = 0.002.*

Roughly 30 - 45% of the measurements resulted in a single binding event. Larger contact forces resulted in multiple binding events in which multiple peaks were present in the force curve measurements. Poisson distribution statistics have been reported that suggest that 30% of the force curves resulting in a single peak reflect a ~ 83% single bond formation and a 15% double bond formation (Merkel, 1999; Chesla, 1998).

As previously mentioned there was a significant difference in the α5β1–fibronectin binding frequency between CaMg and Mn^{2+} treatments as was expected. However, the effect of divalent cation on the α5β1 interaction at 4800 pN/s shows that no significant difference in adhesion force ($P = 0.38$) magnitude existed at a single load rate (Table 3.4).

This surprising result was further investigated at varying tip - substrate separation speeds (see the following section), together with the regulation of α5β1 binding affinity using a more diverse treatment with divalent cation.

Table 3.4 Mean Rupture Force at 4800 pN/s

	Exp 1 (pN)	*Exp 2 (pN)*	*Exp 3 (pN)*	*Exp 4 (pN)*	*Exp 5 (pN)*	*Average(pN)*
CaMg	59 ± 1.0	55 ± 2.3	51 ± 1.4	44 ±1.0	46 ± 2.2	51 ± 2.7
Mn^{2+}	53 ± 1.0	53 ± 4.0	60 ± 2.2	49 ± 1.0	47 ± 3.0	52 ± 2.2

Data: Mean ± S.E.M.; No difference in the mean rupture force was observed ($P = 0.38$).

The specificity of the interaction was investigated using JBS5 monoclonal antibody which blocks the α5β1-fibronectin interaction by binding primarily to the α5 dimer at the fibronectin attachment site. Additionally, EDTA, a chelator of divalent cation was used to disrupt α5β1-fibronectin binding and show the necessity of cation for the interaction. Further experiments involved the use of excess RGD peptide that disrupts α5β1-fibronectin binding by attaching to the fibronectin binding site of α5β1. All specificity experiments showed disruption of the α5β1-fibronectin interaction and significantly reduced the frequency in which this interaction occurred (Figure 3.13).

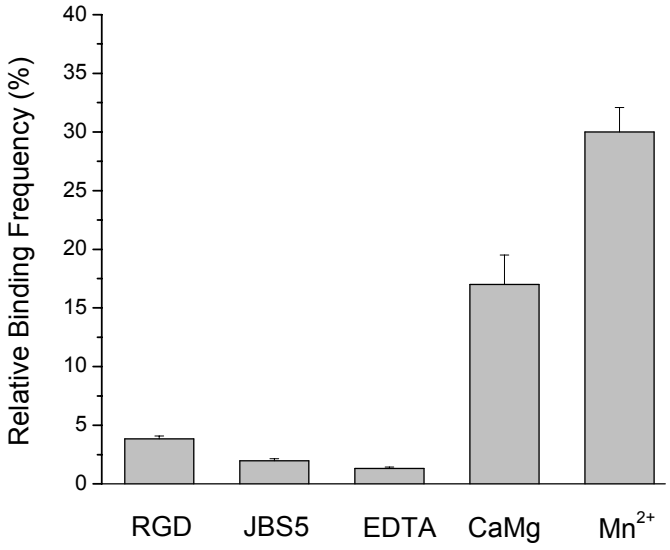

Figure 3.13 Specificity of α5β1-Fibronectin Interaction. The specificity of the molecular interaction was tested using different molecular probes to block fibronectin binding to α5β1 or to disrupt the interaction. Binding of RGD peptide or JBS5 at the fibronectin binding site of α5β1 reduced the number of interactions between α5β1 and fibronectin. EDTA was used to chelate divalent cation for α5β1 treated with 0.5 mM Mn^{2+} and resulted in a loss of binding activity. The sequestering of cation or blocking of the fibronectin binding site in α5β1 resulted in an overall loss of binding activity. The importance of cation for this interaction and the recognition of RGD by α5β1 have been shown in this example. The data is presented as Mean ±S.E.M..

Taken as a whole, the up regulation of α5β1 using Mn^{2+} had an effect on the binding affinity but not the rupture force magnitude at 4800 pN/s. The up regulation with Mn^{2+} affected the frequency of the α5β1–fibronectin interaction by increasing the interaction frequency as compared to basal CaMg treatment. However, the separation force magnitude was not affected by up regulating α5β1 and was not significantly different from basal CaMg treatment.

3.7 EFFECTS OF DIVALENT CATIONS ON ALPHA 5 BETA 1-FIBRONECTIN INTERACTION: MULTIPLE LOAD RATES

To determine the effects of divalent cation on α5β1-fibronectin dynamic rupture force, five different combinations of physiologically relevant cations (i.e. either 1 mM Ca^{2+}, 1mM CaMg, 1 mM Mg^{2+}, 0.5mM Mn^{2+} or CaMn (1 mM: 0.5 mM)) were used as treatments (Table 3.5).

Table 3.5 Divalent Cation Treatment Dosage for Experiments

Divalent Cation	*Treatment Dosage*
Ca^{2+}	1 mM
Mg^{2+}	1 mM
CaMg	1 mM
Mn^{2+}	0.5 mM
CaMn	1 mM:0.5 mM

Divalent cation molarity in 10 mM Hepes buffer containing 150 mM NaCl (pH 6.8).

In addition to five different cation treatments, nine different tip - substrate separation speeds between (0.10 and 19.0 μm/s) were utilized to collect bond separation information. This range of separation rates encompasses reported values for keratinoncyte motility speeds on fibronectin (Galbraith, 1999; De Beus, 1998). Thus, a range of rupture force data was collected that mimics forces most likely experienced by the α5β1-fibronectin interface during cell motility. The range of tip – substrate separation speeds used is shown in (Table 3.6) for either full molecule, plasma fibronectin (pFn) or the 120 kDa cell binding fragment (Fnf120) digested from plasma fibronectin (Chemicon, Temecula, CA).

Table 3.6 Tip – Substrate Retraction Rates for Plasma Fibronectin and Fnf120

	Retraction Speed (μm/s)								
pFn*	0.02	0.08	0.24	0.40	1.0	1.6	2.0	6.0	18.6
Fnf120*	0.01	0.04	0.12	0.20	0.50	0.8	2.0	6.0	12.0

Load rates (pN/s) = retraction speed multiplied by tip spring constant, k_s.

As previously mentioned, the rupture force data was collected as force curves. A prevailing feature of force curves is *the rate* at which the tip and substrate approach or retreat from each other in a cyclic manner. During the single load rate experiments (*Section 3.6*), both the approach and retraction portions of the cycle proceeded at an equal rate. However, when the load rate was varied (i.e. *Section 3.7*), the approach speed was held constant, while only the retraction speed was executed between (0.10 and 19.0 μm/s).

Because the goal of the experiments in this section was to measure the bond rupture force only for the influences of (A) α5β1 binding affinity and (B) varying load rate; the amount of tip – substrate contact time was made equal. The amount of tip – substrate contact time can affect rate dependent events such as bond formation, thus underscoring its importance. The constant approach speed eliminated bias regarding the amount of tip – substrate contact time because the contact time is equal regardless of how the retraction speed varies. In addition, a delay in the retraction cycle of 1.5 ms was implemented to allow longer tip – substrate contact time. Thus, only the characteristics of bond rupture at varying retraction speeds and under the influence of different cation treatments (i.e. different affinity states) were present in the collected data.

The rupture force data was collected for both (pFn) and the cell binding fragment (Fnf120). Note that (Fnf120) only contains the RGD and 'synergy' sequences needed for

adhesion to α5β1. These two ligand forms were used to eliminate possibility that fibronectin regions other than the 'RGD' and 'synergy' sequence were responsible for adhesion to α5β1. The data included at least (*n = 2*00) force curve measurements for each of the nine different tip - substrate separation speeds in *table 3.6* for the 120 kDa fragment; while only (*n = 100*) measurements were collected for each of the nine separation speeds for pFn.

The data for each speed was compiled into a histogram and fit with a Gaussian distribution. The central fit parameter of the histogram was used as the mean bond rupture force. Further, the mean bond rupture force (±S.E.M) was assigned as the representative magnitude in which the α5β1–fibronectin interface ruptures at the corresponding tip – substrate separation speed.

It is reemphasized for clarity that the load rate (pN/s) equals the tip – substrate separation speed (μm/s) multiplied by the tip's spring constant, k_s (pN/nm). Plotting the mean rupture force data versus ln(load rate) in a semi-log manner resulted in a linear region of the data. The plots show two distinct patterns depending on which cation treatments was used.

The first pattern is a single, linear region of the data, whose rupture force increases with increasing load rate. While the second pattern consists of two distinct linear regions of the data that also show increasing rupture force magnitude with increasing load rate (Figures 3.14 & 3.15). The plotted data is shown fit with a single linear regression line for Ca^{2+} or CaMg treatments (Panels A and B); or two linear regressions following treatments with CaMn, Mg^{2+} or Mn^{2+} (Panels C, D and E).

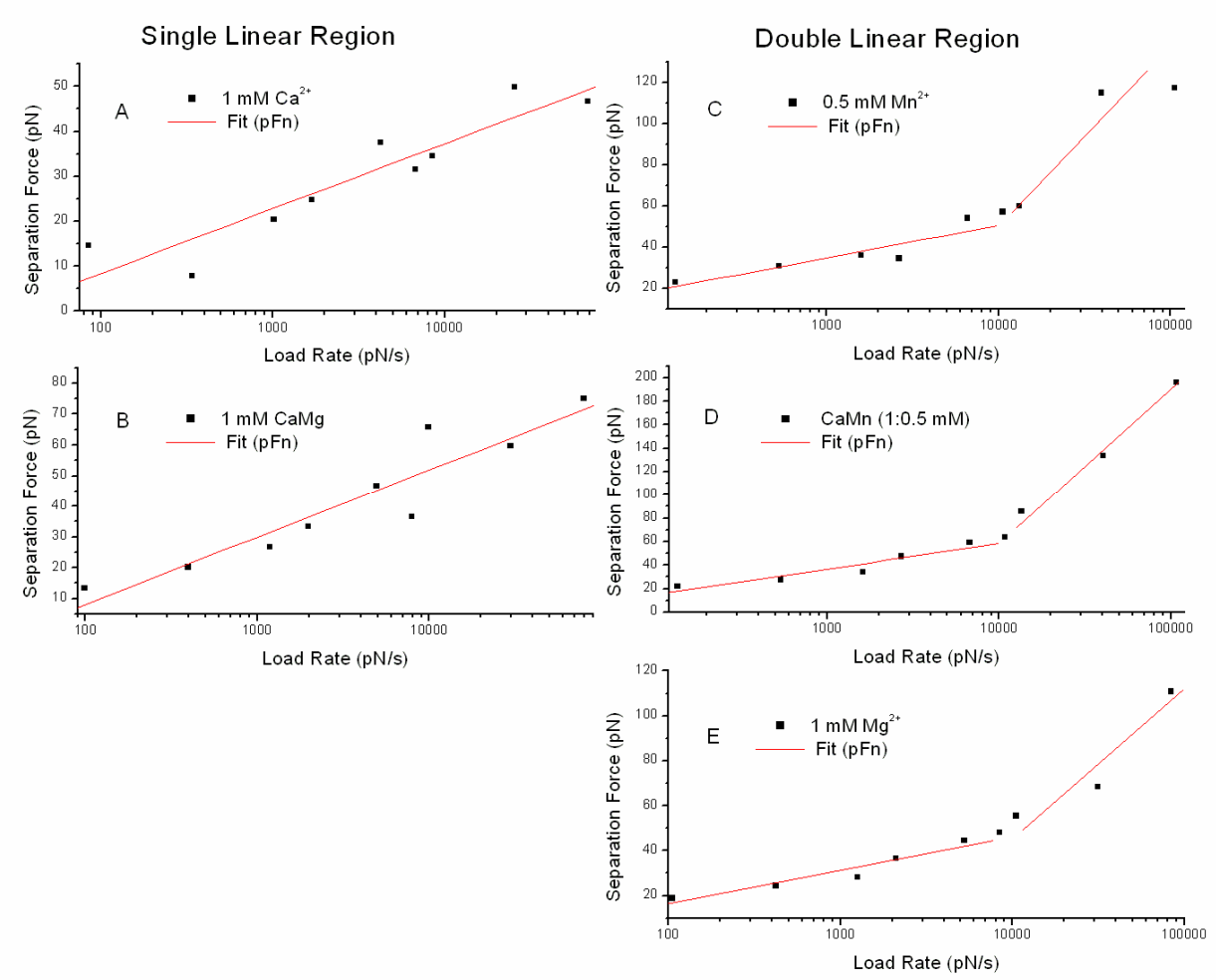

Figure 3.14 Effects of Divalent Cation on α5β1 - pFn Rupture Force at Multiple Load Rates. Mean bond rupture measurements for nine load rates after treatments with either Ca^{2+}, CaMg (Panels A & B respectively) or Mn^{2+}, CaMn, Mg^{2+} (Panels C, D & E respectively). A single α5β1 coated tip was used for each cation treatment. Each plot shows bond rupture force versus load rate and consists of nine data points. Each data point is the mode of distributed values after fitting the data with a Gaussian function. The distribution was generated from (n = 100) force curves per data point. Either a 'single' or 'double' linear regions resulted that depended on divalent cation treatment. Down regulation of α5β1 resulted in the single linear region pattern, while up regulation resulted in two linear regions.

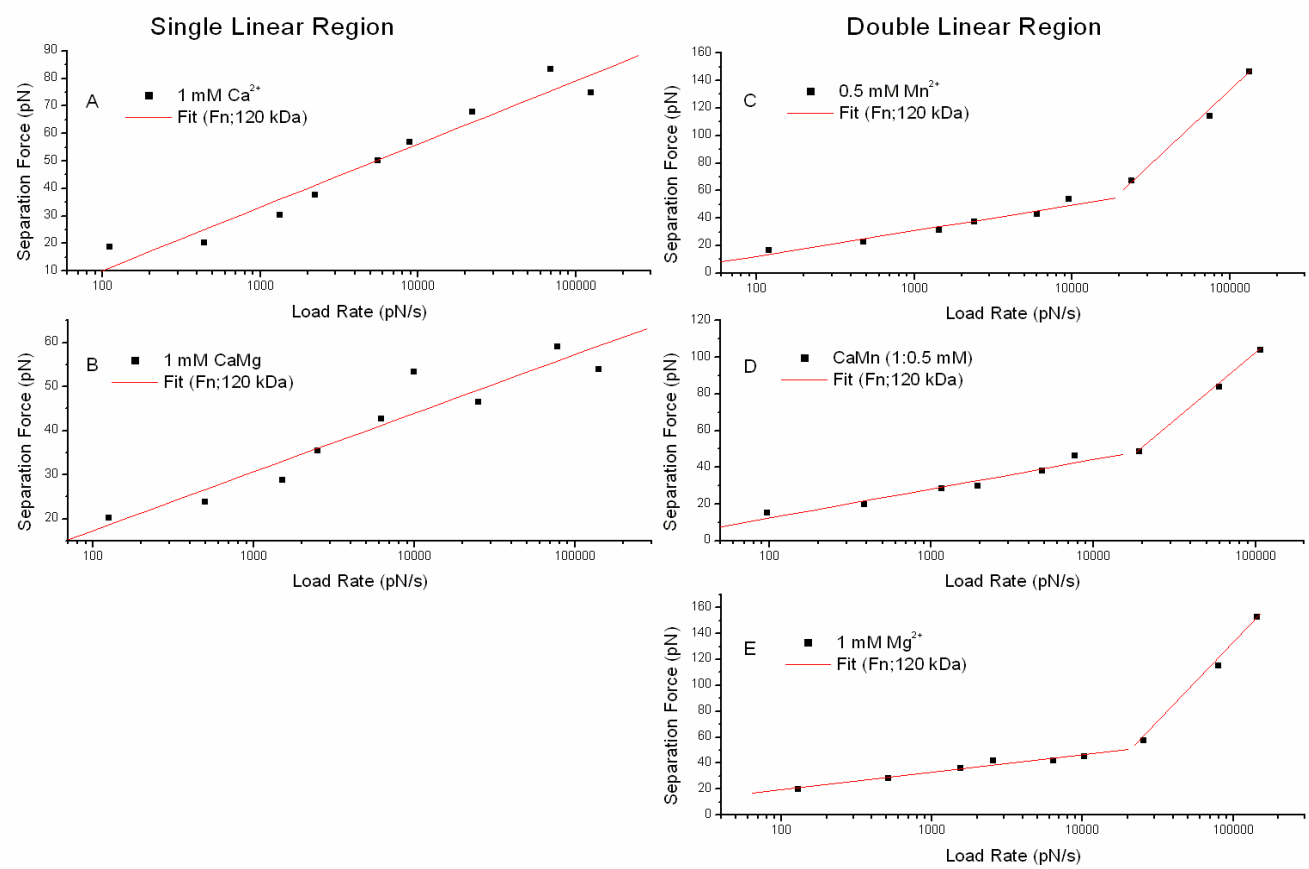

Figure 3.15 Effects of Divalent Cation on α5β1 - Fnf120 Rupture Force at Multiple Load Rates. Mean bond rupture measurements for nine load rates - using the fibronectin fragment (Fnf120) after treatments with either Ca^{2+}, CaMg (Panels A & B respectively) or Mn^{2+}, CaMn, Mg^{2+} (Panels C, D & E respectively). A single α5β1 coated tip was used for each cation treatment. Each plot shows bond rupture force versus load rate and consists of nine data points. Each data point is the mode of distributed values fit with a Gaussian function. The distribution was constructed from roughly (n = 200) force curves for each of nine data points. Either a 'single' or 'double' linear regions resulted that depended on divalent cation treatment. Down regulation of α5β1 resulted in the single linear region pattern, while up regulation resulted in two linear regions.

At this point, the appearance of either a single or double linear region pattern depended on which cation treatment was used. Further, the same two patterns were seen regardless of whether pFn or Fnf120 was used as the ligand. Thus it appears that the two forms of fibronectin ligand used in this study interacted with down regulated or up regulated α5β1 in a nearly identical manner as seen in figures 3.14 and 3.15.

The down regulation of α5β1 (resulting specifically from treatment with 1 mM Ca^{2+} alone or 1 mM CaMg) resulted in the single linear region pattern for the entire range of load rates. While treatment with either 1mM Mg^{2+}, 0.5 mM Mn^{2+}, or a (1: 0.5 mM) CaMn mix resulted in the up regulated form of α5β1. The up regulated binding affinity did not appear to show a difference in rupture force magnitude compared to down regulated binding affinity (i.e. Ca^{2+} or CaMg) for load rates up to 10,000 pN/s. However, the up regulated rupture force magnitude sharply increased for load rates greater than 10,000 pN/s. This sharp increase in rupture force resulted in the second linear region of the data that appears in the pattern showing two linear regions (Figures 3.14 & 3.15, Panels C, D and E).

Therefore, Ca^{2+} and CaMg result solely in the pattern showing a single linear region of the data. While cation treatments with CaMn, Mg^{2+} or Mn^{2+} result in the pattern showing two linear regions of the data. The fact that the sharp increase in rupture force did not appear until the load rate surpassed 10,000 pN/s further suggests that α5β1 binding affinity and the load rate both play a role in the increased rupture force seen in the double region pattern. Thus, the second linear region depends on both an up regulated form of α5β1 and a load rate greater than 10,000 pN/s.

Alternatively, the plots displaying the pattern of two linear regions of data (i.e. Figures 3.14 & 3.15, Panels C, D, and E) can be described according to the range of load rates either less than or greater than 10,000 pN/s. For instance, the linear region of data that corresponds to load rates less than or equal to 10,000 pN/s is also known as the low load region. While the linear region of data corresponding to load rates greater than 10,000 pN/s is known as the high load region. The low load region and the high load region are separated by a transition point located

roughly at 10,000 pN/s. The method of calculation for these transition points is reported in *Section 3.7.1*.

The high load region associated with Mg^{2+} up regulation of α5β1 vanished following the addition of 1 mM Ca^{2+} to the 1 mM Mg^{2+} buffer. Thus the pattern showing two linear regions of the data (Figures 3.14 & 3.15, Panel E) now showed a single linear region of the data for 1 mM CaMg buffer. The single linear region for CaMg was similar to the plots of Ca^{2+} treatment data (Figures 3.14 & 3.15, Panel A, B). The loss of high load region was associated with the down regulation of α5β1 by Ca^{2+}.

The reversion of the Mg^{2+} up regulated, bond rupture force pattern back to the single down regulated linear region pattern associated with Ca^{2+}, led to the question of whether or not Ca^{2+} was able to have the same effect in the presence of Mn^{2+}? The down regulating effects of 1 mM Ca^{2+} were further tested by its addition to Hepes buffer with 0.5 mM Mn^{2+}. This time, the plotted rupture force data showed that Ca^{2+} did not eliminate the high load region associated with up regulating behavior of Mn^{2+}. Both the low load and high load regions remained. Thus, 1 mM Ca^{2+} suppresses the high load region when added to 1 mM Mg^{2+} buffer, *but not* when added 0.5 mM Mn^{2+} buffer. A biochemical analysis of Ca^{2+}, Mg^{2+} and Mn^{2+} interaction with α5β1 is reported on in *section 3.8*.

In summary, the unbinding of α5β1-fibronectin under the five different cation conditions showed that cation regulated binding affinity of α5β1 does not affect rupture force magnitude for load rates less than 10,000 pN/s; however treatments of CaMn, Mg^{2+}, or Mn^{2+} cause a sharp increase in rupture force for load rates greater than 10,000 pN/s. Therefore the increased rupture force suggests that a combination of α5β1 up regulation and high load rates are conditions responsible for the sharp increase in bond rupture force. α5β1. The different divalent cations;

Ca^{2+}, Mg^{2+} or Mn^{2+} seemingly interact dissimilarly either with α5β1 or at the α5β1-fibronectin interface – especially at high load rates.

3.7.1 Determining Distinct Linear Regions for Force – Load Rate Data

The single or double region patterns described in *section 3.7* represent the bond rupture force (vs. load rate) while overcoming two distinct energy barriers. A higher energy barrier exists for load rates up to ~ 10,000 pN/s and for all five cation treatments. A lower energy barrier exists for load rates greater than 10,000 pN/s but only for CaMn, Mg^{2+} or Mn^{2+} treatments. As force increases, the higher energy barrier (systems free energy) is reduced, exposing the new impedance to rupture, the low energy barrier. Thus the high energy barrier is present for either down regulated or up regulated states of α5β1, while the low energy barrier only exists for up regulated α5β1.

Further, the single linear region pattern is associated solely with the high energy barrier; while the double region pattern is associated with both the high energy barrier (< 10,000 pN/s) and low energy barrier (> 10,000 pN/s). The transition between these two energy barrier states occurs at a transition point located where the two described linear regions of data intersect. However, one may question whether the double linear region pattern is statistically different from the single linear region pattern? Put another way, would a single linear regression fit of the two regions have less residual error than a fit of the same data using two separate regression lines? The question of whether or not the two region pattern of data is truly distinct from the single region pattern is answered in this section.

A visual inspection of data in Figures 3.14 and 3.15 indicates that two piecewise linear regions exist only for Mn^{2+}, CaMn, and Mg^{2+} (Panels C, D, and E). In order to examine this

issue quantitatively, we used the following iterative algorithm and associated statistical testing; this procedure was incorporated into a Matlab™ script (Appendix III).

The algorithm began by fitting a single linear line to the entire dataset (reduced model) and calculating the corresponding residual sum of squares (RSS_{total}). Next, the dataset was divided into two subsets: a low load rate region and a high load rate region. This was accomplished by choosing a cut-off value for the load rate. Linear regression analyses were performed for the two individual data subsets (full model). The residual sum of squares (RSS) for the full model was calculated as the sum ($RSS_1 + RSS_2$), where RSS_1 and RSS_2 were the residual sum of squares for the two individual fits. The cut-off value was repeatedly changed until a minimum of ($RSS_1 + RSS_2$) was obtained; this represented the transition from the low load rate region to the high load rate region. The point of intersection of the two linear regression lines corresponding to the minimum ($RSS_1 + RSS_2$) was taken as the optimal estimate of the transition point. These transition point values for the three conditions wherein two linear regions were visually observable are shown in Table 3.7.

Table 3.7 Estimated Transition Point Between Low and High Load Rate Regions

	CaMn	Mg^{2+}	Mn^{2+}
Fnf120	9.9	10.1	9.8
pFn	9.1	9.1	8.4

Values are the calculated transition points [in units of Ln (load rate)] at which the low load rate region becomes the high load region. Results are shown for two ligands (FNf120 and pFn) and for the three cation conditions wherein two linear regions were visually observable.

To determine whether or not the two linear regions were distinct, an F-ratio was calculated. as follows:

$$F = \frac{\dfrac{\left[RSS_{total} - \left(RSS_1 + RSS_2\right)\right]}{2}}{\dfrac{\left[RSS_1 + RSS_2\right]}{N_1 + N_2 - 4}}, \tag{3.2}$$

where, N_1 and N_2 correspond to the number of data points in the low load-rate and high load-rate regions, respectively. The numerator in Equation 3.2 represents the improvement in fit obtained by splitting data into two regions. F-ratio greater than the critical value (P=0.05; degrees of freedom: 2, N_1+N_2-4) would provide a statistical evidence that two distinct linear regions exist.

The values of the calculated F-ratio clearly show that the data plots for CaMn, Mg^{2+} and Mn^{2+} indeed have two distinct linear regions (Table 3.8) and therefore, splitting data into two distinct linear regions significantly improves the fit.

Table 3.8 Results of the Statistical Test for the Existence of Two Distinct Linear Regions

	CaMn	*Mg^{2+}*	*Mn^{2+}*
Fnf120	60.5	273.9	88.5
pFn	71.8	10.2	6.3

Values are the F-ratios calculated according to Equation 3.2. Results are shown for two ligands (FNf120 and pFn) and for the three cation conditions wherein two linear regions were visually observable. The critical F value for P = 0.05 and degrees of freedom = 2, 5 is 5.79.

3.7.2 Statistical Comparison of Low and High Load Regions Using ANCOVA

Previous studies have reported that up regulation of α5β1 resulted in increased rupture force magnitude between α5β1 and fibronectin when compared with down regulated α5β1 rupture force (Garcia, 1998; Li, 2003). The question of whether or not any differences in binding force with respect to effects from divalent cation treatment (i.e. influences on binding affinity) prompted a comparative investigation of rupture force data using statistical analysis. As

previously stated in *section 3.7*, the data showed that bond rupture force was dependent on the load rate and increased linearly as load rate increased. Further, the influence of divalent cation showed that down regulation of α5β1 resulted in a single linear region of the data, while up regulation resulted in two linear regions of data – a low load region (< 10,000 pN/s) and a high load region (> 10,000 pN/s).

While it is readily apparent by visual assessment that the high load rate region associated with CaMn, Mg^{2+} or Mn^{2+} treatments (i.e. up regulated α5β1) results in the data pattern displaying two linear regions of increasing rupture force, the differences in rupture force among the five different cation conditions, if any, is not apparent in the low load rate region. Thus, a formal statistical comparison of the data for all cation treatments was performed for the low load rate and high load rate regions. Specifically, we addressed two questions: (1) How does ligand type (Fnf120 *vs*. pFn) affect the load rate-rupture force relationship? (2) How does cation condition affect the load rate-rupture force relationship? Given that we are interested in examining the effects on a relationship, the Analysis of Covariance (ANCOVA) is the correct statistical method for data analysis. The ANCOVA method controls for the effects of the covariate, *load rate*, while assessing the effects of the variable of interest (ligand type or divalent cation).

The ANCOVA method of comparison of data sets was accomplished using SAS statistical analysis software (SAS Institute, Cary, NC). A Generalized Linear Model (GLM) containing and dependent variable, *force*, two independent variables: *load rate* and *ligand type* or *load rate* and *cation*.

The effects of ligand type were examined for each cation condition separately. In addition, analyses for low (<10,000 pN/s) and high (>10,000 pN/s) load rate regions were

performed separately. The results shown in Table 3.9 indicate that the ligand type (pFn *vs*. Fnf120) had no effect on load rate – force relationship under any of the cation conditions tested. This observation was true for both the low and high load rate regions.

Table 3.9 ANCOVA Analysis for Examining the Effects of Ligand Type (pFn *vs*. Fnf120) on Low Load Rate – Rupture Force Relationship

	Load Rate-Ligand Type Interaction Effect	*Ligand Type Effect*	*Load Rate Effect*
Low load rate			
Ca^{2+}	0.18	0.45	0.0002
CaMg	0.83	0.90	0.0001
Mg^{2+}	0.34	0.29	0.0001
Mn^{2+}	0.86	0.62	0.0001
CaMn	0.1	0.32	0.0001
High load rate			
Mg^{2+}	0.25	0.25	0.03
Mn^{2+}	0.37	0.38	0.04
CaMn	0.08	0.15	0.005

Data are the *P* values.

Given that the ligand type had no effect on the load rate – rupture force relationship, we pooled data from the two ligand groups to investigate the effects of divalent cations. Thus, the low load group was composed of 12 data points from each of the five cation treatments (NL = 60 data points); while the high load group was composed of 6 data points from each of the three cation treatment (NH = 18 data points). The results of the ANCOVA analysis for assessing the

effects of divalent cation are shown in Table 3.10. There *P* value for the interaction term was not significant for both the low and high load rate regions, indicating that the slopes of the load rate – rupture force relationships were not different among the various divalent cation conditions. Furthermore, the *P* values associated with the *cation type* effect were not significant, indicating that the cation type did not affect the load rate – rupture force relationship within each load rate region.

Table 3.10 ANCOVA Analysis for Examining the Effects of Divalent Cations on Low Load Rate – Rupture Force Relationship

	Load Rate-Cation Type Interaction Effect	*Cation Type Effect*	*Load Rate Effect*
Low load rate	0.62	0.69	0.0001
High load rate	0.17	0.33	0.0001

Data are the *P* values.

In summary, the ligand type (pFn *vs*. Fnf120) did not affect the load rate – rupture force relationship in either loading regions (low and high load rate). Furthermore, within each load rate region, cation condition did not affect the load rate – rupture force relationship. It should be noted, however, that the certain divalent cation conditions (Mg^{2+}, Mn^{2+}, CaMn) do up regulate α5β1-fibronectin interaction (i.e., the presence of the second linear region at load rates (> 10,000 pN/s). The Ca^{2+}-induced down regulation of this interaction (i.e., loss of the second linear region at high load rates) occurs only when Ca^{2+} is added to Mg^{2+}, and not when added to Mn^{2+}. Thus, divalent cations do play a role in modulating α5β1-fibronectin load rate – rupture force relationship (up *vs*. down regulation). In the following section, a biochemical assay of cation

binding to α5β1 will be performed to shed light on the cation-induced up or down regulation of α5β1-fibronectin.

3.7.3 Calculation of Bell Model Parameters

The measurement of Bell model parameters (k°, γ) gives information regarding the molecular kinetics of bond dissociation. The dissociation rate, k_r, of the molecular pair can be influenced by the application of a separation force to the bond interface as described by the Bell model (Bell, 1978). The natural dissociation rate constant, k°, is the dissociation rate in the absence of applied force and is increased exponentially by an applied force, *f*. The Bell Model is shown in (Equation 3.3).

$$k(f) = k^{\circ} \exp\left(\frac{f\gamma}{k_B T}\right) \tag{3.3}$$

The bond rupture length, γ, is a parameter describing bond extension from the bound to unbound state along the direction of the applied force.

A modified Bell model (Evans, 1997) describing bond rupture force versus $\ln[r_f]$, where r_f is the load rate, was applied to the bond rupture force data in the present study (See Equations 3.4 & 3.5); in which the energy landscape was sampled over a range of load rates spanning several orders of magnitude. These load rates encompassed reported ranges of cell motility speeds on fibronectin (Galbraith, 1999; De Bues, 1998) and load rates results reported for single molecule α5β1-fibronectin interaction studies (Li, 2003; Kokkoli, 2004).

$$f = \frac{kT}{\gamma}\ln\left(\frac{\gamma}{k^{\circ}k_B T}\right) + \frac{kT}{\gamma}\ln\left(r_f\right). \tag{3.4}$$

$$\text{Slope} = \frac{kT}{\gamma};\ \text{Intercept} = \frac{kT}{\gamma}\ln\left(\frac{\gamma}{k^{\circ}k_B T}\right). \tag{3.5}$$

A comparison of the linear regression fit parameters for the rupture force versus ln[r_f] and the slope and intercept terms (Equation 5) for the modified Bell model resulted in the estimated Bell model parameters. Again, the Bell model parameters include the natural dissociation rate parameter, k°, and the bond rupture length, γ. The bond dissociation rate values range from (1.3 to 3.0 s^{-1}) for pFn and (0.6 to 3.0 s^{-1}) for the 120 kDa fibronectin fragment. The bond rupture length parameters ranged from (4.0 to 7.0 Å; pFn) and (4.6 to 7.0 Å; Fnf120) for the low load region(Tables 3.11 and 3.12).

The bond rupture length parameters for the high load region only existed for cation treatments with CaMn, Mg^{2+} and Mn^{2+}. The high load region bond rupture lengths ranged from (0.8 to 1.5 Å; pFn) and (0.7 to 1.3 Å; Fnf120).The high load rupture lengths and dissociation rates indicate that bond rupture occurs after a much shorter extension of the α5β1–fibronectin interface and at much faster rate compared to the low load region.

Table 3.11 Calculated Bell Parameters for Plasma Fibronectin (pFn) Data

	1st Linear Region		2nd Linear Region	
Divalent Cation	k° (s^{-1})	γ (Å)	k° (s^{-1})	γ (Å)
Ca^{2+}	3.1	6.9	N/A	N/A
CaMg	2.4	6.0	N/A	N/A
Mg^{2+}	1.5	5.9	59.2	1.5
Mn^{2+}	1.3	5.2	42.5	1.4
CaMn	2.5	4.0	53.8	0.8

Table 3.12 Calculated Bell Parameters for 120 kDa Fibronectin Fragment (Fnf120) Data

	1st Linear Region		2nd Linear Region	
Divalent Cation	k° (s^{-1})	γ (Å)	k° (s^{-1})	γ (Å)
Ca^{2+}	3.1	4.6	N/A	N/A
CaMg	1.9	7.0	N/A	N/A
Mg^{2+}	0.6	6.9	168.0	0.7
Mn^{2+}	2.7	5.0	123.2	0.9
CaMn	2.4	5.9	133.2	1.3

Because statistical analysis of the individual rupture force data sets collected in this study for pFn and Fnf120 indicated no significant difference in a generalized linear model (see statistical analysis in next section) they were combined and the Bell model parameters (k°, γ) recalculated (Table 3.13).

Table 3.13 Combined Bell Parameters for pFn and Fibronectin Fragment (Fnf120) Data

	1st Linear Region		2nd Linear Region	
Divalent Cation	k° (s^{-1})	γ (Å)	k° (s^{-1})	γ (Å)
Ca^{2+}	3.6	5.2	N/A	N/A
CaMg	2.2	5.7	N/A	N/A
Mg^{2+}	1.0	6.3	102.2	1.1
Mn^{2+}	2.0	5.1	70.2	1.2
CaMn	2.8	4.6	64.2	1.1

The Bell parameters for the combined data showed much less variation for the dissociation rate and bond rupture parameters compared to individual data sets for pFn and Fnf120. The dissociation rate ranged from (1.0 to 3.6 s^{-1}) and the bond rupture length ranged from (4.6 to 6.3 Å) for the low load region. The high load bond rupture lengths ranged from (1.1 to 1.2 Å) while the dissociation rate ranged from (64 to 102 s^{-1}).

Overall, the natural bond dissociation time, $1/k^{\circ}$, showed that Ca^{2+} (a $\alpha5\beta1$ down regulator of binding affinity) had the fastest molecular dissociation times for the combined data (~280 ms) while Mg^{2+} and Mn^{2+} (up regulators of $\alpha5\beta1$ binding affinity) had slower bond release

times of ~ 1.0 s and ~ 500 ms respectively for load rates less than 10,000 pN/s. However, for load rates greater than 10,000 pN/s, the dissociation time for Mg^{2+} and Mn^{2+} decreased to ~10 ms and 14 ms respectively.

3.8 BIOCHEMICAL ANALYSIS OF CATION BINDING TO ALPHA 5 BETA 1 AND FIBRONECTIN

3.8.1 Analysis of Competitive Binding of Divalent Cation to α5β1

As previously described, the dynamic rupture force measurements for the α5β1 - fibronectin interface showed that for treatments with Mg^{2+}, Mn^{2+} or CaMn, two distinct linear regions existed for plots of bond rupture force versus $\ln[r_f]$; a low load region (< 10,000 pN/s) and a high load region (> 10,000 pN/s). Treatments with Ca^{2+} or CaMg resulted only in a single linear region of the data for all load rates. Thus it was established that only up regulation of α5β1 with CaMn, Mg^{2+} or Mn^{2+} resulted in the appearance of a low load and a high load region for plotted data. Further, it was established that the low and high load regions were statistically different by comparing the residual error for a single linear regression fit versus a double regression fit of the low and high regions using and F-distribution.

However, the addition of 1 mM Ca^{2+} to 1 mM Mg^{2+} resulted in the loss of the high load rate regime, resulting in a single linear region of the rupture force and load rate. The single linear region pattern mimicked the results of Ca^{2+} treatment alone which also resulted in a single linear region pattern for the plotted data. The ability of Ca^{2+} to eliminate the high load rate region when added to Mg^{2+} prompted an experiment in which 1 mM Ca^{2+} was added to 0.5 mM Mn^{2+}. The

results were surprising in that the high load region remained intact. Thus Ca^{2+} could eliminate the high load region in the presence of Mg^{2+} but not Mn^{2+}.

The above results signified that the interaction of Ca^{2+}, Mg^{2+} and Mn^{2+} with α5β1 – fibronectin interface somehow influenced the rupture force magnitude. Further, the effect was assumed to be due to competitive binding of cation sites in α5β1.

Thus a cation binding competition assay using radio-labeled calcium ($^{45}Ca^{2+}$, GE Healthcare) was performed to determine the circumstances under which $^{45}Ca^{2+}$ competitively occupied the integrin's cation binding sites. Hypothetically it was assumed that physiological levels of Ca^{2+} would bind α5β1 in the presence of physiological Mg^{2+} but not 0.5 Mn^{2+}. However, limitations of such a study are that physiological levels of $^{45}Ca^{2+}$ cannot be used for safety reasons.

Also, recent crystal structure models for integrin αVβ3 have shown that only a single cation occupied the β3 dimer at the ADMIDAS site of the unligated receptor (Xiong, 2001, 2002). Because the crystal structure for α5β1 is not yet solved, a structural model based on results obtained for αVβ3 is used (Coe, 2001; Mould, 2004). Thus no certainty about which cation binding site is occupied in the β1 dimer can be arrived at regarding the results of a cation binding assay.

The electrophoretic separation of the α5β1 dimers was done under non-denatured conditions (Figure 3.16). This was to ensure that the protein remained biologically active after transfer to polyvinylidene difluoride (PVDF) membrane (Gailit, 1988). Briefly, a 2 μg sample of

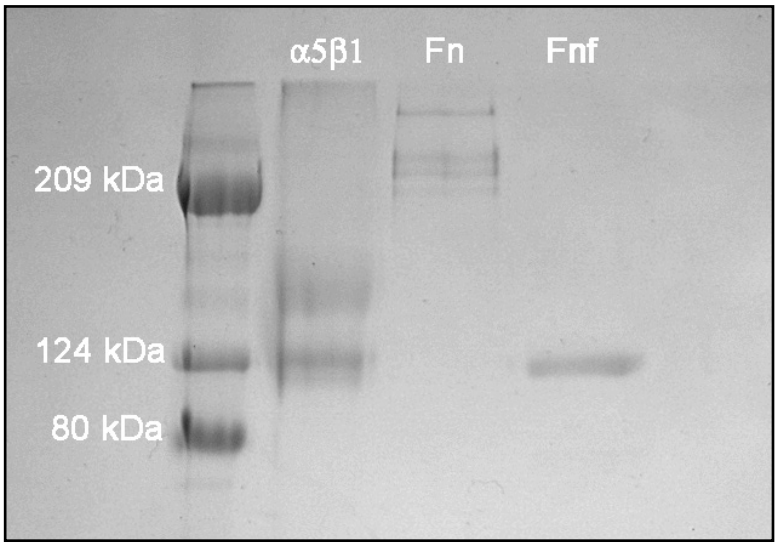

Figure 3.16 SDS-PAGE Gel of α5β1 and Fibronectin: Electrophoretic separation of all proteins used in force separation experiments in 7.5% gel under non-reduced conditions. The left most lane is a standard protein marker. The lane titled 'α5β1' shows non-reduced separation of the α5 dimer (top band, 145 kDa) and the β1 dimer (120 kDa). The third lane from left is human plasma fibronectin (~250 kDa).Note both dimers are visible and roughly the same molecular weight. The last lane is the 120 kDa, cell binding domain from human plasma fibronectin. The protein concentrations are 2μg for α5β1, and 0.8 μg for plasma fibronectin and the120 kDa cell binding fragment.

purified α5β1 (Chemicon; Temecula, CA) was separated using a 12% SDS PAGE gel. The α5β1 dimers were stained using coomassie blue and are compared to a standard molecular weight marker in the left most lane. The top band is the 145 kDa α5 dimer and the 120 kDa β1 dimer follows. The remaining lanes of the gel show full molecule pFn (Invitrogen) and the 120 kDa cell binding fragment from human plasma fibronectin (Chemicon; Temecula, CA).

Transfer of the proteins to the PVDF membrane was accomplished using the method of Towbin (1979). The $^{45}Ca^{2+}$ labeling of the integrin dimers was accomplished according to the method of Maruyama (1984). The PVDF membrane sections containing transferred protein were incubated in imidazole buffer container either 1 mM Mg^{2+} or 0.5 mM Mn^{2+}. Radio labeled calcium was added to the incubating membranes at an activity level of 1 μCi/ mL.

A control PVDF membrane containing no transferred protein was incubated in buffer containing 1 μCi/ mL of $^{45}Ca^{2+}$. The labeled membranes were exposed to x-ray film for 24 hours and the results showed that the small amount of labeled $^{45}Ca^{2+}$ preferentially bound both the α5 and β1 dimers when competing against 1 mM Mg^{2+}. Note that the positions of the dimers are denoted by the (Figure 3.17) arrows. The α5 dimer is more prominently marked due to the availability of four cation binding sites compared to one for the unligated β1 dimer. However, when the $^{45}Ca^{2+}$ competed against 0.5 mM Mn^{2+}, there was only a faint labeling of the α5 and β1 dimers. In addition, a select few molecular weight markers remained labeled after membrane washing to remove excess $^{45}Ca^{2+}$showing the specificity of true calcium binding proteins. The control membrane and the membrane incubated in $^{45}Ca^{2+}$ alone have more non-specific background labeling. Non specific labeling can be controlled somewhat by washing in buffer containing either Mg^{2+} or Mn^{2+}. These experimental results were repeated twice.

After the auto radiographs were complete, the membranes were stained with amido black to confirm the existence of the transferred protein. The stained membranes reveal both molecular weight marker to the far left as well as the α5 and β1 dimers (Figure 3.18).

Densitometry measurements between the auto radiographs and the amido stained PVDF membranes sections were conducted using a Kodak 2000r gel analysis station to remove bias regarding labeling intensity of $^{45}Ca^{2+}$.

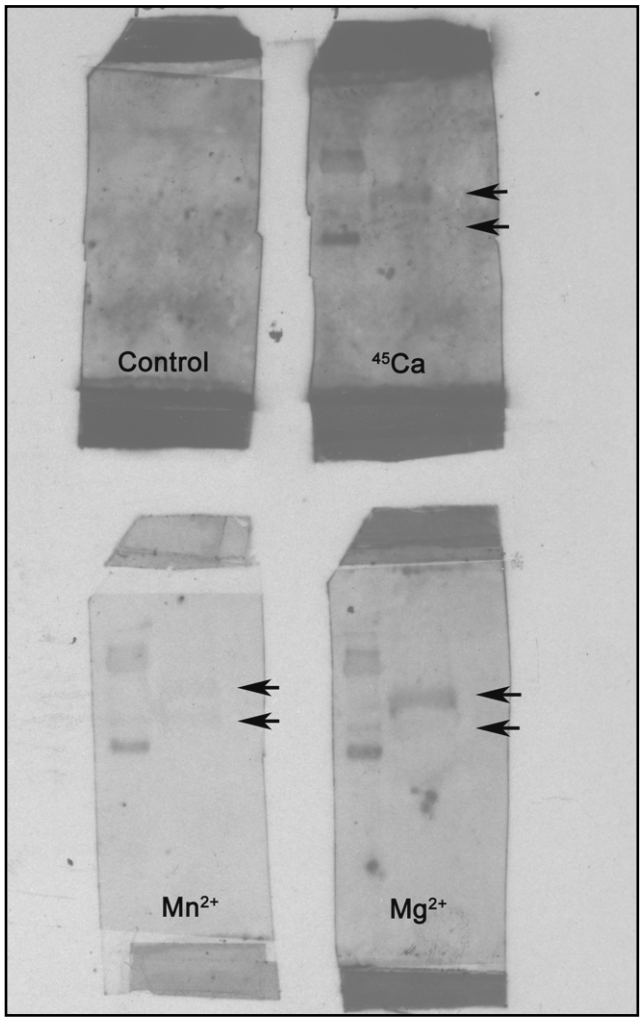

Figure 3.17 Competition Between Mg^{2+}, Mn^{2+} and $^{45}Ca^{2+}$ for Integrin Cation Binding Sites for Separated α5 and β1 Dimers. Exposed x-ray film shows images of PVDF membranes after radio-labeling with $^{45}Ca^{2+}$ (1μCi/mL activity in imidazole buffer, pH 6.8). The control membrane (no protein) was incubated solely in $^{45}Ca^{2+}$ as was the membrane labeled $^{45}Ca^{2+}$. The remaining membranes were first incubated in either 0.5 mM Mn^{2+} or 1 mM Mg^{2+} imidazole buffer before the addition of $^{45}Ca^{2+}$. The results show that $^{45}Ca^{2+}$ alone (or in the presence of Mg^{2+}) preferentially binds the α5 and β1 dimers. However, scarce $^{45}Ca^{2+}$ labeling is observed in the presence of Mn^{2+}. Mn^{2+} is a well known up-regulator of α5β1 binding activity whose role in cellular binding is a mystery (Mould, 1995). Arrows (top) mark the α5 dimer and the (bottom) β1 dimer. Note that the α5 dimer is more prominently labeled. This is attributed to a difference in the number of occupied cation binding sites for non-ligated integrin forms. Solved crystal structure models for the αV beta propeller region and the βA domain of β3 show that unligated aVβ3 has (5) occupied sites for the αV dimer while only the ADMIDAS site is occupied for the βA (Xiong, 2001, 2002). α5β1 has similar structural homology with αVβ3 and thus is regarded to bind cation similarly.

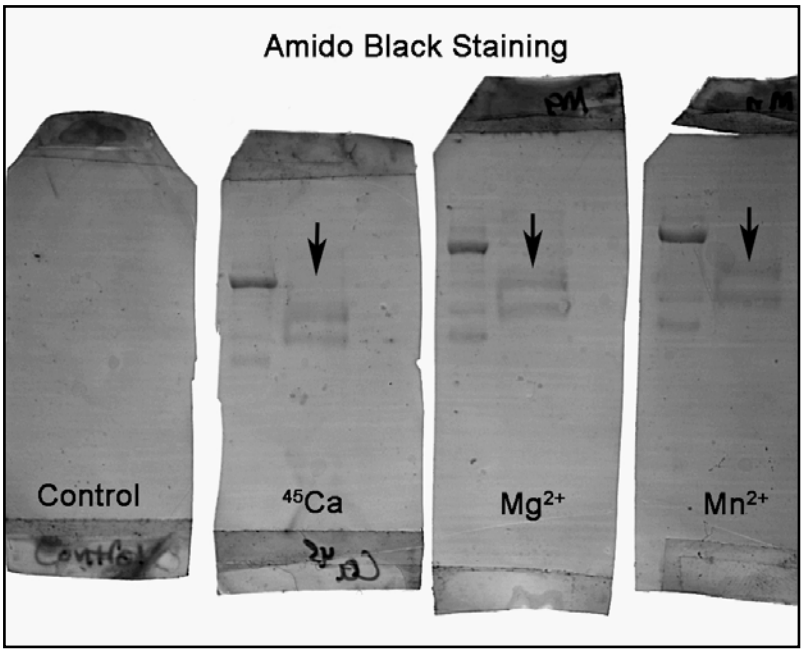

Figure 3.18 Amido Black Staining of α5 and β1 Dimers Transferred to PVDF. Amido black staining of PVDF membrane showing transferred integrin α5β1 used in $^{45}Ca^{2+}$ labeling experiments. Panel labeled control had no loaded protein while the remaining panels resulted from the non-reduced transfer of 2 µg of purified α5β1 loaded per lane in SDS-PAGE gel. Amido black staining was accomplished after radio-labeling was complete. The leftmost lane in panels 2, 3 and 4 is protein standard (209 kDa myosin top band) while the rightmost lanes (marked with arrows) show separated α5β1 where the top band represents the α5 dimer (145 kDa) and the bottom band the β1 dimer (120 kDa). During $^{45}Ca^{2+}$ labeling, panel 2 was incubated solely in while panels 3 and 4 were First incubated in $^{45}Ca^{2+}$ then 1 mM Mg^{2+} and 0.5 mM Mn^{2+} respectively. The $^{45}Ca^{2+}$ activity level in all Experiments was 1 µCi/mL.

Densitometry measurements from individually labeled bands for the $^{45}Ca^{2+}$ treatment alone or the Mg^{2+} + $^{45}Ca^{2+}$ resulted in an intensity ~2.5 times greater when compared to intensity measurements from corresponding amido stained PVDF membranes (Table 3.14). On the contrary, the band intensity measurements for the Mn^{2+} + $^{45}Ca^{2+}$ treatment showed an intensity ~ 0.5 that of the PVDF stained bands. These results give evidence to the observation that Mn^{2+} inhibits the $^{45}Ca^{2+}$ labeling of the α5 and β1 dimers.

Table 3.14 Ratio of Densitometry Measurements ($^{45}Ca^{2+}$/ PVDF) for α5β1

	$^{45}Ca^{2+}$	Mg^{2+}	Mn^{2+}
α5	2.6	3.8	0.4
β1	1.0	0.1	0.3

Table values reflect ratio of densitometry measurements from $^{45}Ca^{2+}$ labeling and Amido Black membrane staining. The $^{45}Ca^{2+}$ measurements were normalized by total protein amido black staining. Measurements were made using a Kodak Image station 2000R which scanned band area. Analysis was done with Kodak 1D software.

The competitive labeling of α5β1 with $^{45}Ca^{2+}$ showed that the α5 and β1 dimers preferentially bind small molar concentrations of Ca^{2+} when in the presence of 1mM Mg^{2+} but only faint traces bind in the presence of 0.5 mM Mn^{2+}. Thus, Ca^{2+} displaces Mg^{2+} from α5β1 but not Mn^{2+}. This result is consistent with the rupture force results of *section 3.7* in which Ca^{2+} added to Mg^{2+} resulted in the loss of the high load region. However, the high load region remained intact when Ca^{2+} was added to Mn^{2+}. Because of the competitive nature of cation binding, the labeling of both the receptor and ligand is investigated. In the following section, labeling of fibronectin with $^{45}Ca^{2+}$ is conducted in the presence of Mg^{2+} and Mn^{2+} to determine if cation binding to fibronectin is also competitive.

3.8.2 Analysis of Competitive Binding of Divalent Cation to Fibronectin

In the previous section, it was shown that radio – labeled Ca^{2+} displaced Mg^{2+} from α5β1 but not Mn^{2+}. This prompted the radio - labeling of fibronectin in this section to determine divalent cation binding properties (if any existed) of this ligand molecule - since little information is available on this topic. Ultimately, the question in which this labeling experiment seeks to

answer is whether or not fibronectin binding affinity is also regulated by the binding of divalent cation. The first step in this process was to determine if any divalent cation binds fibronectin.

The ligands used in this cation binding assay were commercially available (Chemicon, Temecula, CA) and the same protein transfer and labeling techniques used in the previous section was also used in this section. All ligands (other than pFn) were enzymatically digested fragments of human plasma fibronectin (pFn) and included the 30 kDa N-terminus, the 40 kDa gelatin binding domain and the 120 kDa cell binding fragment (Fnf120).

As with the α5β1 labeling experiments, the PVDF control membrane had no protein but was loaded with molecular weight marker (BioRad). The remaining membranes were loaded with 0.8 μg/mL samples for each of the following; (lane 2) pFn, (lane 3) Fnf120 and (lane 4) a mixture of the 30 and 40 kDa fragments. Additionally, each of the non-control membranes was loaded with molecular weight marker with colored reference bands (Invitrogen). The PVDF membranes were incubated in either buffer with no cation, 1 mM Mg^{2+} or 0.5 mM Mn^{2+}. The incubation buffer was loaded radio –labeled calcium with 1μCi/mL activity of $^{45}Ca^{2+}$ and the membranes were incubated further.

Exposed x-ray film showed that only pFn (lane 2) and the 120 kDa cell binding fragment (lane 3) bound $^{45}Ca^{2+}$. Although the exact location of bound cation is unknown, the cation binding sites were narrowed solely to the 120 kDa region of fibronectin because the 120 kDa fragment is digested from pFn. Both the 120 kDa fragment and pFn consist solely of type III structural repeats, which implies that one or more type III domains contains cation binding sites.

Further, $^{45}Ca^{2+}$ was able to bind fibronectin in the presence of either Mg^{2+} or Mn^{2+}. This result differs from the labeling of α5β1 in that $^{45}Ca^{2+}$ preferentially bound ligand samples in the presence of Mg^{2+} but not Mn^{2+} (See Figure 3.19 top panels). Also, it appears that divalent cation

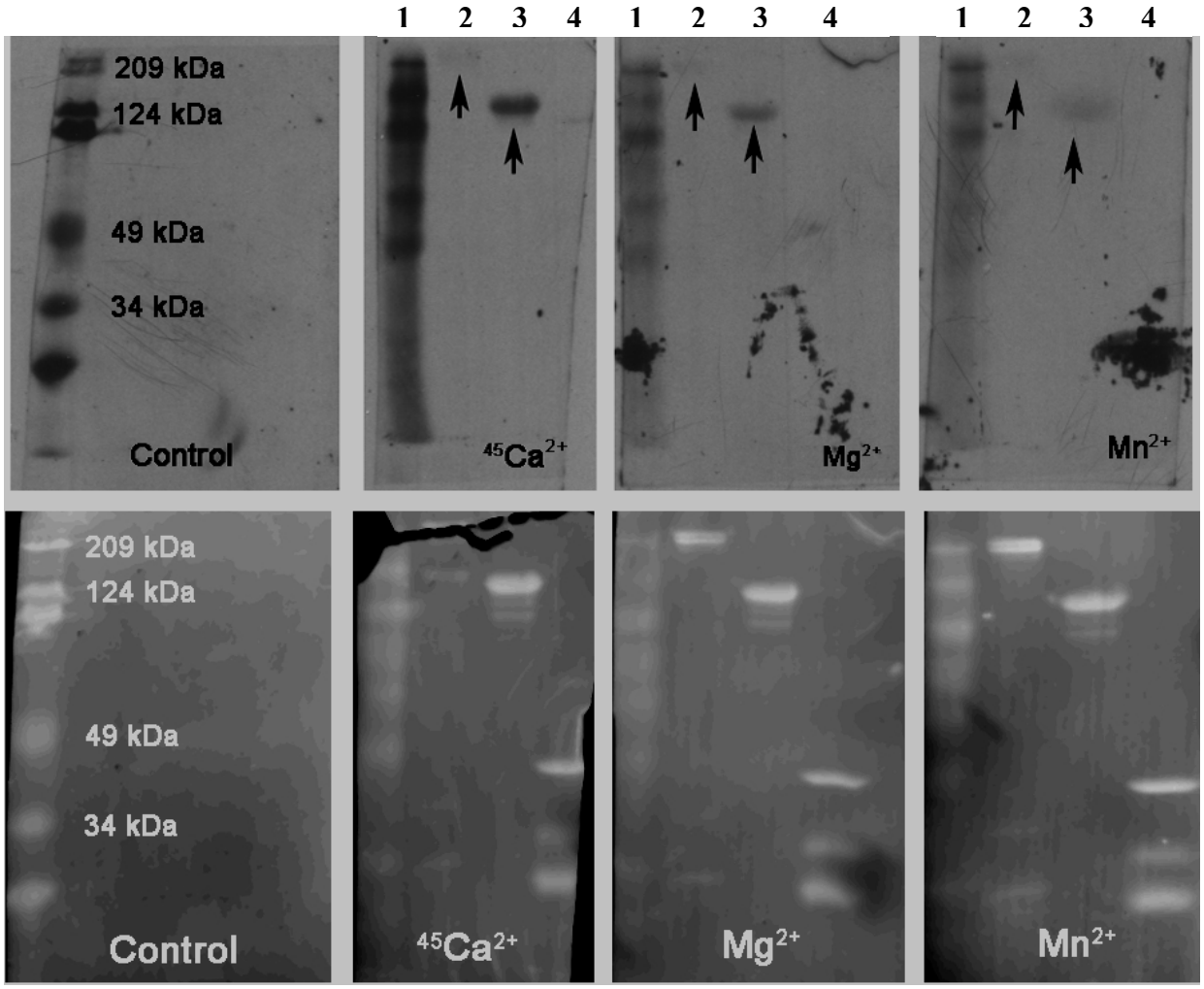

Figure 3.19 $^{45}Ca^{2+}$ Labeling of pFn, Fnf120 and N-Terminus Fragments. The fibronectin cation binding properties were investigated using competitive labeling with $^{45}Ca^{2+}$. An activity level of 1 uCi/mL of $^{45}Ca^{2+}$ was used to compete against 1 mM Mg^{2+} or 0.5 mM Mn^{2+}. The top panels are x-ray film after 24 hour exposure to PVDF membranes competitively labeled with $^{45}Ca^{2+}$. The bottom panels are the corresponding top panels after amido black staining. The control panels contain only protein marker but no fibronectin. The remaining panels were loaded with a color coded, protein marker (lane 1), pFn (lane 2), Fnf120 (lane 3) and 30 kDa and 40 kDa N-terminus fragments (lane 4). The amido black staining indicates presence of transferred protein in PVDF membrane and is thus available for $^{45}Ca^{2+}$ labeling. All loaded samples were at a concentration of 0.8 μg/mL. The $^{45}Ca^{2+}$ labeled top panels show that only pFn (lane 2) and Fnf120 (lane 3) were labeled, while the N-terminus fragments were not labeled at all. The difference in labeling intensity of pFn and Fnf120 is due to a difference in molecular molarity. This result supports a previous reports finding in which the N-terminus of fibronectin did not bind divalent cation (Amphlett, 1983). Cation binding activity is shown to be limited to the 120 kDa fragment which contains only Type III module structure.

only labels pFn (whole molecule) or 120 kDa pFn fragment (Figure 3.20) indicating that cation only binds fibronectin in locality of the molecule containing the 120 kDa cell binding region. The densitometry measurements for pFn and Fnf120 were obtained for the $^{45}Ca^{2+}$ labeling and amido black staining (Figure 3.19, bottom panels) using a Kodak 2000r station. The $^{45}Ca^{2+}$ intensity was normalized using the amido stain measurements and the ratio of intensities show that the $^{45}Ca^{2+}$ labeling was more prominent in the presence of either Mg^{2+} or Mn^{2+} (Table 3.15).

The dissimilarity in labeling intensity for pFn and the Fnf120 is due to the difference in molecular molarity as each was loaded as a 0.8 μg/mL sample. The molarity of pFn was 1.6 pM, while the molarity for the 120 kDa fragment was 6.7 pM. Thus, the number of 120 kDa fragments was four times the number of pFn molecules.

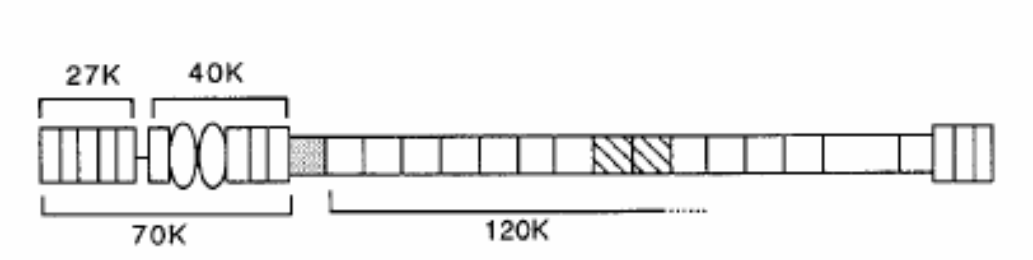

Figure 3.20 45Ca^{2+} Only Binds the 120 kDa Cell Attachment Fragment. The schematic illustrates a single fibronectin dimer divided at digestion sites. The 120 kDa fragment contains both the RGD and 'synergy' sequences, while the n – terminus contains the 30 kDa heparin binding fragment and the 40 kDa gelatin binding fragment. Radio labeling of pFn, and the digested fragments resulted in 45Ca2+ only binding either pFn or the 120 kDa fragment, thus suggesting that cation only binds fibronectin in this region. (Figure from Hocking, et al. 1994).

Table 3.15 Ratio of Densitometry Measurements for pFn & Fnf120 ($^{45}Ca^{2+}$/ Amido Stain)

	$^{45}Ca^{2+}$	Mg^{2+}	Mn^{2+}
pFn	1.1	1.4	0.9
Fnf120	3.8	2.8	2.9

Table values reflect ratio of densitometry measurements from $^{45}Ca^{2+}$ labeling and Amido Black membrane staining. The $^{45}Ca^{2+}$ measurements were normalized by total protein amido black staining. Measurements were made using a Kodak Image station 2000R which scanned band area. Analysis was done with Kodak 1D software.

In summary, the radio-labeling of fibronectin in competition with 1 mM Mg^{2+} or 0.5 mM Mn^{2+} resulted in the preferential binding of calcium. Additionally, $^{45}Ca^{2+}$ only bound to either the full molecule pFn or the 120 kDa cell binding fragment, but not the 30 kDa N-terminus or 40 kDa gelatin binding domain. However, it is not known if fibronectin binds any other cation besides calcium or where the location of cation binding in the 120 kDa region is located. The measurement of conformational change in either α5β1 or fibronectin upon binding divalent cation or during molecular association was investigated using circular dichroism spectroscopy in the following section. In α5β1, conformational change resulting from binding of divalent cation has been correlated with changes in binding affinity.

3.9 CD ANALYSIS OF MOLECULES IN THE PRESENCE OF DIVALENT CATION

3.9.1 CD Analysis of pFn in the Presence of Divalent Cation

The role of fibronectin in α5β1 binding is that of a passive ligand. Although cation binding to integrin and its relationship to binding affinity and bond rupture force has been the focus of this

study, the response of fibronectin to the binding of cation (e.g. change in conformation or binding affinity) is unknown and therefore examined this issue using circular dichroism spectroscopy (CD). Specifically, the conformation change in fibronectin structure upon binding cation was measured using (CD). The measurements were performed on human plasma fibronectin in hepes buffer at a pH of 6.8 and at room temperature.

Circular dichroism spectroscopy utilizes the UV range of wavelengths from the electromagnetic spectrum to measure content of secondary structure or changes in protein conformation. A general definition of CD is the difference in absorbance of left handed and right handed circularly polarized light (Equation 3.6). The measurements of CD are usually reported in units (deg*cm^2*dMol^{-1}), which is the simply the difference of the extinction coefficients.

$$\begin{aligned} &\Delta A = (\varepsilon L - \varepsilon R) C \ell \\ &\varepsilon = extinction\ coefficient. \\ &C = Molecular\ Concentration. \\ &\ell = Cuvical\ Path\ Length. \end{aligned} \tag{3.6}$$

Circular Dichroism spectroscopy can be used to measure structural content of a protein (i.e. helix or beta sheet content) using the far UV spectra (220 – 260 nm). The near UV (260 – 320 nm) can be used to measure changes in conformation of proteins by monitoring changes in absorbance in the aromatic amino acids (tyrosine, 280; phenylalanine 260 nm; and tryptophan, 290 nm).

The measurements of fibronectin were in the near UV spectra range using a concentration of 1.67 mg/mL and under the following conditions; plain buffer, buffer with either 1 mM Ca^{2+},

1mM Mg^{2+}, 1 mM Ca^{2+} + 1mM Mg^{2+}, 0.5 mM Mn^{2+}, or 1mM Ca^{2+} + 0.5mM Mn^{2+} (Figure 3.21).

The absorbance spectra for fibronectin in plain buffer (no cation) or buffer containing Ca^{2+}, Mn^{2+}, CaMg or CaMn were nearly identical showing strong recordings at 290 nm.

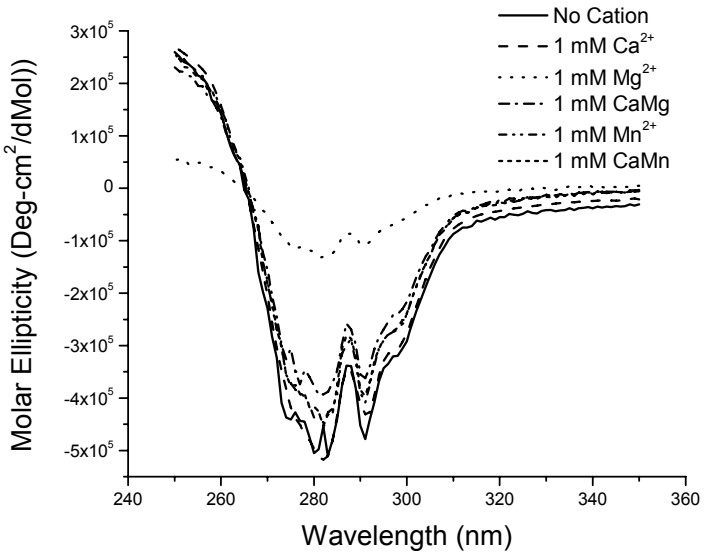

Figure 3.21 CD Spectrographs of pFn for Various Divalent Cation**.** pFn was diluted in hepes buffer (pH 6.8) at a concentration of 1.67 mg/mL. Various divalent cation was added to samples; 1 mM Ca^{2+}, 1 mM Mg^{2+}, 1mM CaMg, 0.5 mM Mn^{2+} or 1: 0.5 mM CaMn. The individual spectra for no cation or divalent cation show typical absorbance at 290 nm due to trytophan residues. The absorbance was lost when 1 mM Mg^{2+} was used. The absorbance was reestablished by the addition of 1 mM Ca^{2+} to the Mg^{2+} sample.

However, a loss in absorbance at 290 nm was observed only when Mg^{2+} buffer was used. The addition of 1 mM Ca^{2+} to the Mg^{2+} buffer sample resulted in the return of absorbance at 290 nm to levels consistent with samples containing plain buffer, Ca^{2+}, Mn^{2+} or CaMn. The return of absorbance demonstrated that the loss of signal was a result of the interaction of fibronectin with Mg^{2+} and not due to precipitation of protein out of solution. A previous study monitoring

conformational changes in pFn using CD have reported the loss of spectral absorption due to interaction heparin; however the addition of Ca^{2+} reversed the loss in absorption (Khan, 1988). Further, the loss of tryptophan activity (290 nm) was observed for CD measurements of plasma fibronectin in buffer containing GdmCl (Alexander, 1979). Overall, these results may indicate that Ca^{2+} (and possibly Mn^{2+}) stabilizes fibronectin against denaturing and preferentially binds to fibronectin's cation binding sites.

Previous studies have measured the conformational change in α5β1 structure using (CD) after treatment with divalent cation (Barneres et al, 1998, 2000). Banerese et al, used a recombinant α5β1 fragment containing the four EF-hand cation binding sites in the α5 (160-448) dimer and the entire βI domain of the β1 (121-329) dimer, which contains the MIDAS, ADMIDAS and LIMBS cation binding sites (Mould, 2004; Xiao, 2004). The CD measurement of α5β1 under different cation conditions was not performed in this study. This was because the fragmented form of α5β1 was not available during this study.

The fragmented form of α5β1 reportedly retained its ability to bind a fibronectin. A fibronectin fragment containing type III modules 3 – 7 was used and CD measurements were made of the bound complex that showed increased absorbance activity for phenylalanine (270 nm) and tryptophan (290 nm). It is further noted that CD measurements of a fragmented form of a protein containing the region of interest is more sensitive. Differences in structural conformation (i.e. shape change) are more apparent due to the lack of constraints of surrounding protein structure on the region of interest being measured.

3.9.2 CD of α5β1-Fibronectin Complexation in the Presence of Divalent Cation

In this study, attempts were made to measure changes in secondary structure for complexed full molecule α5β1 and plasma fibronectin. The absorbance spectra for individual α5β1 and fibronectin molecules were measured at the far UV (180 - 240 nm) in hepes buffer containing 0.5 mM Mn^{2+}, and then for a 1:1 mixture (Figure 3.22).

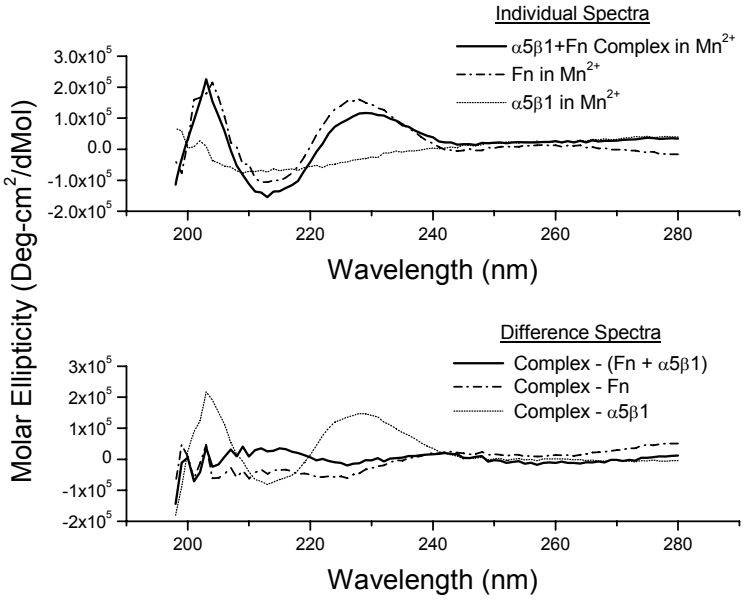

Figure 3.22 CD Spectra for Bound α5β1 and pFn**.** Individual CD spectra for α5β1, pFn and a 1:1 mixture of both molecules (Top). To investigate whether structural changes at the far UV occur (200 -240 nm) for bound α5β1-pFn, the difference spectra between the mixture for each of the two and their individual spectra were calculated. The difference of the complex and a pFn results in the α5β1 waveform and vice versa. The difference between the complex and the sum of the two individual waveforms results in a baseline waveform with zero absorbance. This result indicates that the far UV absorbance for structural conformation remains unchanged during binding. Measurement of absorbance at the near UV (220-300 nm) requires fragmented forms of the proteins to eliminate constraint of changes in conformation by protein structure surrounding the target structure.

The measurements sought to specifically identify changes in peptide bond orientation due to protein binding (i.e. complex formation). Changes in conformation at the near UV for non-fragmented molecules are highly unlikely to be observed due to constraints of using the entire protein structure to measure very subtle changes (sensitivity inherent to CD technique) in structure due to cation or ligand binding.

The difference between the full molecule complex formation spectra (α5β1 + plasma fibronectin) and the individual α5β1 and pFn spectra resulted in a baseline signal with zero absorbance; demonstrating that the spectrograph representing the complex formation was solely the superposition of the individual α5β1 and fibronectin spectra. Thus no measurable changes in absorbance were noted for non-fragmented protein forms.

Previous measurements by Banerese et al. with the fragmented molecules resulted in measurable changes in absorbance for the aromatic amino acids in the near UV spectra for complexed α5β1 and fibronectin fragment. Conformational changes in structure can result in the exposure (or packing) of aromatic acids. Again, a lack of sensitivity to changes in conformation in our data was attributed to a masking effect by molecular protein structure adjacent to the integrin cation binding regions.

CD measurements of proteins can uncover changes in conformation; however these changes can be masked by non – changing regions of the target protein. This was most likely the case for our data as the full molecule form of α5β1 was used and not a fragmented form as in the study by Baneres. Although attempts were made to uncover changes in protein shape for the complex, the results show that our attempts were thwarted due to the full molecule α5β1 used. On the other hand, full molecule pFn showed large changes in conformation for individual samples tested but the region of change in the protein are unknown. This is an additional reason

to consider fragmented forms of proteins that include only the regions known to be active for performed experimental functions.

4.0 DISCUSSION

In the present study, the dynamic loading properties of the α5β1-fibronectin interface were evaluated under conditions where the integrin binding affinity was regulated by divalent cation. The specific cation effect of down regulation or up regulation of α5β1 was examined for the forced separation of bound molecular α5β1 and fibronectin using AFM.

This discussion first examines the protein modified AFM tips used in this study and the initial measurements using these test tips in *Section 4.1*. The effects of integrin binding affinity on (A) *binding frequency* and (B) *rupture force magnitude,* at a single tip – substrate separation speed are discussed in *Section 4.2*. The effect of divalent cation regulation and varying tip – substrate separation speeds on rupture force magnitude is discussed in *Section 4.3*. The possible mechanisms responsible for the data patterns of rupture force versus ln(load rate) resulting from cation regulation of α5β1 are described following *Section 4.3*. Further, the possible mechanisms for increased rupture force when load rate is increased is described in terms of bond separation energy and probability of bond failure with time. A crystal structure model of αVβ3 with bound Mn^{2+} and cyclic RGD peptide is discussed and related to the results of the present study. A mathematical model describing the transition point or the transition from the low load to the high load region (as described in the results section) and its association with increased rupture force is explained as it pertains to divalent cation regulation of α5β1 and the resulting patterns of rupture

force versus load rate. Finally, a diagrammed model of cation binding pathways, which lead to down or up regulation of α5β1 and the associated linear patterns of rupture force versus ln(load rate) is also proposed.

4.1 BINDING ASSAY TO MEASURE ALPHA 5 BETA 1-FIBRONECTIN RUPTURE FORCE

4.1.1 Tip Modification

The modification of the AFM tip using an attached silica microsphere was performed to exploit the more abundant SiO_x groups for chemical modification with silane. The standard silicon nitride material used to fabricate AFM tips has less available SiO_x groups for the attachment of silane molecules and thus less attachment of α5β1 was achieved as shown through fluorescents labeling (Figure 3.5). The labeling showed that the microsphere area was completely covered with α5β1 and emitted a bright red hue typical of excited Cy3 labeling; while adjacent silicon nitride showed erratic attachment of α5β1 and no uniform color signal typical of a uniform layer.

Further, control experiments showed no fluorescence signal for α5β1 modified tips that were not first incubated in anti – α5β1 primary antibody but then incubated in secondary fluorescing antibody. Two different primary antibodies were used; a monoclonal (JBS5) that attaches to the fibronectin binding site or a polyclonal (H – 104) that attaches to the c – terminus of the α5 dimer.

Overall, the fluorescence signal shows that the covalent attachment of α5β1 to the tip was successful and that the fibronectin binding site of α5β1 is accessible for binding and not impeded by protein cross linking. However the extent of the crosslinking of the integrin is unknown.

4.1.2 Initial Measurements of the α5β1–Fibronectin Interaction

The initial measurements of the α5β1–fibronectin interaction were made to test the functional integrity of the modified tips. The interaction between α5β1 modified tips and whole molecule plasma fibronectin was tested using AFM. The background adhesion between tips at various stages of construction and the substrate was first tested (Figure 3.4). No background adhesion between the bare or fibronectin coated substrates and silane coated tips or with the subsequent addition of cross - linker was observed. However, multiple peaks were observed between fibronectin coated substrates and tips with attached α5β1. Further the interaction could be disrupted using anti - α5β1, function blocking monoclonal antibody that attaches to the fibronectin binding site, showing the specificity of the interaction (Figure 3.9).

The modified tips in this study gave results that are comparable to other AFM experiments in which the tip and substrate were modified with pairs of binding molecules in which distinctive bond rupture peaks appeared upon molecular separation (Florin, 1994; Hinterdorfer, 1996). Florin *et al.,* showed that avidin - coated AFM tips and biotin - coated beads produce bond rupture force peaks where the interaction could be disrupted using an excess of free avidin. While Hinterdorfer *et al.,* showed that interactions between AFM tips modified with anti – serum albumin antibody and substrates coated with serum albumin could be blocked with excess serum albumin in solution, showing the function and specificity of the experiments.

Interactions involving α5β1 and fibronectin, and subsequent disruption of the interactions with function blocking antibody establishes the specificity of the tip modification process and confirms that the tips were functioning as intended. The lack of background adhesion ensures that the majority of the interactions involve only the α5β1–fibronectin interaction.

4.2 EFFECTS OF DIVALENT CATIONS ON ALPHA 5 BETA 1-FIBRONECTIN INTERACTION: SINGLE LOAD RATE

Initially, the binding force measurements for this study were limited to a single tip – substrate separation load rate of 4800 pN/s and divalent cation treatment with either 1 mM CaMg or 0.5 mM Mn^{2+}. The goal was to determine whether increased α5β1 binding affinity in the presence of Mn^{2+} resulted in a higher frequency of interaction with fibronectin as reported in cell binding or solid phase binding assays (Gailit, 1988; Mould, 1995).

A mixture of physiological levels of Ca^{2+} and Mg^{2+} (1 mM each) was chosen as the basal activation state (down regulated) of the integrin. Results for the basal state were compared with those from the up regulated integrin state (i.e. the activation state of α5β1 following treatment with 0.5 mM Mn^{2+}). The rational for choosing these concentrations of Ca^{2+} and Mg^{2+} was based on levels reported for wound fluid analysis. During wound healing, more fibronectin is expressed and α5β1 binding is therefore increased accordingly (Grzesiak, 1995). The concentration of Mn^{2+} chosen for this study (0.5 mM) was comparable with the concentration used by (Mould, *et al.,* 1995), which resulted in maximal binding between purified α5β1 and fibronectin in a solid phase binding assay.

The rupture force data collected at 4800 pN/s yielded distributions for each cation treatment. Each distribution contained 100 single peak, rupture force magnitudes, determined from 100 individual force curves measurements. The distributions were fit with a Gaussian function, where the mode rupture force value (most frequent force value) represented the overall rupture force magnitude at 4800 pN/s as described by (Evans, 1997). Although the effects of divalent cation on binding frequency were not surprising, the apparent lack of effect on rupture force magnitude was surprising given that previous studies reported an increase in rupture force due to up regulation of α5β1 as compared to the basal state or down regulated state (Xiao, 1996; Garcia, 1998; Li, 2003).

The discussion now focuses specifically on two adhesion properties resulting from cation regulated binding affinity observed at 4800 pN/s; (A) the influence of divalent cation regulated binding affinity on rupture force magnitude in *section 4.2.1* and (B) the influence of cation regulated binding affinity on the frequency of occurrence of the α5β1–fibronectin interaction in *section 4.2.2*.

4.2.1 Effects of Divalent Cations on Rupture Force Magnitude

Previous studies have reported that α5β1–fibronectin rupture force increased for up regulated α5β1 binding affinity (Garcia, 1998; Li, 2003). Li, *et al.,* showed that a range of load rates from (50 – 10,000 pN/s) resulted in higher rupture forces for activated (i.e. up regulated) α5β1 when compared to inactivated (i.e. down regulated) α5β1. For this study however, despite Mn^{2+} up regulation of α5β1 binding affinity, the increased receptor affinity did not affect rupture force magnitude at 4800 pN/s. This conclusion was reached following a comparison of the mode

rupture force values from multiple experiments at 4800 pN/s for CaMg and Mn^{2+}. The mode rupture force values from CaMg (n = 5) and Mn^{2+} (n = 5) distributions were grouped according to cation treatment and compared using a students t - test. The results showed no statistical difference between the mean rupture force values for the CaMg and Mn^{2+} groups ($P = 0.38$).

The first point that will be made regarding the lack of difference in rupture force is that measurements at a single load rate (i.e. 4800 pN/s) only represent a single point in a broad continuum of rupture force magnitudes that are dependent on load rate. That is, rupture force for weak, non – covalent bonds is not a constant value but increases with increasing load rate (Evans, 1997). The second point is that when weak, non – covalent bonds rupture, they reflect the relationship between force, bond lifetime and bond chemistry at the molecular level and the dynamic force spectroscopy method of measurement (e.g. AFM) is most revealing when bonds are ruptured over a wide range of load rates (Evans, 2001). Thus a broader, dynamic sampling of the α5β1–fibronectin rupture force is needed to properly assess the contribution that divalent cations make on rupture force magnitude. The analysis of the influence of divalent cation on rupture force for an increasing span of load rates is presented in *section 4.3*.

Although a more in depth analysis regarding the lack of difference in rupture force magnitude at 4800 pN/s is not offered at this point, it is apparent that the non covalent bonds associated with the bond interface (i.e. α5β1, cation and fibronectin) require the same amount of force (~ 50 pN) to dissociate regardless of which cation is used at this single load rate.

Further, the loading of the α5β1-fibronectin interface at 4800 pN/s corresponds to cellular motility speeds between 0.08 and 0.5 μm/s using appropriate spring constant values from this study. These speeds are within known physiological motility rates (Burton, 1999; Galbraith, 1999; De Beus, 1998) and thus the results from this study indicate that CaMg or Mn^{2+} most

likely do not affect rupture force magnitude between the α5β1 receptor and fibronectin for motile cells.

As an aside, the two main receptors implicated in cellular motility on fibronectin substrates are α5β1 (a.k.a. fibronectin receptor) and the vitronectin receptor, αVβ3 (Hynes, 1992; Zamir, 2001). However, it is unknown whether or not the αVβ3 receptor also exhibits a similar lack of difference in rupture force at 4800 pN/s for CaMg or Mn^{2+} treatments.

In summary, the surprising lack of statistical difference in bond rupture force between the up regulated and the basal state of α5β1, at a single load rate of 4800 pN/s, prompted new experiments measuring bond rupture force over a range of separation speeds. The new experiments were performed to better elucidate whether any differences in rupture force really exist and are reported on in *section 4.3*. However, at this point, no difference in rupture force can be determined to exist between CaMg or Mn^{2+} treated α5β1 at 4800 pN/s. Although it is unknown whether or not, Mn^{2+} plays a physiological role similar to Ca^{2+} or Mg^{2+} in cell binding, these results indicate that cellular retraction forces at 4800 pN/s would not differ if the α5β1 – fibronectin interface contained either Mn^{2+} or Ca^{2+} ions.

4.2.2 Effects of Divalent Cations on Interaction Frequency

As stated in the results section, a single bond rupture *interaction* between α5β1 and fibronetin was determined by the existence of a single cantilever deflection peak per force curve measurement. However, not all force measurements will result in a molecular interaction (no peak), thus the binding frequency is the number of curves resulting in an *interaction*, N_{peak}, divided by the total number of measurements collected, N_{Total} (Equation 4.1).

$$Binding\ Frequency = \frac{N_{peak}}{N_{Total}} \tag{4.1}$$

The average *binding frequency* for Mn^{2+} (30%) was higher when compared to the average *binding frequency* of CaMg (17%) for the same number of collected force curve measurements (See Table 3.3). The incidence of increased binding frequency for Mn^{2+} (compared to CaMg) was observed for repeated experiments (n = 5) and is consistent with previously reported results (Gailit, 1988; Mould, 1995). The binding frequency was reduced following treatments with JBS5 antibody (to ~ 3% binding), RGD peptide (~ 5% binding) or 5 mM EDTA (~ 3 % binding) (See Figure 3.13). The treatments show the specificity of the α5β1 - fibronectin interaction for RGD located in fibronectin and the necessity for divalent cation in bond formation. Excess concentrations of either RGD peptide or JBS5 block access of fibronectin to α5β1, leaving few receptors available for binding, thus very few interaction peaks are observed and subsequent reduction of binding frequency results.

Solid phase assays between α5β1 and fibronectin (or cellular assays using K562 cells producing only α5β1 and fibronectin) display increased levels of binding in the presence of Mn^{2+}, which was 2 - 3 times higher than Ca^{2+} or Mg^{2+} alone; when all treatments were at a cation concentration of 1mM (Gailit, 1988, Mould 1995). The trace element Mn^{2+} is essential for metabolic health (Hussain, 1998; Gong, 1999; Gulberti, 2003) and is also a well known stimulator of increased integrin binding. As a caveat, however it is unknown whether or not Mn^{2+} actually plays a physiological role similar to Ca^{2+} or Mg^{2+} in cellular binding.

The exact reasons for increased binding frequency due to Mn^{2+} up regulation of α5β1 are largely unknown. However, it has been reported in the literature that conformational changes in

integrin shape are responsible for increased binding frequency due to exposure of hidden ligand binding sites (Mould, 1998; Mould, 2000; Takagi, 2001). For instance, in one study by Mould *et al.,* it was shown that α5β1 binding affinity for various stimulatory (i.e. up regulating) or inhibitory (i.e. function blocking) antibodies could be regulated using Ca^{2+}, Mg^{2+} and Mn^{2+}. The antibodies all bound to epitopes on either the α5 or β1 dimers, which form the fibronectin binding site. The binding affinity of the individual integrin dimers was increased or decreased, depending on which divalent cation was used. The differences in α5β1 affinity for individual antibody, following treatment with different cation, suggested that conformational change lead to masking or unmasking of partially exposed epitopes. Further, the changes in integrin conformation are thought to allow for a better mating with fibronectin surfaces (type III_9 and type III_{10}) modules at the molecular interface. Crystal structure analysis of fibronectin has shown that the RGD loop of type III_{10} and the 'synergy' sequence of type III_9 modules are aligned in the same plane in 3D space (Leahy, 1996). Thus conformational change in the α5 and β1 dimers, due to cation uptake, is thought to result in a more (or less) complete mating with the planar orientation of the fibronectin modules depending on which individual cation is used (Leahy, 1996; Redick, 2000).

It has also been reported that the synergy sequence of fibronectin increases cellular binding frequency via α5β1. Together with the RGD sequence, the synergy sequence increases binding to α5β1. Mutant fibronectin fragments lacking the synergy sequence reduce cellular binding forty - fold (Redick, 2000; Krammer, 2001).

The atomic properties of the divalent cations used in this study are tabulated below (Table 4.1). The cations are in order from highest to lowest electro - negativity: $Mn^{2+} > Mg^{2+} > Ca^{2+}$. However, Ca^{2+} has the largest atomic radius while Mn^{2+} has the smallest. Perhaps the

higher electro – negativity, and thus higher reactivity of Mn^{2+}, causes higher binding frequency. Additionally, the small atomic radius of Mn^{2+} (with respect to Ca^{2+} or Mg^{2+}) has led to the presence of space filling, H_20 molecules in αVβ3 (Xiong, 2002). The addition of a polar molecule such as H_20 may also affect binding frequency by coordinating (along with adjacent amino acids) with ligands through electrostatic interactions. More on the possible relationship between atomic properties and conformational change in α5β1 is discussed in the following sections.

Table 4.1 Atomic Properties of Divalent Cation Used in Study

	*Electronegativity**	*Atomic Radius (pm)*
Ca^{2+}	1.00	180
Mg^{2+}	1.31	150
Mn^{2+}	1.55	140

Based on Pauling scale: (0 – 4), where 4 is the most electronegative.

For future reference and comparison, the duration of the tip – substrate contact time for measurements at 4800 pN/s was estimated. The contact time between the tip and substrate was observed to be less than 250 ms for all rupture force measurements at 4800 pN/s. For illustration purposes, an example of contact between a bare tip and mica substrate measured in air for both the 'approach' and 'retraction' at 0.5 Hz is displayed below (Figure 4.1).

For data collected at 4800 pN/s, the approach and retraction speeds between the tip and substrate were equal for all measurements. The tip – substrate contact force was limited to no more than (20 – 150 pN) – thus limiting the cantilever deflection and ultimately, the contact

time. However, the tip – substrate contact time alone cannot explain the frequency of binding; and because force plays a catalytic role in governing kinetic rate constants, another method of analysis was needed to investigate the influence of time on binding affinity.

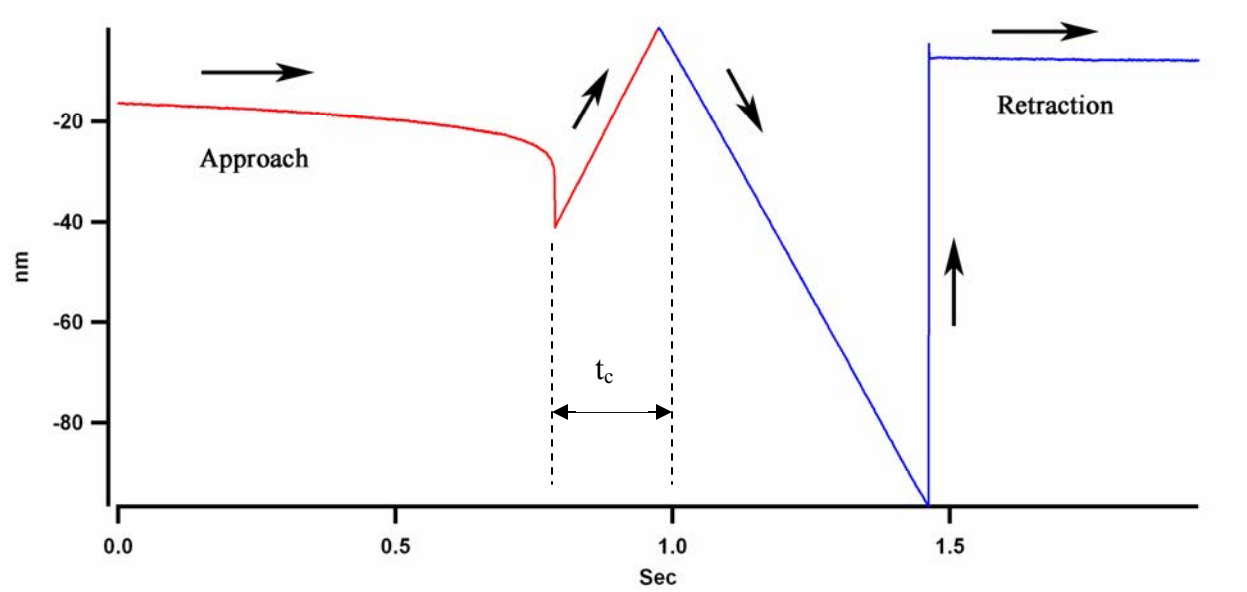

Figure 4.1 Cantilever Deflection Versus Time for Bare AFM Tip on Mica at 0.5 Hz. The approach (red) and retraction (blue) cycle for a bare tip on mica substrate in air. The linear slope during the approach (red) is due to tip contact with the substrate. The contact time, t_c, lasts about 250 ms before the retraction cycle begins..

The probability, $P(t, f)$, of a single bond rupture during a time interval, $(t, t + \Delta t)$, was calculated according to reliability theory (Tees, 2001), where the probability function is a function of force and time. The probability function used for these calculations produced values greater than the random probability ($P > 1$), (Equation 4.2).

$$P(t,f)=[k^{\circ}e^{\left(\frac{\gamma r_f \Delta t}{k_B T}\right)}][e^{\left\{\left(\frac{k^{\circ}k_B T}{r_f \gamma}\right)[1-e^{\left(\frac{\gamma r_f \Delta t}{k_B T}\right)}]\right\}}] \qquad (4.2)$$

The Bell model parameters for CaMg and Mn^{2+} treatments were previously calculated for multiple load rates (Table 3.8 & 3.9) and were used as factors in the probability calculation; where, k^0, is the dissociation rate in the absence of forced bond rupture and γ is the distance from the bound state to the energy transition state. The load rate, r_f = 4800 pN/s, is a constant parameter multiplied by a time increment, Δt = 0.00001 seconds, over a time interval from (0 – 15 ms).

The most probable time interval for single bond rupture at 4800 pN/s (for CaMg treatment) corresponded to the time interval between (8.05 – 8.06 ms). While the probability for single bond rupture for Mn^{2+} treatment at 4800 pN/s corresponded to a time interval between (9.89 – 9.90 ms), (Figure 4.2).

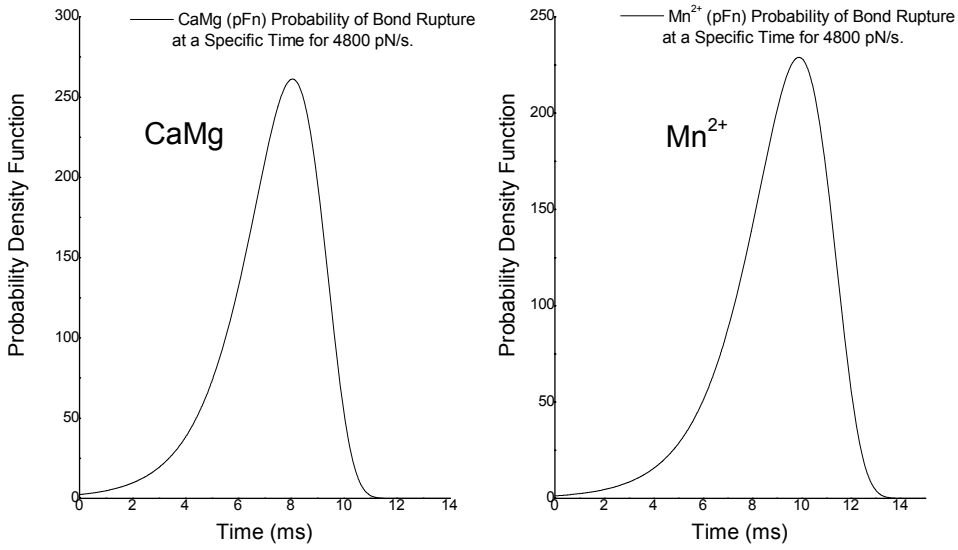

Figure 4.2 Probability of Bond Rupture at Time, t, for CaMg and Mn^{2+}. The most probable time for a single bond rupture at 4800 pN/s was calculated using Bell model parameters for CaMg and Mn^{2+} treatments respectively. The probability model is a function of both time and force, *P*(f, t). The CaMg treatment showed that rupture most probably occurs at ~ 8.0 ms, while rupture occurs at ~ 10 ms for Mn^{2+} treatment. Overall, the Mn^{2+} bonds have a higher probability of being intact and thus being detected during forced dissociation by AFM.

The probability that CaMg treatments result in faster bond dissociation under force than Mn^{2+} treatments may explain the higher frequency of binding between α5β1 and fibronectin for Mn^{2+} treatments. This is because the most probable time of rupture for CaMg is less than the probable dissociation time for Mn^{2+}, thus more frequently; the interaction peaks will be detected during rupture force measurements for Mn^{2+}.

Another possibility for the difference in CaMg and Mn^{2+} binding frequency is the fact that integrin posture is dissimilar for the down regulated (basal state) and up regulated states. While down regulated integrins adopt a physical posture which folded downward and impedes ligand accessibility (See Figures 2.3 and 2.4), up regulated integrins adopt an upright posture' as seen by scanning electron microscopy (SEM). Different conformations (e.g. up right or folded down ward) of αVβ3 or αIIbβ3 have been observed using scanning SEM following treatment with Ca^{2+} or Mn^{2+} (Takagi, 2002).

When the up regulated form of these integrins adopts the 'upright posture', the head region is fully exposed for ligand binding. Conversely, the down regulated form is folded like a switch blade knife, leaving the head region less exposed for ligand binding (Hynes, 2002, Liddington, 2002). The binding impedance due to the down regulated integrin shape has been previously been suggested to result in decreased binding frequency especially for integrin adhesion during leukocyte rolling (Beglova, 2002; Salas, 2004). Further, the down regulated integrin state is the default state in cells such a circulating blood platelets, which suggests a biological strategy for inhibiting cellular binding at inappropriate times.

Thus, both the difference in probable dissociation times between CaMg and Mn^{2+} and binding impedance, due to the CaMg-induced, folded conformation of down regulated α5β1,

most likely contributed to the reduction in binding frequency seen in this study. In the next section, the influence of divalent cation on rupture force magnitude over a range of load rates is discussed.

4.3 EFFECTS OF DIVALENT CATIONS ON ALPHA 5 BETA 1-FIBRONECTIN INTERACTION: MULTIPLE LOAD RATES

The plotted rupture force versus ln(load rate) patterns observed in this study are similar to those reported on in the literature (Kokkoli, 2004; Li, 2003; Tees, 2001). The potential mechanisms underlying these patterns are discussed in the following sections.

4.3.1 Energy Barriers Along the Dissociation Path Affect Rupture Force Data Patterns

Previous studies have shown that rupture force increased in magnitude as the load rate increased for a variety of molecular pairs (e.g. α5β1–fibronectin and avidin – biotin) and for various techniques such as bio - membrane probes and AFM (Evans, 1997; Merkel, 1999; Li, 2003). Further, the increased rupture force magnitudes associated with increasing load rate resulted from prominent energy barriers (i.e. kinetic impedances) that are overcome along the path of forced dissociation.

The overcoming of these barriers results in distinct patterns for the rupture force versus load rate data. For the avidin – biotin interactions, these patterns result in piecewise, continuous

segments of linearly increasing rupture force versus ln(load rate); where each linear segment is associated with a specific energy barrier along the dissociation path (Evans, 1997).

The molecular pair used in this study (i.e. α5β1 and fibronectin) resulted in the same linear, piecewise continuous patterns for plotted rupture force data versus ln(load rate) as the avidin – biotin data above. Further, the down regulated form of α5β1 (following treatment with Ca^{2+} or CaMg) resulted in a single linear pattern of rupture force versus ln(load rate). For the up regulated form of α5β1 (following treatment with Mg^{2+}, Mn^{2+} or CaMn), the data pattern resulted in two linear segments of rupture force versus ln(load rate) (Figures 3.14 & 3.15). Thus two distinct patterns of rupture force versus load rate existed between down regulated (a single linear segment) and up regulated (two linear segments) forms of α5β1.

The presence of the single linear segment for the down regulated form of α5β1 indicates that only a single energy barrier exists, while the two linear segments associated with the up regulated form of α5β1 indicates that two energy barriers exist along the dissociation path – one for each linear segment (Figure 4.3).

The α5β1–fibronectin interaction has previously been reported to result in two distinct patterns of rupture force versus load rate (Li, 2003). In agreement with the results from this study, one pattern has two different segments of linearly increasing rupture force versus ln(load rate), where each segment is associated with a different energy barrier. Just as in this study, one segment is associated with load rates less than ~ 10,000 pN/s, while the second segment is associated with load rates greater than ~ 10,000 pN/s.

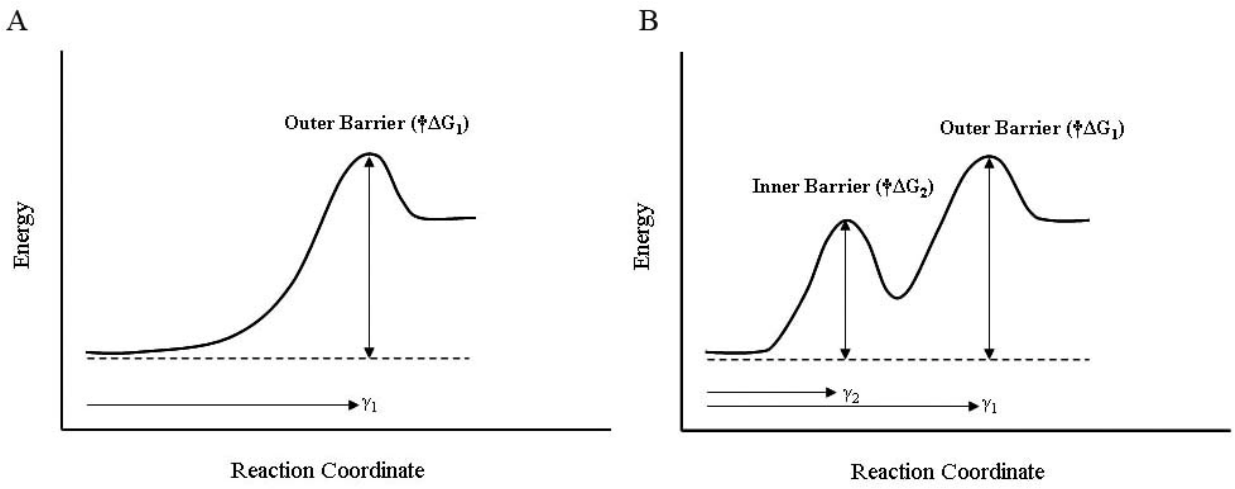

Figure 4.3 Idealized Energy Barriers Which Impede α5β1–Fibronectin Dissociation. Illustration of idealized energy barriers overcome during dissociation of the α5β1–fibronectin complex. The energy barrier height, $\dagger\Delta G_x$, is the difference in energy between a bound and unbound state and is also the energy necessary to overcome for bond dissociation to occur. The Reaction Coordinate, γ, is the distance along the dissociation path in which the complex is stretched before rupture occurs or can be thought of as the distance along the dissociation path to the energy barrier. (A) The down regulated form of α5β1, resulting from Ca^{2+} or CaMg treatments, yields a single, outer energy barrier that produces a single linear region of increasing rupture force versus increasing load rate. (B) The up regulated form of α5β1 (resulting from Mg^{2+}, Mn^{2+} or CaMn treatments) yields and outer and inner energy barrier, that produces two linear regions of increasing rupture force versus increasing load rate (See Figures 3.14 & 3.15). The outer barrier specifically produces the linear region of rupture force values associated with load rate values up to ~10,000 pN/s (i.e. low load region), while the inner barrier produces the rupture force values associated with the load rates greater than ~ 10,000 pN/s (i.e. high load region).

However, the two linear segments of rupture force versus ln(load rate) reported by (Li *et al.,* 2003) were present regardless of whether or not, α5β1 was down regulated or up regulated. This differed from the results in this study, where only up regulation of α5β1 binding affinity resulted in two linear segments and down regulation resulted in a single, linear segment.

Further, the two barriers were described by Li *et al.,* as an outer barrier for load rates less than 10,000 pN/s and an inner barrier for load rates greater than 10,000 pN/s. Multiple energy barriers emerge in succession from outer to inner to impede bond rupture. These barriers are distinguished by their associated bond rupture length, γ, which is referenced from the bound state

molecular state. The concept of inner and outer energy barriers was initially described for avidin – biotin rupture force data collected at multiple load rates using a bio - membrane probe (Evans, 1997; Merkel, 1999). The terminology used to describe the multiple energy barriers (i.e. inner barrier, outer barrier) in previous studies has been adopted by this study.

The second pattern reported by (Li, *et al.,* 2003) was a single linearly increasing segment associated with the deletion of the RGD (but not the synergy sequence) from fibronectin. Thus, it appeared that the RGD interaction with α5β1 determined the existence second linear region and deletion of RGD from fibronectin resulted in elimination of the inner barrier associated with load rates greater than 10,000 pN/s. This result indicates that non – covalent bonds at the α5β1 – fibronectin interface (such as RGD and adjacent amino acids of α5β1) are responsible for generating the impedances associated with outer energy barrier.

It has also been reported that the many non covalent bonds (e.g. hydrogen bonds, hydrophobic interactions, electrostatic interactions, etc….) between α5β1 and fibronectin are responsible for the resistance between molecules that give rise to the different energy barriers for avidin and biotin molecular binding (Merkel, 1999; Evans, 2001).

The force scale (or slope) governing the force range for each linear segment (at each energy barrier) is the product of Boltzmann's constant and temperature, divided by reaction coordinate, γ, which is the distance to the energy barrier along the dissociation path (Equation 4.3).

$$f_{scale} = \frac{k_B T}{\gamma} \tag{4.3}$$

The energy required to separate bound α5β1 and fibronectin, ΔG(0), is the height of a single barrier along the dissociation path that's needs to be overcome for molecular separation to occur. The addition of force applied to the bonds, not only results in increased kinetics (e.g. increased dissociation rate), but also reduces the barrier height, ΔG(0), by a factor, γf, where gamma is multiplied by separation force, f. The Gibbs' free energy of an individual bond, $\Delta G(f)$, is described in (Equation 4.4).

$$\Delta G(f) = \Delta G(0) - \gamma f \tag{4.4}$$

The linear decrease in free energy occurs as loading force is increased. As was previously stated, the increase in load rate results in an increase in bond rupture force magnitude. For this study, up regulated α5β1 results in the appearance of two linear segments. A low load segment for load rates up to 10,000 pN/s and a high load region for load rates greater than 10,000 pN/s. While the load rate does not exceed 10,000 pN/s, both down regulated and up regulated α5β1 encounters a dominant outer barrier, $\Delta G_1(0)$. However, as the load rate exceeds 10,000 pN/s, $\Delta G_1(0)$ is reduced energy wise by γf and the bound molecules now encounter a previously hidden inner barrier, $\Delta G_2(0)$ (Figure 4.3). Thus, $\Delta G_1(0)$ (outer barrier) is responsible for the low load linear region while $\Delta G_2(0)$ (inner barrier) is responsible for high load region.

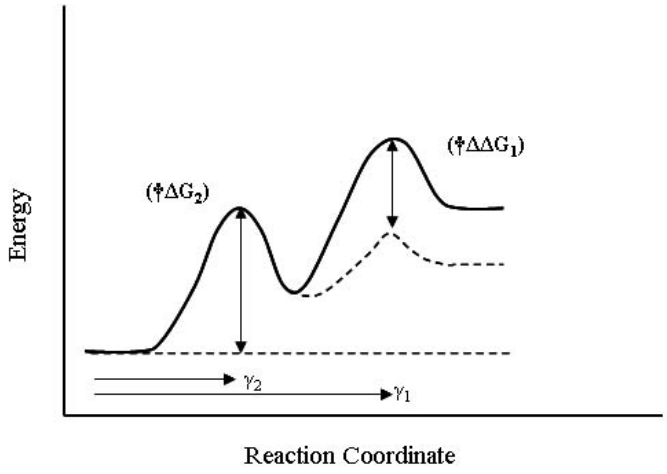

Figure 4.4 Reduction of Prominent Outer Energy Barrier as α5β1–Fibronectin Rupture Force Increases. Illustration of the two, idealized energy barriers associated with the up regulated form of α5β1 following treatments with either Mg^{2+}, Mn^{2+} or CaMn. The barriers are overcome during dissociation of the α5β1–fibronectin complex. The outer barrier is initially the most prominent kinetic impedance, but its influence is reduced as rupture force increases ($\dagger\Delta\Delta G_1$), leaving the inner barrier ($\dagger\Delta G_2$) as the new kinetic impedance to overcome for bond rupture to occur. The increase in rupture force, as load rate increases, reduces the outer barrier energy below that of the inner barrier. The switch in barrier prominence, from outer to inner, occurs when the load rate exceeds ~ 10,000 pN/s. The Gibb's free energy for the bond is reduced according to Equation 4.4.

The bond energy for each cation treatment was calculated for the low load and high load regions for both ligands used in this study (i.e. pFn and Fnf120). The Bell model parameters used in the bond energy calculations was previously determined from rupture force versus ln(load rate) data from this study (See tables 3.9, 3.10 & 3.11). The dissociation rate in the absence of force, k^0, and the reaction coordinate, γ, were calculated using the modified Bell model (Equation 3.3). However, k^0 can be solved for when the force equals zero in Equation 3.4, therefore, k^0 can be represented symbolically as follows in (Equation 4.5).

$$k^\circ = \left(\frac{r_f \gamma}{k_B T} \right) \tag{4.5}$$

The dissociation rate, k^0, in the absence of force can also be described as follows using the Eyring formula (Equation 4.6) when $f = 0$, $-\Delta G$ is $-\Delta G(0)$ and where h is Planck's constant.

$$k(0) = \frac{k_B T}{h} e^{\left(\frac{-\Delta G}{k_B T}\right)} \tag{4.6}$$

Thus, $\Delta G(0)$ can be determined by equating (Equations 4.5 and 4.6). The actual calculation of $\Delta G(0)$ was accomplished using (Equation 4.7) and the calculations shown in figure 4.5.

$$\Delta G(0) = -k_B T \ln\left(\frac{hk^\circ}{k_B T}\right) \tag{4.7}$$

The down regulated or up regulated forms of α5β1 both encounter the same outer barrier, $\Delta G_1(0)$, during separation with fibronectin. That is, the outer barrier always exists for down regulated α5β1 for load rates up to 10,000 pN/s. However, when the load rate reached the transition point, C, at ~ 10,000 pN/s, the $\Delta G_1(0)$ barrier no longer existed and the second barrier, $\Delta G_2(0)$, was now dominant.

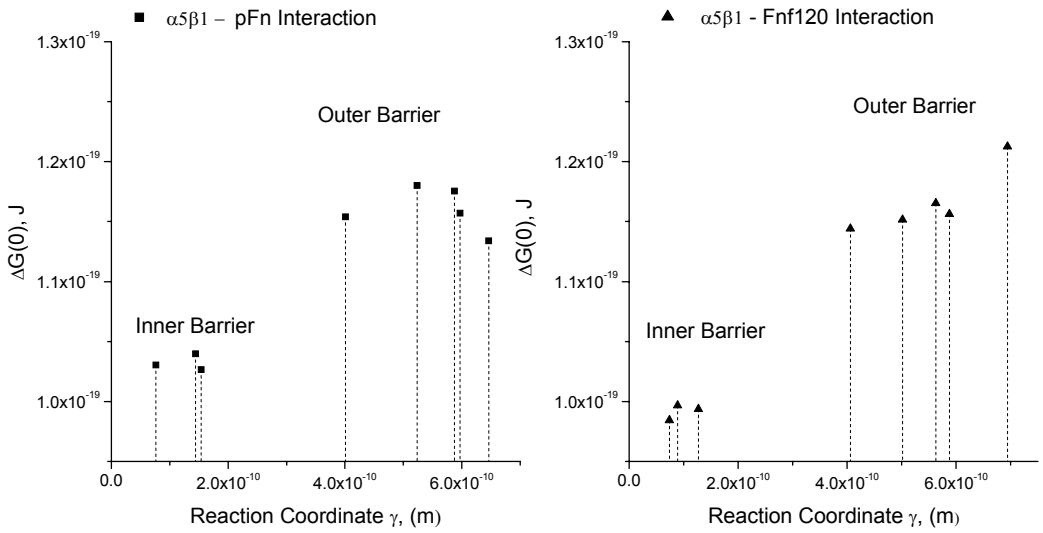

Figure 4.5 Molecular Bond Energy Calculations , ΔG(0), for Inner and Outer Barriers. The individual calculated bond energies, ΔG(0), required to overcome inner and outer energy barriers during bond rupture is shown for pFn (left panel) and Fnf120 (right panel). The outer barrier is the first impedance along the dissociation path and is reduced by a factor, *γf,* during tensile loading of the bond until the inner barrier becomes the major impedance to bond separation. It is further noted that the inner barrier is only encountered for load rates greater than (~ 10,000) pN/s and only when α5β1 is up regulated. The outer barrier is encountered for both down and up regulated α5β1 but the up regulated form only encounters the outer barrier for load rates up to (~ 10,000) pN/s, before transition to the inner barrier occurs. A difference in energy greater than k_BT (~ 4 pN*nm) exists between the inner and outer barriers, which signifies an energy magnitude (~ 20 k_BT) which is sufficient for transition from the outer to the inner barrier.

Nevertheless, only up regulated α5β1 encountered $\Delta G_2(0)$, resulting in the sharply increasing, high load region segment. The down regulated form of α5β1 continuously encountered the outer barrier ($\Delta G_1(0)$) for the low load and high load regions. Further, down regulation of α5β1 results in suppression or elimination of the inner energy barrier.

Only a small difference in energy magnitude between the barriers (~ 20 k_BT) is apparent in Figure 4.4. However, a difference in energy between the barriers greater than k_BT (~ 4 pN*nm) is sufficient to reduce the outer barrier height below that of the inner barrier, which

results in the inner barrier becoming the dominant impedance. Thus, the rupture force must increase to a level where (γf) is greater than k_BT.

The cluster of five data points in each panel of figure 4.4 represents all five of the different cation treatments (Ca^{2+}, CaMg, Mg^{2+}, Mn^{2+} and CaMn) for the low load region for which $\Delta G_1(0)$ was the impeding barrier. The remaining three data points in each panel of figure 4.4 represent the up regulating treatments of $\alpha5\beta1$ for which the outer barrier, $\Delta G_2(0)$, existed. The data points are grouped according to the distance to the energy barrier (e.g. reaction coordinate, γ). The bond extension distance for the inner barrier, γ_2 (~ 1 Å), is much shorter than the extension distance for the outer barrier (~ 4 Å). Further, the shape and location of these barriers changes little under applied force and the inner barrier is much more invariant to force than the outer barrier (Merkel, 1999; Evans, 2001).

During rupture force measurements, the AFM cantilever loads the bonds with a constant rate of linear ramping force that depends on the tip - substrate separation speed. However, the chemical bonds formed at the bond interface and the molecular structure of the pair molecules resist the cantilevers' pull in such a way that rupture force magnitude depends on load rate (Evans, 2001). In essence, a series of springs contributes to an effective spring constant. That is, the spring constants associated with extension of the pair molecules and cross linkers during tensile loading as well as the cantilever spring constant combine to arrive at an overall spring constant. However, in this study only the cantilever spring constant was known and an effective spring constant was not calculated. Thus, the rupture force data in this study is modeled and discussed in terms of effective spring constants whose values are unknown. The multi – regression model that immediately describes this data is formulated below in (Equation 4.8).

$$Force = k_0 + k_1 x + k_2 (x - C) z$$

$$z = \begin{cases} 1; \; x > C \\ 0; \; x < C \end{cases} \tag{4.8}$$

The constant, k_0, is the elastic spring constant of the system when no forced extension exists. The governing parameter, z, is zero for all load rate values below C. The data plots from this study (Figures 3.14 & 3.14) further show that the α5β1–fibronectin interface responded to bond rupture with force magnitudes that followed a linear spring model with a single spring constant, k_1, for all load rates following treatments with Ca^{2+} or CaMg. However, a stiffer spring constant, $k_1 + k_2$, existed after the transition point, C (~ 10,000 pN/s), but only for treatments with Mg^{2+}, Mn^{2+} or CaMn. Thus a softer spring constant, k_1, was present for load rates less than the transition point, C, regardless of which cation treatment was used. Whereas a stiffer spring constant, $k_1 + k_2$, existed only for cation treatments resulting in up regulation (i.e. Mg^{2+}, Mn^{2+} or CaMn).

The transition point, C, represents the load rate at which a transition from one energy barrier to another occurs. In the case of this study, C, represents the transition from $\Delta G_1(0)$ (outer barrier) to $\Delta G_2(0)$ (inner barrier). The barriers show a small difference in energy which must be related to additional bonding between up regulated α5β1 and fibronectin.

In summary, the data for this study showed that a single energy barrier, $\Delta G_1(0)$, existed for down regulated forms of α5β1; while the up regulated form showed a second barrier, $\Delta G_2(0)$, existed following the transition point C (~ 10,000 pN/s). The reasons for the second barrier, $\Delta G_2(0)$, seem to point to specific molecular interactions with the cation that up regulate α5β1 (i.e. Mg^{2+} and Mn^{2+}). It is further emphasized that $\Delta G_1(0)$ is identical for both down and up

regulated forms of a5b1 and is encountered The cation interaction and its influence on rupture force are discussed in the following section.

4.3.2 Influence of Cation Regulated α5β1 Binding Affinity on Rupture Force Magnitude

The α5β1–fibronectin interaction was reported by (Li, *et al.,* 2003) to be affected by up regulation of α5β1 using stimulatory antibody, when compared to the default, down regulated state. Specifically, the up regulation of α5β1 using the stimulatory antibody, TS2/16, resulted in increased rupture force magnitude for the low load region (< 10,000 pN/s) when compared to the default, down regulated form of α5β1. However, up regulating antibody treatment did not result in a difference in rupture force for high load rates (> 10,000 pN/s) between down regulated and up regulated α5β1. Overall, Li's results showed that up regulation of α5β1 using TS2/16 resulted in an increase in rupture force magnitude only for low load rates (< 10,000 pN/s). Further, both the down regulated and up regulated forms of α5β1 resulted in the two linear segment pattern of rupture force versus ln(load rate) typically associated only with the up regulated form of α5β1 in this study.

The results for the experiments in this study also showed that regulation of α5β1 binding affinity, coupled with varying load rate, resulted in increased rupture force for the separation of α5β1 and fibronectin. However, the results from this study differed from those of Li *et al.,* in that no statistical difference in rupture force magnitude existed between the down regulated and up regulated forms of α5β1 for rupture force measurements at low load rates (<10,000 pN/s). Additionally, the down regulated form of α5β1 resulted in a single linear segment pattern whose rupture force magnitudes at high load rates (i.e. > 10,000 pN/s) differed greatly from the up

regulated form of α5β1. Only the up regulated form of α5β1 from this study resulted in the two segmented, linear pattern where the second segment displayed sharply increasing rupture force values for high load rates (>10,000 pN/s) as compared to down regulated α5β1.

Of further interest is the fact that Li et al, observed the two linear segmented pattern of rupture force versus ln(load rate) for both down regulated and up regulated α5β1. To offer a possible explanation as to why the α5β1–fibronectin rupture force data patterns between these two studies differed, it is first necessary to comment on the molecular systems utilized. In this study, purified α5β1 and fibronectin were used as the molecular binding pair while Li *et al.,* attached a live, K562 cell (which expressed only α5β1) to an AFM tip. The unknown in Li's study is the activation state of the cells used. If activated, the cellular integrins (i.e. α5β1) would adopt the 'up right' posture, as opposed to the folded posture associated with down regulation (See figure 2.3 & 2.4). The 'up right' posture fully exposes the integrin's head region, which contains the fibronectin binding site. Further, it has been reported that the stimulatory antibody, TS2/16, results in a higher frequency of cellular binding when compared to Mn^{2+} (Takada, 1993; Bazzoni, 1995; Mould, 1995, Mould, 1998). Thus, Li *et al.,* may have been comparing activated integrin states of α5β1, where activation was from two sources, (1) cellular signaling (2) and stimulatory antibody. This would be in contrast to the intended state comparison (i.e. down regulated verses up regulated state). Consequently, naturally occurring cell activation could explain why treatments with or without α5β1 stimulating antibody resulted in two linear patterns of rupture force versus ln(load rate) for Li's data.

While there is no convenient way of determining whether or not a cell's integrin receptors were down regulated (or up regulated), the affinity state of purified receptors is less ambiguous. Individual α5β1 receptors have been confirmed, through scanning electron

microscopy (SEM) images, to adopt a folded conformation (due to down regulation via Ca^{2+} treatment) and the 'up right' conformation (due to Mn^{2+} treatment) (Takagi, 2001). Thus, working with purified receptors has advantages regarding control in regulating receptor binding affinity states.

At this point in the discussion, it is apparent that cation plays a role in the generation of rupture force data patterns and in the regulation of α5β1 binding affinity. That is, down regulation of α5β1, due to treatments with Ca^{2+} or CaMg results in a single, linear segment pattern of rupture force versus ln(load rate); while up regulation with Mg^{2+} or Mn^{2+} results in a pattern with two linear segments.

An attempt will now be made to establish a link between conformational change in dimer shape and the data patterns observed for this study. Following the discussion on cation induced, conformational change in dimer shape, the focus will be on identifying mechanisms responsible for the generation of the inner and outer energy barriers and their relationship to α5β1 binding affinity (i.e. the down and up regulated integrin states).

Previous studies have reported that cation induced conformational changes in integrin shape accompany changes in α5β1 binding affinity (Bazzoni, 1995; Mould, 1998). Further, the cations responsible for α5β1 up regulation (Mg^{2+} and Mn^{2+}) have been reported to induce conformational changes in both the α5 and β1 dimers (Baneres, 2000). Baneres, *et al.,* used circular dichroism spectroscopy (CD) to measure conformational changes in a fragmented form of α5β1 that lacked the cytoplasmic tail domains and stalk regions, but contained all cation binding sites and remained functional as a receptor. The measurements were performed in the presence of either Ca^{2+}, Mg^{2+} or Mn^{2+} and showed interesting changes in conformation for the individual dimers of α5β1.

The α5 dimer showed equal amounts of change in conformation in response to equal concentrations of either Ca^{2+}, Mg^{2+} or Mn^{2+}. Surprisingly, there was no difference in cation binding affinity for the α5 dimer. However, in some previous studies, the EC_{50} values for α5β1 or cellular binding assays showed Ca^{2+} and Mn^{2+} concentrations at about 50 μM each, while Mg^{2+} was roughly 1.2 mM showing that α5β1 has a higher affinity for Ca^{2+} or Mn^{2+} (Gailit, 1988, Mould 1995).

While no difference in cation dependent conformational change occurred in the α5 dimer between Ca^{2+}, Mg^{2+} and Mn^{2+}, the β1 dimer did show changes in conformation which were cation specific. Changes in conformation for the β1 dimer, resulting from Mg^{2+} or Mn^{2+} treatments, produced a maximal amount of change based on molar concentration ranging from 1 μM to 1 mM. Further, the β1 dimer showed a higher binding affinity for Mn^{2+}, reaching maximal conformational change for a much lower concentration (0.02 mM Mn^{2+}) compared to (0.1 mM) Mg^{2+}. On the other hand, Ca^{2+} produced no change in β1 conformation despite gradually increased concentrations up to 100 mM. Hence, a striking difference in conformation occurs in the β1 dimer depending on which cation is used. Thus, the up regulated form of α5β1 undergoes a conformational transformation that does not occur for down regulated forms of α5β1.

The conformational changes to the β1 dimer, resulting from Mg^{2+} or Mn^{2+} treatments, are likely associated with the increased rupture force observed for up regulated α5β1 at high load rates.

Further, the up regulated conformational shape of α5β1 allows optimal alignment of fibronectin modules III_9 (synergy site) and III_{10} with α5β1, resulting in more frequent molecular interactions (Danen, 1995; Redick, 2000). It is further noted that two types of conformational change affect binding frequency; (1) a lack of conformational change in the β1 dimer (due to

Ca^{2+} uptake) results in less than optimal alignment and interaction between α5β1 and fibronectin and (2) the down regulated form of α5β1 results in integrin folding (See Figures 2.3 & 2.4) that conceals the integrin head region, and thus disrupts fibronectin binding.

The RGD sequence is recognized by amino acid residues from both the α5 and β1 dimers, while the synergy site is primarily recognized by the α5 dimer (Mould, 1998; Redick, 2000). The recent crystal structure model by (Xiong, 2002) showed integrin αVβ3 binding a cyclic RGD peptide (Figure 4.6; Generated from MMDB, RCSB protein data bank). The peptide is coordinated with different amino acids as well as a single divalent cation, Mn^{2+}. The aspartate acid (D) of the RGD peptide is associated directly with the Mn^{2+} cation bound at the MIDAS site of the β3 dimer. The arginine residue (R) from the RGD peptide mainly associates with the αV dimer, but also associates to a much lesser extent, with the β3 dimer. The glycine (G), from the RGD peptide, associates with the αV dimer via hydrophobic interactions.

The β3 dimer contains two other cation binding sites (ADMIDAS and LIMBS) that appear to function as stabilizers of the up regulated conformational shape of β3, rather than interact with the RGD peptide. The ADMIDAS site is located adjacent to MIDAS site, and near the periphery of the β3 dimer. Xiong *et al.,* determined that only the ADMIDAS site is occupied

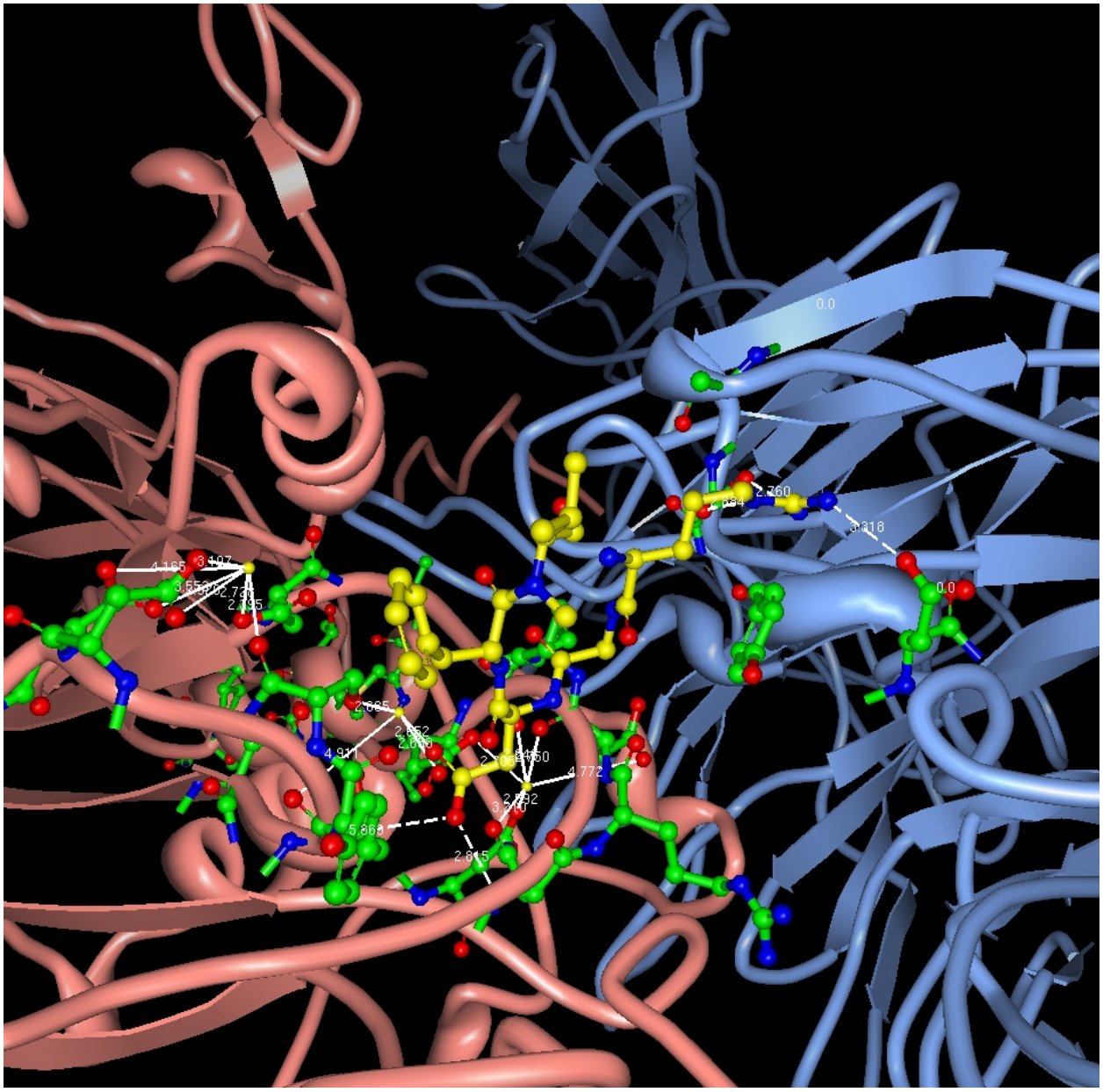

Figure 4.6 Crystal Structure of αVβ3 with Bound RGD Peptide. The structural model shows coordinating amino acid residues from the αV and β3 dimers (green) interacting with the RGD peptide (gold) and bound Mn^{2+} (gold spheres). Amino acid - cation interactions are illustrated with solid white lines, while dashed lines indicate interactions between amino acid residues and the RGD peptide. The (R) residue from RGD interacts with both the αV and β3 dimer residues, while the Aspartic acid interacts solely with the β3 dimer and MIDAS (center) bound cation. An extension of this model to α5β1 leads to the proposal that the (R) residue (along with the synergy site) and none cation interactions with (D) from RGD is responsible for the outer energy barrier. The interaction of the (D) from RGD and either Mg^{2+} or Mn^{2+} at the MIDAS site results in the inner barrier. Model of αVβ3 crystal structure from protein data base (Xiong, 2002).

by cation in the un - liganded state. The ADMIDAS site is also thought to regulate cation access to the MIDAS site through conformational changes in shape. The LIMBS binding site, (Ligand Induced Metal Ion Binding Site) is located adjacent to the MIDAS site, but at the αV and β3 interface. Unlike the ADMIDAS site, the LIMBS (and MIDAS) site is occupied by cation only after integrin ligation occurs. The LIMBS bound cation associates solely with amino acid residues in the β3 dimer, contributing significantly to the stability of its conformational shape.

The integrin α5β1 also contains the ADMIDAS, LIMBS and MIDAS cation binding sites in its β1 dimer (Mould, 1998) and shares the same fundamental, structural homology with αVβ3. After examining the crystal structure model for αVβ3, from which the current structural model for α5β1 is based (Coe, 2001; Li, 2003), it is plausible that the resistance generated during bond rupture is the result of various non – covalent interactions such as; (1) the RGD – cation interaction, (specifically the Aspartic acid interaction with cation at the MIDAS site) and (2) the association of the Arginine (of the RGD peptide) with the α5 dimer (3) the additional association of water molecules surrounding the cation occupying the MIDAS site and various hydrogen and other electrostatic bonds.

Although, the synergy sequence from fibronectin has been reported to associate with both the α5 and β1 dimers, it most likely functions to properly align the III_{10} module and thus aligns the RGD sequence for up regulated α5β1 (Redick, 2000; Mould, 1998). However, the interaction apparently does not affect rupture force magnitude (Li, 2003).

The focus of the discussion will now move away from conformational change in α5β1 and refocus on determining the mechanisms responsible for generating the energy barriers discussed in *Section 4.3.1.*

Determining the specificity of a molecular reaction is essential for identifying possible mechanisms responsible for binding behavior. The specificity of the α5β1-fibronectin interaction for this study was investigated using a variety of tests that disrupted molecular binding, including saturation levels of RGD peptide (Sigma, St. Louis, MO) or function blocking monoclonal antibody (JBS5; Chemicon). The JBS5 antibody binds to the fibronectin binding site of α5β1, thus restricting adhesion to fibronectin. The specific epitope is the 2^{nd} and 3^{rd} repeats of the beta propeller structure in the α5 dimer (Mould, 1998).

Mould *et al.,* established that JBS5 *did not bind* to α5β1 ligated with fibronectin fragment containing both the RGD and synergy homologies. However, it was also established that JBS5 *did bind* to α5β1 ligated with RGD peptide, or with mutated fibronectin fragment, which lacked the III_9 module, which contains the synergy sequence. Taken together, these results establish that (A) JBS5 does indeed primarily contact the α5 dimer, and (B) more importantly establishes that the synergy sequence of fibronectin also primarily binds the α5 dimer. The reduction in frequency of binding for the α5β1-fibronectin interaction in this study, following treatment with JBS5, indicates that molecular recognition (of fibronectin by α5β1) was reduced due to the lack of synergy site interaction (See *Section 3.6*).

The specificity of the α5β1-fibronectin interaction was also tested using EDTA chelation of divalent cation. The addition of 5 mM EDTA to buffer in these experiments also resulted in loss of the α5β1-fibronectin binding, showing the necessity of divalent cation to the interaction and perhaps its glue – like qualities.

Overall, the α5β1–fibronectin interaction can be disrupted if either RGD or JBS5 has previously bound to α5β1, or if divalent cation is sequestered. Further, JBS5 binds primarily to the α5 dimer, disrupting attachment of the III_9 module (synergy sequence). The RGD peptide

attaches primarily to the β1 dimer, blocking attachment of the III_{10} module which contains the RGD sequence (Mould, 1995; Mould, 1998; Xiong, 2002). These observations point to possible mechanistic chemical bonding from each dimer that is responsible for the impedance resulting in the two energy barriers observed in this study.

A further analysis of rupture force data from this study addresses whether or not, down regulation of α5β1 with Ca^{2+} results in a single segment pattern due to circumstances of bond dissociation kinetics (Figure 4.7). The analysis compares the ratio of the pull time (Tp) required to dissociate a α5β1-fibronectin bond using AFM and the natural dissociation time, 1/k(f).

If the pull time is less than the natural dissociation time (i.e. ratio < 1) then the rupture force magnitude resulted from a completed AFM pull. Conversely, a (ratio > 1) implies that the bond naturally dissociated before the AFM pull was complete, resulting in a bond rupture force of reduced magnitude. The natural dissociation time, 1/k(f), was calculated using the Bell model (Equation 3.3) where the natural dissociation rate, k^0, increases exponentially under applied force. The AFM pull time (Tp) was calculated by dividing the Bell model parameter, γ (distance bond is extended before rupture occurs), by the AFM tip speed. The results of the analysis shows that down regulated α5β1 (treated with either Ca^{2+} or CaMg) resulted in an average of two data points at high tip speeds (> 0.7 μm/s) in which the bond dissociated before the AFM pull was complete.

Although it is unlikely that the down regulated form of α5β1 results in a single linear pattern of rupture force (and not two segments) due to natural dissociation before bond rupture from AFM extension occurs from AFM extension, this suggestion cannot be ruled out. However, there is overshadowing evidence from the CD measurements of conformational change due to α5β1 cation uptake (Baneres, 2000) and crystal structure evidence of the RGD – cation

interaction (Xiong, 2002) that point to specific cation interactions as responsible for the data patterns observed in this study.

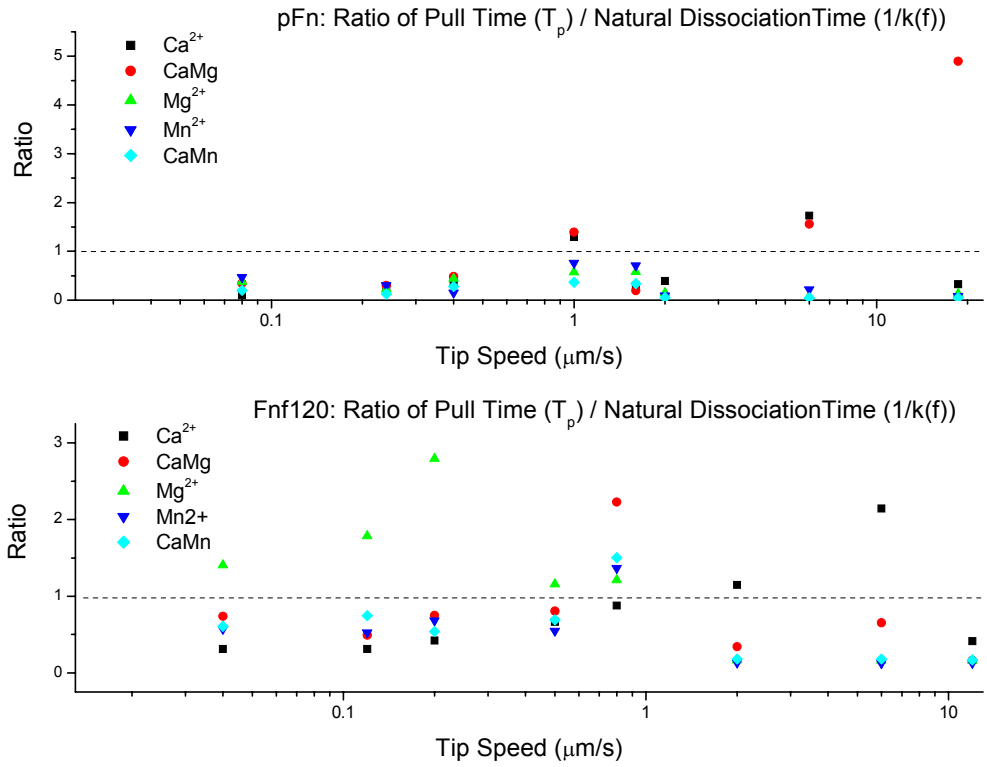

Figure 4.7 Ratio of Bond Rupture Pull Time and Natural Dissociation Time for all Tip Speeds. The ratios for the AFM pull time, Tp (i.e. γ / tip speed), and natural bond dissociation time influenced by force, 1/ k(f), for pFn (top) and Fnf120 (bottom). The ratio was calculated to investigate if bonds naturally dissociated faster than the time frame, Tp, in which the AFM applied force. When the ratio was (< 1) the AFM ruptured the bond before natural dissociation occurred. This analysis further investigates the possibility that down regulated α5β1 results in a single linear pattern of rupture force due to premature bond dissociation before the AFM pull is complete at high tip speeds. The ratio for the majority of data for all cation treatments shows that less time was taken for the AFM to rupture the bond than for the bond to naturally dissociate. The high load region data (tip speeds > 0.7 μm/s) for Ca^{2+} and CaMg treatments a some data points (red, black) that naturally dissociated before the AFM pull was finished.

A further question regarding the reliability of rupture force measurements in this study stems from the use of two different fibronectin ligands (i.e. pFn and Fnf120). There have been

reports that the amino terminus of full molecule fibronectin (pFn), which is important in matrix assembly, binds to α5β1 (McKeown, 1985; Hocking, 1998). Although the appearance of rupture force data patterns (i.e. one or two linear segments) depended on which cation was used for α5β1 treatment, the fibronectin ligands used (i.e. pFn or Fnf120) did not matter, as no statistical difference in rupture force between the groups was found.

Further, a recent follow up study to Hocking *et al.,* demonstrated that labeled amine terminus from fibronectin (or labeling of full molecule fibronectin amine terminus) show that the terminus actually associate with integrin α6β1, but not α5β1 (Johansson, 2006). The statistical comparison of the rupture force data from this study for pFn and Fnf120 ligands was accomplished using a generalized linear model (GLM) that controlled for load rate effects (See *Section 3.7.3*).

The Bell model parameters calculated for this study were as much as two orders of magnitude different from other studies measuring rupture force between α5β1 and fibronectin (Kokkoli, 2004; Li, 2003) and a study measuring kinetic parameters between this molecular pair using surface plasmon resonance techniques (Takagi, 2001). The study by (Li, 2003) reported measurements for the dissociation rate, k^0, of (0.13 s^{-1}) for down regulated α5β1 and (0.012 s^{-1}) for up regulated α5β1 in the low load region; while (Kokkoli, 2004) reported (0.015 s^{-1}) for up regulated α5β1 in the low load region. Because the modified Bell model (Equation 3.5) used to calculate, k^0, required that data from this study be fit using a regression model, the parameters of the regression fitted data from this study were examined using propagation of error (i.e. slope and intercept). The error in k^0 associated with all cation treatments showed slope errors of ~ 20%, however the ~ 80% of the error in k^0 was attributed to the y- intercepts. The full detailed set of propagated errors is available in the Appendix IV.

In summary, the binding affinity of α5β1 is regulated through its' interaction with divalent cation. The binding of various cation leads to conformational changes in shape for the α5 and β1 dimers that accommodate binding of fibronectin's synergy and RGD sequences. The changes in shape for the α5 dimer are the same regardless of whether Ca^{2+}, Mg^{2+} or Mn^{2+} is used as a treatment. However, only Mg^{2+} or Mn^{2+} produce a change in shape for the β1 dimer. Thus down regulation and up regulation differ by an overall change in shape for α5β1, which is attributed to the change in shape of the β1 dimer or the lack of it.

Further, up regulated, α5β1 binding affinity contributes to a better key – lock fit between α5β1 and fibronectin due to the change in β1 dimer shape; allowing Mg^{2+} or Mn^{2+} to interact with the aspartic acid from RGD, which produces higher rupture force magnitudes at load rates greater than ~ 10,000 pN/s. The RGD – cation interaction at the MIDAS site is most likely responsible for the inner energy barrier; while the interaction between α5 and β1 amino acid residues and arginine (from RGD) results in the outer energy barrier. The relationship between α5β1 cation binding and the appearance of single or double linear segment data patterns is also load rate dependent.

The rupture force data from this study clearly shows that down regulation of α5β1 (with Ca^{2+}) results in a single linear segment pattern of rupture force versus ln(load rate) for both low and high load rates. However, only up regulated α5β1 results in the pattern which displays two linear segments, but only for high load rates (> 10,000 pN/s). This suggests that for up regulated α5β1, the inner barrier (i.e. RGD – cation interaction) is inactive for load rates less than ~ 10,000 pN/s, while the outer barrier (i.e. arginine - α5 dimer interaction) becomes inactive when the load rate exceeds ~ 10,000 pN/s. For the down regulated form of α5β1, the less than optimal

alignment between α5β1 and fibronectin results in a lack of RGD – cation interaction, thus no inner barrier or associated second linear segment data pattern occurs.

Unlike the α5β1–fibronectin interaction where measurements were taken at a single load rate (See *Section 4.2.1*); there was a distinct difference in rupture force magnitude that depended on divalent cation treatment, but also load rate. Thus, a broad range of load rates is necessary to properly determine if binding affinity indeed affects rupture force magnitude. It is quite apparent that the up regulated form of α5β1 produces higher rupture forces than down regulated α5β1 but only when load rates exceed ~ 10,000 pN/s. This result suggests that the RGD – cation interaction plays a role (as does load rate) in the generation of the rupture force magnitude differences associated with high load rates in this study.

Overall, this section has establishesed that a relationship exists between α5β1 binding affinity and conformational change in the α5 and β1 dimers due to distinct cation binding. This relationship is believed to promote the access of Mg^{2+} or Mn^{2+} to the aspartic acid residue from RGD; however it is also believed to restrict Ca^{2+} access due to a lack of conformational change in the β1 dimer. The ability of Ca^{2+} to down regulate α5β1, following up regulation with Mg^{2+} (but not Mn^{2+}) is investigated in the following section by testing the cation binding affinity of α5β1 using a competitive cation labeling assay.

4.4 BIOCHEMICAL ANALYSIS OF CATION BINDING TO ALPHA 5 BETA 1

The rupture force versus ln(load rate) data for this study has shown that α5β1 down regulation, through treatments with Ca^{2+} or CaMg, leads to a single linear segment pattern; while up

regulation with Mg^{2+} or Mn^{2+} leads to a pattern with two linear segments. Further, the single and double linear patterns are associated with one or two bond dissociation impedances (i.e. energy barriers) respectively. Thus, it was apparent that the interaction between receptor bound Mg^{2+} or Mn^{2+} and fibronectin was responsible for the sharp increases in rupture force at high load rates (i.e. > ~ 10,000 pN/s); which result in the second linear segment and the inner energy barrier. The molecular bond chemistry at the bond interface has been previously implicated as the source of impedance responsible for the energy landscape (i.e. energy barriers) (Merkel, 1999; Evans, 2001).

Interestingly, Ca^{2+} added to Mg^{2+} buffer was able to eliminate the second linear segment pattern (i.e. eliminate the inner energy barrier) that was associated with Mg^{2+} up regulation. Thus it was determined that Ca^{2+} was able to down regulate α5β1 in the presence of Mg^{2+}. However, the addition of Ca^{2+} to buffer containing Mn^{2+} was not able to eliminate the second linear region pattern. Therefore, the question of why Ca^{2+} could down regulate α5β1 in the presence of Mg^{2+}, but not Mn^{2+} was asked.

A qualitative investigation of α5β1's binding affinity for the divalent cations, Ca^{2+}, Mg^{2+} and Mn^{2+} was performed using an assay, where radio – labeled calcium ($^{45}Ca^{2+}$) competed with Mg^{2+} and Mn^{2+} for binding to α5β1. The α5β1 samples were separated into individual dimers (i.e. α5 and β1) in a non – denatured manner using SDS-PAGE. Radio-labeled calcium, at an activity level of 1 μCi/mL, was added to sample buffer in which samples were initially incubated in either 0.5 mM Mn^{2+} or 1 mM Mg^{2+}. The membranes were then exposed to x-ray film for 24 hours and compared with a sample incubated solely in ($^{45}Ca^{2+}$) as a control.

The assay results showed that ($^{45}Ca^{2+}$) bound preferentially to both the α5 and β1 dimers in the presence of Mg^{2+} but not Mn^{2+}, thus leading to the conclusion that Ca^{2+} displaced Mg^{2+}

(but not Mn^{2+}) from the cation binding sites in α5β1. This further supported the rupture force data results from this study, in which it was proposed that the Mg^{2+} or Mn^{2+} interaction with the RGD sequence in fibronectin was responsible for the second energy barrier (i.e. inner barrier) that gives rise to the second, linear pattern for up regulated α5β1. Further, the assay results qualitatively showed that α5β1 has a higher binding affinity for Mn^{2+} as compared to Ca^{2+} or Mg^{2+}. The affinity ranking for each cation following the results from this study is as follows: $Mn^{2+} > Ca^{2+} > Mg^{2+}$.

The cation binding affinity also shows that α5β1 remains in an up regulated or 'up right' conformation when Mn^{2+} is bound and may be difficult to down regulate by competing cation. On the other hand, the α5β1 receptor can most likely be down regulated by Ca^{2+} during motility, if the only affinity regulating cations available are Ca^{2+} and Mg^{2+}. This is most likely the physiological case as cation are needed for the α5β1–fibronectin interaction to occur and $Mn^{2+}$is a trace element, available only in minute concentrations compared with Ca^{2+} and Mg^{2+}.

A conceptual model illustrating the effects of cation uptake by α5β1 is shown in (Figure 4.8). The model shows; (1) the cation binding affinity of α5β1 (2) the binding affinity state of α5β1 following cation uptake (i.e. down or up regulation) and (3) the resulting rupture force data pattern (i.e. either single linear or double linear segments).

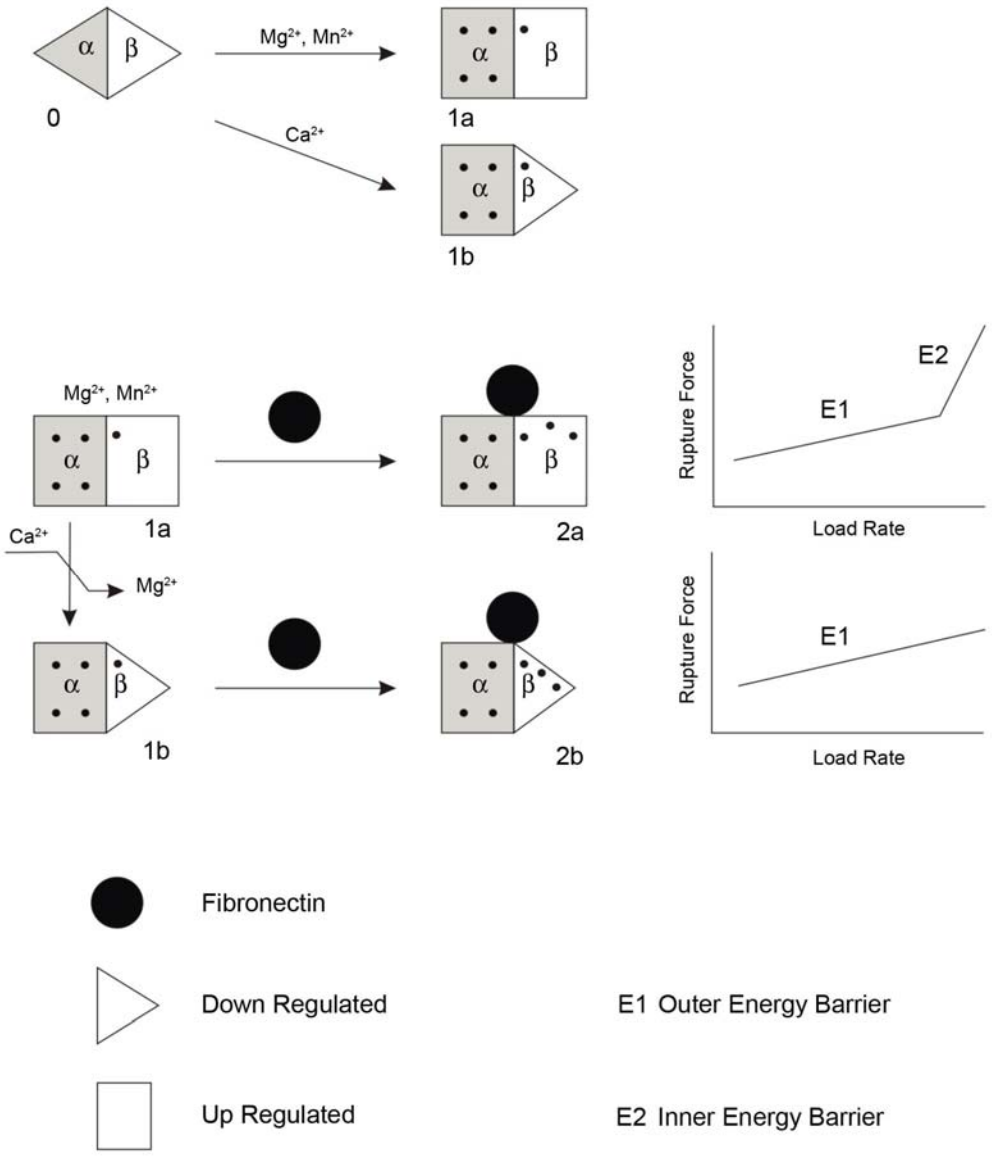

Figure 4.8 Divalent Cation Regulated Pathways for α5β1 Binding Affinity. Model illustrating divalent cation regulation of α and β dimer conformations responsible for one or two linearly increasing patterns of bond rupture force versus load rate regimes. The presence of any cation species up regulates the α5 dimer indistinguishably while the β1 dimer is only up regulated by Mg^{2+} or Mn^{2+} but is down regulated by Ca^{2+}. When not ligated, the α dimer's 4 cation sites are filled while only the ADMIDAS site in the β dimer is filled (Xiong, 2001). Following ligation, the β dimer has 3 bound cation. When Ca^{2+} fills all the β dimer sites during ligation, the result is a conformation whose interaction with fibronectin is limited and thus only a single linear, load pattern appears. Mn^{2+} and Mg^{2+} induce a β1 conformation whose ligand interaction results in two linear, load patterns, indicating the importance of β dimer conformation in rupture force magnitude. Competitive binding of cation showed that Ca^{2+} can displace Mg^{2+} (but not Mn^{2+}) from the β dimer, thus eliminating the second linear pattern and resulting in a single pattern.

4.5 CONCLUSIONS

The conclusions from this study are that up regulated binding affinity (which results from conformational changes in β1 dimer shape) results in a better fit between α5β1 and fibronectin and thus more bonds formed at the molecular interface. The extra bonds are ultimately responsible for the higher rupture forces observed between the down and up regulated forms of α5β1 at high load rates (i.e. > ~ 10,000 pN/s). The interaction between RGD and receptor bound cation is most likely the reason why rupture forces increase dramatically with load rates exceeding ~ 10,000 pN/s. Specifically, the interaction between Mn^{2+} or Mg^{2+} and the aspartic acid of RGD results in the inner energy barrier. Nevertheless, this interaction is sensitive to load rate and thus (for reasons unknown) does not contribute to rupture force magnitudes for low load rates (< ~ 10,000 pN/s). The Mg^{2+} or Mn^{2+} interaction with α5β1 results in a conformational shape change that aligns the β1 dimer such that the RGD sequence from fibronectin module III_{10} can interact with bound cation.

It has also been reported that Ca^{2+} results in no conformational change in the β1 dimer (Bazzoni, 1995; Baneres, 2000), thus it is proposed that the fibronectin III_{10} module (which contains RGD) is a significant distance away from bound cation, therefore eliminating the key interaction responsible for the inner barrier. Further, Ca^{2+} has been shown to reduce α5β1 – fibronectin binding frequency (Gailit, 1988; Mould, 1995). This is the result of (1) a folded conformation, in which the fibronectin binding domain is no longer openly exposed (Takagi,

2001) and (2) the lack conformational change in the β1 dimer, which does not allow interaction between the aspartic acid from RGD and the MIDAS bound cation. However, Ca^{2+}, Mg^{2+} or Mn^{2+} produce the same conformational shape change in the α5 dimer (Baneres, 1999, 2000) and thus all cation from this study produce the interfacial bonding which results in the outer energy barrier. Specifically, the outer barrier results from the interaction between the Arginine from RGD and primarily the α5 dimer and to a lesser extent, the β1 dimer.

Although Ca^{2+} can occupy the MIDAS site of β1 (Xiong, 2001); it is proposed that it does not interact with the aspartic acid of RGD. As previously stated, this is because of the large distance between the Ca^{2+} ion and the RGD sequence due to a lack of conformational change in β1. Instead, the majority of resistance from down regulated α5β1 results when the Arginine from RGD interacts with amino acid residues from the α5 and β1 dimers to produce the outer barrier; which results in the single linear segment. Although, the aspartic acid from the RGD sequence does not interact with Ca^{2+}, it most likely interacts with to some degree with amino acid residues from the β1 dimer.

The rupture force data from this study displays the fact that the single, linear pattern only results when α5β1 is treated with Ca^{2+} and the pattern of two linear segments results only when α5β1 is treated with Mg^{2+} or Mn^{2+}. This shows that the down or up regulated form of α5β1 is related to rupture force patterns.

The biochemical assay results from this study confirm that Ca^{2+} does indeed displace Mg^{2+} from α5β1. However, Ca^{2+} does not displace Mn^{2+} from α5β1. These results support (along with the lack of conformational change in the β1 dimer) a previous conclusion that the outer barrier can result from Ca^{2+} uptake by α5β1 and the inner barrier results from Mg^{2+} and Mn^{2+} uptake by α5β1 and subsequent interaction with RGD. The biochemical assay results also

support the fact that Ca^{2+} is capable of down regulating α5β1, which was previously up regulated with Mg^{2+}, resulting in the loss of RGD – Mg^{2+} interaction and the influence of the inner barrier. However, Ca^{2+} is not able to disrupt the RGD – Mn^{2+} interaction, as was observed through (1) the rupture force data and (2) the biochemical assay data. These observations may be due to the fact that H_2O molecules (along with surrounding amino acids) coordinate with Mn^{2+} at the MIDAS site (Xiong, 2002). The smaller atomic volume of Mn^{2+} (compared with Ca^{2+} or Mg^{2+}) is thought to allow H_2O molecules to fill the void space and coordinate stronger a stronger interaction capable of withstanding displacement by competing cation. A further conclusion is that the α5β1 cation binding affinity is as follows: $Mn^{2+} > Ca^{2+} > Mg^{2+}$, where Ca^{2+} can displace Mg^{2+} bound to α5β1 but not Mn^{2+}.

Although, it has not been established that Mn^{2+} actually participates in cellular adhesion under physiological conditions, it is plausible that this trace element can result in an up regulated conformation of α5β1 that resists down regulation by physiological levels of Ca^{2+}. However, it appears that physiological levels of Mg^{2+} could not resist down regulation by physiological levels of Ca^{2+}.

As a future direction of this study, mutations that disrupt cation binding at the MIDAS, ADMIDAS and LIMBS cation binding sites of α5β1 are in order to investigate the hypothesis that the inner energy barrier results from interactions between the aspartic acid of RGD and Mg^{2+} or Mn^{2+}. These mutations would also test the assumption that amino acid residues surrounding the LIMBS and ADMIDAS sites indeed function as stabilizers of the up regulated conformational shape of α5β1. Also, mutations that disrupt binding of the Arginine from RGD, and the synergy sequence from fibronectin, to the α5 and β1 dimers, are in order to investigate the origins of the outer energy barrier.

APPENDIX A

METHODS

Tip Modification; Standard silicon nitride probes customized with silica microspheres were used to exploit the abundance of SiOx surface groups needed for covalent linking of receptor proteins. Briefly, 7 μm diameter microspheres (Bangs Labs, Fishers, IN) were attached to previously calibrated cantilevers using epoxy (Pacer Technology, Rancho Cucamonga, CA). The tips were soaked in pure ETOH for 30 minutes and rinsed in milliQ H_2O before irradiation with UV for 30 minutes. The tips were then incubated in a (1:100) solution of 3-mercatopropyltrimethoxysilane (Sigma) diluted in pure ETOH for 1 hr, rinsed twice in ETOH and dried under pure argon for 1 hr. The tips were then crosslinked in a 12.8 mM solution of 3-(2-Pyridyldithio) propionic acid N-hydroxysuccinimide ester (Sigma, St. Louis, MO) for 1 hr and then rinsed 2x in ETOH and 2x in 10 mM hepes buffer (150 mM NaCl, pH 7.4) before incubation in α5β1 (3 μg/ml) for 1 hr. Non-linked proteins were removed by extensive rinsing in 10 mM hepes buffer. The probes were used immediately following modification for experiments. All AFM probes used in this study had an approximate cantilever length of 320 μm and k ~ 10 pN/nm or 200 μm and a k~ 60 pN/nm (Veeco Probes; Santa Barbara, CA).

Probe Labeling; Tips covalently linked with α5β1 were labeled with fluorescent antibody to test for: 1) The presence of α5β1 receptor on the probe and 2) whether (or not) the receptor's fibronectin binding domain was available for ligand binding. After being functionalized with α5β1 (as described above), the tips were incubated in 0.5 mM Mn^{2+} to up regulate receptor binding affinity and hence ensure a structural conformation in which the fibronectin binding domain is exposed. The tips were also incubated in a 0.5 % BSA solution to control non-specific adsorption of antibody. The tips were then either incubated in a primary antibody that blocked adhesion of fibronectin or a non-function blocking polyclonal antibody. The function blocking antibody (JBS5 clone, Chemicon, Temecula, CA) binds an epitope located between the second (R2) and third (R3) repeats of the beta propeller domain of the α5 subunit - which specifically inhibits synergistic activity by $FnIII_{10}$ (Mould, 1997). The non-function blocking antibody binds the c –terminal epitope a.a.840-943 (Santa Cruz Biotech). The tips were then incubated in species specific secondary anti-body labeled with Cy3 dye (Chemicon, Temecula, CA) and washed in hepes buffer. The fluorescence was measured at 1 minute intervals using a Nikon dissecting /fluorescence microscope in the red channel (550 -620 nm). Background measurements were also made in the blue and green channels to detect auto-fluorescing. Experimental control tips consisted of either bare standard silicon nitride or α5β1 functionalized tips and were not incubated in primary antibody. The control tips were solely incubated in secondary, fluorescent antibody after initially incubation in a 0.5 % BSA solution to control for non-specific adsorption of antibody. Fluorescence measurements were compared between the control and labeled tips in figure 3.5.

Force Spectroscopy Measurements in Divalent Cation; Single molecule separation force between α5β1 and fibronectin was measured under the conditions of; 1) varying load rate and 2) in the presence of divalent cations which up or down regulate α5β1 in an effort to investigate how these conditions affected separation force magnitude. The separation force was measured using a Digital Instruments AFM with a Nanoscope III controller (Veeco; Santa Barbara, CA). Briefly, fibronectin coated substrates were brought into contact with α5β1 functionalized tips using a piezo electric translator during an approach –contact –retraction cycle. The substrate approached the functionalized tip at a constant speed and then was retracted at speeds between (0.01 – 19 um/s). A single approach-contact-retraction cycle was recorded as a data measurement and 100 measurements (n = 100) were collected for each of nine tip retraction speeds. Contact force with the tip was minimized between (0.5 – 1 nN) for a 0.5 s duration before being retracted. During the tip retraction phase, α5β1-fibronectin interactions were subjected to tensile loading due to tethering constraints, which eventually resulted in bond rupture. Rupture events result in cantilever deflections and are denoted as one or more peaks in data measurements (see figure 3). The cantilever deflections are sensed by photo detection of a laser beam focused at the end of the cantilever. The rupture force is calculated as the product of cantilever deflection for a binding event, (Δd), and the cantilever spring constant. All experiments were conducted at room temperature in hepes buffer (10 mM, 150 mM NaCl, pH 7.4) containing either 1 mM Ca^{2+}, (1 mM Ca + 1 mM Mg^{2+}), 1 mM Mg^{2+}, 0.5 mM Mn^{2+} or (1 mM Ca^{2+} + 0.5 mM Mn^{2+}). Only force data with a single rupture peak were considered for analysis in this study to avoid multiple bond analysis. A frequency of a single binding event per force curve was observed for every 7-10 curves. A single tip and substrate was used for each experiment and 100 force measurements were collected for each of nine retraction speeds retraction speed over the range between (0.01 –

19 μm/s). Data values were averaged for each of nine tip retraction speeds to determine the mode rupture force for each load rate. Each averaged value was then plotted versus the natural-log of the load rate and fit with a linear regression line. This method of averaging the load rate values to determine the mode deviates from the fitting of a distribution to arrive at the modal rupture force however it has been shown to be a suitable and more robust alternative using Monte Carlo simulations (Tees, 2001). The baseline system noise was ~ 0.7 nm cantilever deflection, which translated to noise peaks ranging (7 - 10 pN). Binding separation events with force magnitudes less than or equal to (10 pN) were excluded from the analysis.

Inhibition of Binding Force and Binding Specificity: The molecular separation force was blocked (significantly reduced) using a 1:500 dilution of stock JBS5 (mouse anti-human α5 antibody, Chemicon) that targets the R2/R3 region of the α5 subunit and blocks adhesion to the synergy site in fibronectin. After the collection of data, the experimental buffer was replaced by antibody diluted in the experimental buffer and allowed to incubate for 30 minutes before force measurements resumed.

Additionally, the separation force was significantly reduced by replacing the experimental buffer with a solution containing an excess of GRGDS peptide (Sigma-Aldrich, St. Louis, MO). The GRGDS peptide has been used previously to block α5β1 adhesion to fibronectin by occupying the RGD recognition site in α5β1 and thus establishes the specificity of the α5β1-fibronectin interaction. The post experiment buffer was replaced by a 2uM GRGDS peptide solution followed by a 30 minute incubation period before force measurements resumed. The dependence of α5β1-fibronectin interaction on divalent cation was measured by replacing the experimental buffer enriched with cation with a 5 mM solution of EDTA. As with all

experiments, the EDTA solution was allowed to equilibrate before measurements of separation force resumed.

Substrate Preparation; Purified human plasma fibronectin (Chemicon International, Temecula, CA) was diluted from stock in 10 mM Hepes buffer (150 mM NaCl, pH 7.4) to a concentration of 50 μg/ml. 200 ul volumes were deposited onto freshly cleaved mica incubated for 30 minutes at room temperature to allow for passive adsorption of fibronectin. Unbound fibronectin was removed through rinsing the substrate with Hepes buffer. To cover bare regions not covered by fibronectin, the substrate was incubated in a 1% BSA solution for 30 minutes at room temperature. The substrates were used immediately following preparation.

Spring Constant Measurement; Spring Constant Measurement; An Asylum MPF 3D AFM or the thermal noise method of Bechhoefer & Hutter was used to calibrate all cantilevers. Briefly, the area of the thermal noise resonance peak was calculated and converted to the average cantilever fluctuation $\langle x^2 \rangle$. The formula, $k = k_B * T / \langle x^2 \rangle$ yielded values between 8.5 and 13.2 pN/nm for the 320 um long cantilever (Model # MLCT-AUNM) and 41 to 75 pN/nm for NPS tips (Veeco NanoProbe, Santa Barbara, CA). All spring constants were measured prior to attachment of micro-sphere.

APPENDIX B

MATLAB ® SCRIPT TO ANALYZE RUPTURE FORCE DATA

```
%////////////////////////////////////////////////////////////////////////
////////////////////
% PeakEval.m is a Matlab script that was developed to evaluate binding force
data curves
% (i.e. measure peak height & peak separation) using a dual cursor platform.
The script is
% specific for use with data generated by a Digital Instruments AFM using
Ver. 4.42 nanoscope III
% software. However the script can easily be modified to accommodate other
versions of nanoscope software.
%////////////////////////////////////////////////////////////////////////
////////////////////
% This script offers time saving conveniences such as:

% 1) Directly reading AFM data files in their native, binary format
% 2) Determines peak height (delta Y) and peak separation (delta X)
% 3) Quickly finds and Reads pertinent header parameters to properly scale or
convert data

     clear
     clear
%The following line allows files to be ENTERED using the click of a mouse
     [name] = uigetfile('*.*','Choose Data File');

% File Identifier (fid) tells whether or not file has any data content
     fid = fopen(name)

% The following lines read pertinent numerical header parameters needed to
calculate
% the Z-PIEZO range and to convert CANTILEVER DEFLECTION data to nanometers
     [Y, ZScanSens] = textread(name,'%16c %9.15f',1,'headerlines',52);
     [B, DeflSens]  = textread(name,'%21c %n',1,'headerlines',122);
     [X, ZScanSize] = textread(name,'%51c %n',1,'headerlines',188);
     [Z, SampLn]    = textread(name,'%13c %9.15f',1,'headerlines',213);
     [C, ZScale]    = textread(name,'%35c %n',1,'headerlines',232);

 % The following positions the file indicator to read the BINARY data and
then
```

```
 % converts the DEFLECTION data (voltage) to nanometers. Next, the data is
reformed into two column vectors that represent the Extension and Retraction
curve data.
     status = fseek(fid,-2048,1);
     [data,count] = fread(fid,8192,'short');
     %data=(data*(In1max/32768))*(InSens/DetSens)*(InputAtt);
     data=(data*DeflSens*ZScale);
     maxY=max(data);
     minY=min(data);
     data2=data(513:1024,1);
     data3=data(1:512,1);

  % The following calculates the Z_PIEZO range and INCREMENTS for plotting
versus DEFLECTION.
     %z=((ScanSize)*(Zmax/32768))*(Zsens);
     %x=linspace(-z,0,SampLn);
     dx=(ZScanSize*ZScanSens);
     x=linspace(-dx,0,SampLn);


  % The data is plotted here. The axis labels are automatically added and the
FILE NAME can
  % be placed anywhere on the plot area by pointing and clicking
     hold
     plot(x,data2)
     plot(x,data3,'r')
     %axis([-dx, 0, -20, 20])
     axis([-dx, 0, minY, maxY])
     hold off
     title('Peak Height Determination');
     xlabel('Z (nm)');
     ylabel('Cantilever Deflection (nm)');
     legend('Blue is Retraction Data');
     gtext(name)
     hold off

   % Finally, the data analysis begins by calling the function, dualcursor
(written by Scott Hirsch, Mathworks).
   % Dualcursor allows two movable cursors to be positioned at any location
   % on the force curve.
   % The difference in the horizontal & vertical cursor positions is use to
determine binding force
   % peak height and separation. The values are manually entered into EXCEL
for further data processing.
     dualcursor


%////////////////////////////////////////////////////////////////////////////
//////////////
   % Script Author: Nicolas Perrusquia, November 2003

%////////////////////////////////////////////////////////////////////////////
//////////////
```

APPENDIX C

MATLAB ® SCRIPT TO LOCATE TRANSITION POINT BETWEEN LOW AND HIGH LOAD REGIONS

```
% Matlab script to find optimized transition point, C,
% from intersection of two linear regions in which transition point is
% not known.

clear
clear
%The following line allows files to be ENTERED using the click of a mouse
     [name] = uigetfile('*.*','Choose Data File');

% File Identifier (fid) tells whether or not file has any data content
     fid = fopen(name)
     [X, Y] =textread(name);

% Plot File Data
     hold
     %plot(X,Y,'r.')

% plot Linear Fit of File Data
     coeff = polyfit(X,Y,1);
     newY=polyval(coeff,X);
     plot(X,Y,'r.', X,newY)
     xlabel('Load Rate Ln(pN/s)');
     ylabel('Separation Force (pN)');
     hold off

% 1) Guess Transition Data Point from plot of all data and enter a integer
(Limited to points 4 thru 7 from origin).
% 2) The next few lines of code separates data into TWO separate sets to plot
TWO NEW linear regions.
% 3) The TWO new data sets are subplotted, fit and R^2 calculated.

     dpt=input('Enter Data Point Number (limited to 3 thru 7) from Left
','s');
     C=hex2dec(dpt);
     Y1=Y(1:C);
     Y2=Y(C+1:9);
     X1=X(1:C);
```

```
    X2=X(C+1:9);

    %plot(X1, Y1, 'r.', X2, Y2, '.')



    coeff1 = polyfit(X1,Y1,1);
    newY1=polyval(coeff1,X1);

    coeff2 = polyfit(X2,Y2,1);
    newY2=polyval(coeff2,X2);
    %plot(X1,newY1,'r.',X2, newY2,'.')
    subplot(2,1,1); plot(X, Y, 'r.',X, newY)
    ylabel('Separation Force (pN)');
    residtot=Y-newY;
    Rt=norm(residtot);
    R2tot=Rt*Rt;
    title(['Sum of Rss All Data ='  , num2str(R2tot, '%3.2f')]);

    subplot(2,1,2); plot(X1, Y1, 'r.', X2, Y2, '.', X1, newY1,'b',X2, newY2,
'b')

% Insert axis Labels

    xlabel('Load Rate Ln(pN/s)');
    ylabel('Separation Force (pN)');




    disp(R2tot)

    resid1=Y1-newY1;
    R1=norm(resid1);
    R21=R1*R1;
    disp(R21);

    resid2=Y2-newY2;
    R2=norm(resid2);
    R22=R2*R2;
    disp(R22);
    disp(R21+R22);
    title(['Sum of Rss1 + Rss2 ='  , num2str(R22+R21, '%3.2f')]);

    F=(((R2tot)- (R21+R22))/2)/((R21+R22)/5)
    disp(F)

    gtext(name)

    hold off
  %[a,b] = ginput(1)
  %datacursormode on
  hold off

  %bar(X,resid);
```

APPENDIX D

ERROR PROPAGATION FOR BELL MODEL PARAMETERS

Formulas used to Calculate Bell Model Parameters

$$k^0 = \frac{1}{m} e^{\frac{-b}{m}} \text{ (Formula used to Calculate Dissociation Rate, } k^0\text{).}$$

$$\begin{cases} m = \text{Linear Regression Slope;} \dfrac{\sum (\text{x} - \bar{\text{x}})(y - \bar{y})}{\sum (\text{x} - \bar{\text{x}})^2}, \Delta m = \text{error in slope.} \\ b = Y - \text{intercept;} \ \bar{y} - m\bar{x}, \ \Delta b = \text{error in Y - intercept.} \end{cases}$$

$$\gamma = \frac{k_B T}{m} \text{(Formula used to Calculate Energy Barrier Location, } \gamma\text{).}$$

Formulas used to Calculate of Error in Bell Parameters

$$f = f[m,b]; \ \ \sigma_f = \pm\sqrt{\left(\frac{\partial f}{\partial m}\right)^2 \Delta m^2 + \left(\frac{\partial f}{\partial b}\right)^2 \Delta b^2} \text{ (General Error Propagation Equation).}$$

$$\Delta f = \text{Standard Error of Mean for } f = \frac{\sigma_f}{n}$$

$$\begin{cases} \sigma_f = \text{Propagated Error (Variance).} \\ n = \text{Number of Data Points for Linear Fit.} \end{cases}$$

$$\sigma_{k^0} = \pm\sqrt{\left[e^{\frac{-b}{m}}\left(\frac{b}{m^3}-\frac{1}{m^2}\right)\right]^2 \Delta m^2 + \left(\frac{-e^{\frac{-b}{m}}}{m^2}\right)^2 \Delta b^2}$$ (Error Propagation Formula, k^0).

$$\sigma_{\gamma} = \pm\sqrt{\left(\frac{-k_B T}{m^2}\right)^2 \Delta m^2}$$ (Error Propagation Formula, γ).

Calculated Bell Parameters and Standard Error of the Mean (S.E.M.)

Low Load Rate (i.e. < 10,000 pN/s) Bell Parameters (pFn)

	k^0	$\pm\Delta k^0$	γ	$\pm\Delta\gamma$
Ca^{2+}	3.1	1.5	6.9E-10	3.6E-23
CaMg	2.4	0.7	6.0E-10	2.1E-23
Mg^{2+}	1.5	0.2	5.9E-10	1.2E-23
Mn^{2+}	1.3	0.4	5.2E-10	1.7E-23
CaMn	2.5	0.5	4.0E-10	9.7E-24

Low Load Rate (i.e. < 10,000 pN/s) Bell Parameters (Fnf120)

	k^0	$\pm\Delta k^0$	γ	$\pm\Delta\gamma$
Ca^{2+}	3.1	0.7	4.4E-10	1.2E-23
CaMg	1.9	0.5	5.6E-10	1.7E-23
Mg^{2+}	0.6	0.1	6.9E-10	1.2E-23
Mn^{2+}	2.7	0.5	5.0E-10	1.0E-23
CaMn	2.4	0.4	5.9E-10	1.2E-23

Low Load Rate (i.e. < 10,000 pN/s) Bell Parameters (Combined Data: pFn + Fnf120)

	k^0	$\pm\Delta k^0$	γ	$\pm\Delta\gamma$
Ca^{2+}	3.6	1.1	5.2E-10	1.8E-23
CaMg	2.2	0.4	5.7E-10	1.2E-23
Mg^{2+}	1.0	0.1	6.3E-10	8.4E-24
Mn^{2+}	2.0	0.3	5.1E-10	9.9E-24
CaMn	2.8	0.6	4.6E-10	1.2E-23

High Load Rate (i.e. > 10,000 pN/s) Bell Parameters (pFn)

	k^0	$\pm\Delta k^0$	γ	$\pm\Delta\gamma$
Mg^{2+}	59.2	90.8	1.5E-10	1.8E-23
Mn^{2+}	42.5	91.7	1.4E-10	2.3E-23
CaMn	53.8	26.6	7.7E-11	2.7E-24

High Load Rate (i.e. > 10,000 pN/s) Bell Parameters (Fnf120)

	k^0	$\pm\Delta k^0$	γ	$\pm\Delta\gamma$
Mg^{2+}	168.0	52.1	7.4E-11	1.5E-24
Mn^{2+}	123.2	48.1	8.9E-11	2.4E-24
CaMn	133.2	16.4	1.3E-10	1.1E-24

High Load Rate (i.e. > 10,000 pN/s) Bell Parameters (Combined Data: pFn + Fnf120)

	k^0	$\pm\Delta k^0$	γ	$\pm\Delta\gamma$
Mg^{2+}	102.4	89.8	1.1E-10	6.5E-24
Mn^{2+}	70.0	63.6	1.2E-10	7.7E-24
CaMn	63.9	180.3	1.1E-10	2.2E-23

Regression Parameters

pFn Data

	Ca	CaMg	Mg low	Mg High	Mn Low	Mn High	CaMn Low	CaMn High
m	5.7	6.8	6.9	26.3	7.7	28.1	10.1	52.9
±Δm	1.8	1.4	0.9	9.1	1.5	13.7	1.5	5.7
b	-17.0	-18.8	-16.1	-193.5	-18.0	-199.2	-32.7	-420.6
±Δβ	12.6	10.2	6.2	94.4	11.3	144.7	11.1	59.9

Fnf120 Data

	Ca	CaMg	Mg low	Mg High	Mn Low	Mn High	CaMn Low	CaMn High
m	9.1	7.2	5.8	54.8	8.1	45.5	6.9	31.9
±Δm	1.5	1.3	0.6	3.4	1.0	3.6	0.9	0.8
b	-30.3	-18.9	-7.3	-500.2	-24.9	-392.6	-19.3	-266.3
±Δβ	11.0	9.6	4.5	37.7	7.4	40.2	6.3	8.9

Grouped Data

	Ca	CaMg	Mg low	Mg High	Mn Low	Mn High	CaMn Low	CaMn High
m	7.7	7.1	6.4	38.2	7.9	34.4	8.9	37.1
±Δm	1.6	0.9	0.5	7.1	0.9	6.7	1.4	22.7
b	-25.8	-19.4	-11.9	-316.0	-21.8	-267.6	-28.4	-288.4
±Δβ	11.8	6.7	3.8	76.1	7.0	72.8	10.2	243.2

BIBLIOGRAPHY

1. Akiyama, S.K., et al., *The interaction of fibronectin fragments with fibroblastic cells.* J Biol Chem, 1985. **260**(24): p. 13256-60.

2. Alexander, S.S., Jr., G. Colonna, and H. Edelhoch, *The structure and stability of human plasma cold-insoluble globulin.* J Biol Chem, 1979. **254**(5): p. 1501-5.

3. Almqvist, N., et al., *Elasticity and adhesion force mapping reveals real-time clustering of growth factor receptors and associated changes in local cellular rheological properties.* Biophys J, 2004. **86**(3): p. 1753-62.

4. Altieri, D.C., *Occupancy of CD11b/CD18 (Mac-1) divalent ion binding site(s) induces leukocyte adhesion.* J Immunol, 1991. **147**(6): p. 1891-8.

5. Amphlett, G.W. and M.E. Hrinda, *The binding of calcium to human fibronectin.* Biochem Biophys Res Commun, 1983. **111**(3): p. 1045-53.

6. Aota, S., M. Nomizu, and K.M. Yamada, *The short amino acid sequence Pro-His-Ser-Arg-Asn in human fibronectin enhances cell-adhesive function.* J Biol Chem, 1994. **269**(40): p. 24756-61.

7. Argraves, W.S., et al., *Amino acid sequence of the human fibronectin receptor.* J Cell Biol, 1987. **105**(3): p. 1183-90.

8. Arroyo, A.G., A. Garcia-Pardo, and F. Sanchez-Madrid, *A high affinity conformational state on VLA integrin heterodimers induced by an anti-beta 1 chain monoclonal antibody.* J Biol Chem, 1993. **268**(13): p. 9863-8.

9. Baly, D.L., J.S. Schneiderman, and A.L. Garcia-Welsh, *Effect of manganese deficiency on insulin binding, glucose transport and metabolism in rat adipocytes.* J Nutr, 1990. **120**(9): p. 1075-9.

10. Baneres, J.L., et al., *The cation-binding domain from the alpha subunit of integrin alpha5 beta1 is a minimal domain for fibronectin recognition.* J Biol Chem, 1998. **273**(38): p. 24744-53.

11. Baneres, J.L., et al., *A minimized human integrin alpha(5)beta(1) that retains ligand recognition.* J Biol Chem, 2000. **275**(8): p. 5888-903.

12. Barillari, G., et al., *Inflammatory cytokines stimulate vascular smooth muscle cells locomotion and growth by enhancing alpha5beta1 integrin expression and function.* Atherosclerosis, 2001. **154**(2): p. 377-85.

13. Bazzoni, G., et al., *Divalent cations and ligands induce conformational changes that are highly divergent among beta1 integrins.* J Biol Chem, 1998. **273**(12): p. 6670-8.

14. Bazzoni, G., et al., *Monoclonal antibody 9EG7 defines a novel beta 1 integrin epitope induced by soluble ligand and manganese, but inhibited by calcium.* J Biol Chem, 1995. **270**(43): p. 25570-7.

15. Bell, G.I., M. Dembo, and P. Bongrand, *Cell adhesion. Competition between nonspecific repulsion and specific bonding.* Biophys J, 1984. **45**(6): p. 1051-64.

16. Best, R.B., et al., *Can non-mechanical proteins withstand force? Stretching barnase by atomic force microscopy and molecular dynamics simulation.* Biophys J, 2001. **81**(4): p. 2344-56.

17. Blindt, R., et al., *Characterization of differential gene expression in quiescent and invasive human arterial smooth muscle cells.* J Vasc Res, 2002. **39**(4): p. 340-52.

18. Bork, P., et al., *Structure and distribution of modules in extracellular proteins.* Q Rev Biophys, 1996. **29**(2): p. 119-67.

19. Bottger, B.A., et al., *Integrin-type fibronectin receptors of rat arterial smooth muscle cells: isolation, partial characterization and role in cytoskeletal organization and control of differentiated properties.* Differentiation, 1989. **41**(2): p. 158-67.

20. Briesewitz, R., A. Kern, and E.E. Marcantonio, *Assembly and function of integrin receptors is dependent on opposing alpha and beta cytoplasmic domains.* Mol Biol Cell, 1995. **6**(8): p. 997-1010.

21. Briesewitz, R., et al., *The membrane-cytoplasm interface of integrin alpha subunits is critical for receptor latency.* Mol Biol Cell, 1996. **7**(10): p. 1499-509.

22. Carrion-Vazquez, M., et al., *Mechanical and chemical unfolding of a single protein: a comparison.* Proc Natl Acad Sci U S A, 1999. **96**(7): p. 3694-9.

23. Chen, J., A. Salas, and T.A. Springer, *Bistable regulation of integrin adhesiveness by a bipolar metal ion cluster.* Nat Struct Biol, 2003. **10**(12): p. 995-1001.

24. Chen, J., et al., *The relative influence of metal ion binding sites in the I-like domain and the interface with the hybrid domain on rolling and firm adhesion by integrin alpha4beta7.* J Biol Chem, 2004.

25. Clausen-Schaumann, H., et al., *Force spectroscopy with single bio-molecules.* Curr Opin Chem Biol, 2000. **4**(5): p. 524-30.

26. Coe, A.P., et al., *Generation of a minimal alpha5beta1 integrin-Fc fragment.* J Biol Chem, 2001. **276**(38): p. 35854-66.

27. Colombatti, A., P. Bonaldo, and R. Doliana, *Type A modules: interacting domains found in several non-fibrillar collagens and in other extracellular matrix proteins.* Matrix, 1993. **13**(4): p. 297-306.

28. Dammer, U., et al., *Specific antigen/antibody interactions measured by force microscopy.* Biophys J, 1996. **70**(5): p. 2437-41.

29. Danen, E.H., et al., *Requirement for the synergy site for cell adhesion to fibronectin depends on the activation state of integrin alpha 5 beta 1.* J Biol Chem, 1995. **270**(37): p. 21612-8.

30. de Beus, E. and K. Jacobson, *Integrin involvement in keratocyte locomotion.* Cell Motil Cytoskeleton, 1998. **41**(2): p. 126-37.

31. Enderlein, J., *A theoretical investigation of single-molecule fluorescence detection on thin metallic layers.* Biophys J, 2000. **78**(4): p. 2151-8.

32. Evans, E., *Probing the relation between force--lifetime--and chemistry in single molecular bonds.* Annu Rev Biophys Biomol Struct, 2001. **30**: p. 105-28.

33. Evans, E. and K. Ritchie, *Dynamic strength of molecular adhesion bonds.* Biophys J, 1997. **72**(4): p. 1541-55.

34. Fisher, T.E., P.E. Marszalek, and J.M. Fernandez, *Stretching single molecules into novel conformations using the atomic force microscope.* Nat Struct Biol, 2000. **7**(9): p. 719-24.

35. Florin, E.L., V.T. Moy, and H.E. Gaub, *Adhesion forces between individual ligand-receptor pairs.* Science, 1994. **264**(5157): p. 415-7.

36. Francis, S.E., et al., *Central roles of alpha5beta1 integrin and fibronectin in vascular development in mouse embryos and embryoid bodies.* Arterioscler Thromb Vasc Biol, 2002. **22**(6): p. 927-33.

37. Gailit, J. and E. Ruoslahti, *Regulation of the fibronectin receptor affinity by divalent cations.* J Biol Chem, 1988. **263**(26): p. 12927-32.

38. Galbraith, C.G. and M.P. Sheetz, *Keratocytes pull with similar forces on their dorsal and ventral surfaces.* J Cell Biol, 1999. **147**(6): p. 1313-24.

39. George, E.L., H.S. Baldwin, and R.O. Hynes, *Fibronectins are essential for heart and blood vessel morphogenesis but are dispensable for initial specification of precursor cells.* Blood, 1997. **90**(8): p. 3073-81.

40. George, E.L., et al., *Defects in mesoderm, neural tube and vascular development in mouse embryos lacking fibronectin.* Development, 1993. **119**(4): p. 1079-91.

41. Georges-Labouesse, E.N., et al., *Mesodermal development in mouse embryos mutant for fibronectin.* Dev Dyn, 1996. **207**(2): p. 145-56.

42. Goh, K., J. Yang, and R. Hynes, *Mesodermal defects and cranial neural crest apoptosis in alpha5 integrin-null embryos.* Development, 1997. **124**(21): p. 4309-4319.

43. Goh, K.L., J.T. Yang, and R.O. Hynes, *Mesodermal defects and cranial neural crest apoptosis in alpha5 integrin-null embryos.* Development, 1997. **124**(21): p. 4309-19.

44. Gong, H. and T. Amemiya, *Optic nerve changes in manganese-deficient rats.* Exp Eye Res, 1999. **68**(3): p. 313-20.

45. Grinnell, F., *Manganese-dependent cell-substratum adhesion.* J Cell Sci, 1984. **65**: p. 61-72.

46. Grinnell, F. and R. Backman, *Role of integrin receptors in manganese-dependent BHK cell spreading on albumin-coated substrata.* Exp Cell Res, 1991. **195**(1): p. 218-23.

47. Hocking, D.C., J. Sottile, and P.J. McKeown-Longo, *Fibronectin's III-1 module contains a conformation-dependent binding site for the amino-terminal region of fibronectin.* J Biol Chem, 1994. **269**(29): p. 19183-7.

48. Hocking, D.C., J. Sottile, and P.J. McKeown-Longo, *Activation of distinct alpha5beta1-mediated signaling pathways by fibronectin's cell adhesion and matrix assembly domains.* J Cell Biol, 1998. **141**(1): p. 241-53.

49. Huang, C., et al., *Structural and functional studies with antibodies to the integrin beta 2 subunit. A model for the I-like domain.* J Biol Chem, 2000. **275**(28): p. 21514-24.

50. Hughes, P.E., et al., *Breaking the integrin hinge. A defined structural constraint regulates integrin signaling.* J Biol Chem, 1996. **271**(12): p. 6571-4.

51. Humphries, J.D., et al., *Molecular basis of ligand recognition by integrin alpha5beta 1. II. Specificity of arg-gly-Asp binding is determined by Trp157 OF THE alpha subunit.* J Biol Chem, 2000. **275**(27): p. 20337-45.

52. Humphries, M.J., *Integrin structure.* Biochem Soc Trans, 2000. **28**(4): p. 311-39.

53. Hussain, S. and S.F. Ali, *Manganese scavenges superoxide and hydroxyl radicals: an in vitro study in rats.* Neurosci Lett, 1999. **261**(1-2): p. 21-4.

54. Hutter, J.L., Bechhoefer, J., *Calibration of atomic-force microscope tips.* Rev. Sci. Instrum., 1993. **64**(7): p. 1868-1873.

55. Hynes, R.O., *Integrins: a family of cell surface receptors.* Cell, 1987. **48**(4): p. 549-54.

56. Hynes, R.O., *Integrins: versatility, modulation, and signaling in cell adhesion.* Cell, 1992. **69**(1): p. 11-25.

57. Hynes, R.O., *The dynamic dialogue between cells and matrices: implications of fibronectin's elasticity.* Proc Natl Acad Sci U S A, 1999. **96**(6): p. 2588-90.

58. Hynes, R.O., *Integrins: bidirectional, allosteric signaling machines.* Cell, 2002. **110**(6): p. 673-87.

59. Hynes, R.O., *The emergence of integrins: a personal and historical perspective.* Matrix Biol, 2004. **23**(6): p. 333-40.

60. Hynes, R.O. and K.M. Yamada, *Fibronectins: multifunctional modular glycoproteins.* J Cell Biol, 1982. **95**(2 Pt 1): p. 369-77.

61. Hynes, R.O. and Q. Zhao, *The evolution of cell adhesion.* J Cell Biol, 2000. **150**(2): p. F89-96.

62. Kamata, T., et al., *Membrane-proximal {alpha}/{beta} stalk interactions differentially regulate integrin activation.* J Biol Chem, 2005. **280**(26): p. 24775-83.

63. Keen, C.L., et al., *Nutritional aspects of manganese from experimental studies.* Neurotoxicology, 1999. **20**(2-3): p. 213-23.

64. Khan, M.Y., et al., *Structural changes in the NH2-terminal domain of fibronectin upon interaction with heparin. Relationship to matrix-driven translocation.* J Biol Chem, 1988. **263**(23): p. 11314-8.

65. Kim, S., et al., *Regulation of Angiogenesis in Vivo by Ligation of Integrin {alpha}5{beta}1 with the Central Cell-Binding Domain of Fibronectin.* Am J Pathol, 2000. **156**(4): p. 1345-1362.

66. Krammer, A., et al., *A structural model for force regulated integrin binding to fibronectin's RGD-synergy site.* Matrix Biol, 2002. **21**(2): p. 139-47.

67. Krammer, A., et al., *Forced unfolding of the fibronectin type III module reveals a tensile molecular recognition switch.* Proc Natl Acad Sci U S A, 1999. **96**(4): p. 1351-6.

68. Leahy, D.J., I. Aukhil, and H.P. Erickson, *2.0 A crystal structure of a four-domain segment of human fibronectin encompassing the RGD loop and synergy region.* Cell, 1996. **84**(1): p. 155-64.

69. Lee, J.O., et al., *Crystal structure of the A domain from the alpha subunit of integrin CR3 (CD11b/CD18).* Cell, 1995. **80**(4): p. 631-8.

70. Li, F., et al., *Force measurements of the alpha5beta1 integrin-fibronectin interaction.* Biophys J, 2003. **84**(2 Pt 1): p. 1252-62.

71. Liao, Y.F., et al., *The EIIIA segment of fibronectin is a ligand for integrins alpha 9beta 1 and alpha 4beta 1 providing a novel mechanism for regulating cell adhesion by alternative splicing.* J Biol Chem, 2002. **277**(17): p. 14467-74.

72. Lin, H., R. Lal, and D.O. Clegg, *Imaging and mapping heparin-binding sites on single fibronectin molecules with atomic force microscopy.* Biochemistry, 2000. **39**(12): p. 3192-6.

73. Litvinovich, S.V. and K.C. Ingham, *Interactions between type III domains in the 110 kDa cell-binding fragment of fibronectin.* J Mol Biol, 1995. **248**(3): p. 611-26.

74. Loftus, J.C. and R.C. Liddington, *New insights into integrin-ligand interaction.* J Clin Invest, 1997. **100**(11 Suppl): p. S77-81.

75. Maroudas, N.G., *Adhesion and spreading of cells on charged surfaces.* J Theor Biol, 1975. **49**(2): p. 417-24.

76. Maruyama, K., T. Mikawa, and S. Ebashi, *Detection of calcium binding proteins by 45Ca autoradiography on nitrocellulose membrane after sodium dodecyl sulfate gel electrophoresis.* J Biochem (Tokyo), 1984. **95**(2): p. 511-9.

77. McDonald, J.A., et al., *Fibronectin's cell-adhesive domain and an amino-terminal matrix assembly domain participate in its assembly into fibroblast pericellular matrix.* J Biol Chem, 1987. **262**(7): p. 2957-67.

78. Meadows, P.Y.B., J. E.; Walker, G. C., *Single Molecule Force Spectroscopy of Isolated and Aggregated Fibronectin Proteins on Negatively Charged Surfaces in Aqueous Liquids." Langmuir*, 2003. **19**: p. 9566-9572.

79. Merkel, R., et al., *Energy landscapes of receptor-ligand bonds explored with dynamic force spectroscopy.* Nature, 1999. **397**(6714): p. 50-3.

80. Michishita, M., V. Videm, and M.A. Arnaout, *A novel divalent cation-binding site in the A domain of the beta 2 integrin CR3 (CD11b/CD18) is essential for ligand binding.* Cell, 1993. **72**(6): p. 857-67.

81. Mould, A.P., S.K. Akiyama, and M.J. Humphries, *Regulation of integrin alpha 5 beta 1-fibronectin interactions by divalent cations. Evidence for distinct classes of binding sites for Mn2+, Mg2+, and Ca2+.* J Biol Chem, 1995. **270**(44): p. 26270-7.

82. Mould, A.P., et al., *Defining the topology of integrin alpha5beta1-fibronectin interactions using inhibitory anti-alpha5 and anti-beta1 monoclonal antibodies. Evidence that the synergy sequence of fibronectin is recognized by the amino-terminal repeats of the alpha5 subunit.* J Biol Chem, 1997. **272**(28): p. 17283-92.

83. Mould, A.P., J.A. Askari, and M.J. Humphries, *Molecular basis of ligand recognition by integrin alpha 5beta 1. I. Specificity of ligand binding is determined by amino acid sequences in the second and third NH2-terminal repeats of the alpha subunit.* J Biol Chem, 2000. **275**(27): p. 20324-36.

84. Mould, A.P., et al., *Role of ADMIDAS cation-binding site in ligand recognition by integrin alpha 5 beta 1.* J Biol Chem, 2003. **278**(51): p. 51622-9.

85. Mould, A.P., et al., *Regulation of integrin alpha 5 beta 1 function by anti-integrin antibodies and divalent cations.* Biochem Soc Trans, 1995. **23**(3): p. 395S.

86. Mould, A.P., et al., *Regulation of integrin function: evidence that bivalent-cation-induced conformational changes lead to the unmasking of ligand-binding sites within integrin alpha5 beta1.* Biochem J, 1998. **331 (Pt 3)**: p. 821-8.

87. Mould, A.P. and M.J. Humphries, *Cell biology: adhesion articulated.* Nature, 2004. **432**(7013): p. 27-8.

88. Moy, V.T., E.L. Florin, and H.E. Gaub, *Intermolecular forces and energies between ligands and receptors.* Science, 1994. **266**(5183): p. 257-9.

89. Obara, M., M.S. Kang, and K.M. Yamada, *Site-directed mutagenesis of the cell-binding domain of human fibronectin: separable, synergistic sites mediate adhesive function.* Cell, 1988. **53**(4): p. 649-57.

90. Oberhauser, A.F., et al., *The mechanical hierarchies of fibronectin observed with single-molecule AFM.* J Mol Biol, 2002. **319**(2): p. 433-47.

91. Oberhauser, A.F., et al., *Single protein misfolding events captured by atomic force microscopy.* Nat Struct Biol, 1999. **6**(11): p. 1025-8.

92. Ohashi, T., D.P. Kiehart, and H.P. Erickson, *Dynamics and elasticity of the fibronectin matrix in living cell culture visualized by fibronectin-green fluorescent protein.* Proc Natl Acad Sci U S A, 1999. **96**(5): p. 2153-8.

93. Pankov, R. and K.M. Yamada, *Fibronectin at a glance.* J Cell Sci, 2002. **115**(Pt 20): p. 3861-3.

94. Plaxco, K.W., et al., *A comparison of the folding kinetics and thermodynamics of two homologous fibronectin type III modules.* J Mol Biol, 1997. **270**(5): p. 763-70.

95. Powell, R.D., et al., *A covalent fluorescent-gold immunoprobe: simultaneous detection of a pre-mRNA splicing factor by light and electron microscopy.* J Histochem Cytochem, 1997. **45**(7): p. 947-56.

96. Pytela, R., M.D. Pierschbacher, and E. Ruoslahti, *Identification and isolation of a 140 kd cell surface glycoprotein with properties expected of a fibronectin receptor.* Cell, 1985. **40**(1): p. 191-8.

97. Rabinovitch, M. and M.J. DeStefano, *Manganese stimulates adhesion and spreading of mouse sarcoma I ascites cells.* J Cell Biol, 1973. **59**(1): p. 165-76.

98. Radmacher, M., et al., *Mapping interaction forces with the atomic force microscope.* Biophys J, 1994. **66**(6): p. 2159-65.

99. Redick, S.D., et al., *Defining fibronectin's cell adhesion synergy site by site-directed mutagenesis.* J Cell Biol, 2000. **149**(2): p. 521-7.

100. Rief, M., M. Gautel, and H.E. Gaub, *Unfolding forces of titin and fibronectin domains directly measured by AFM.* Adv Exp Med Biol, 2000. **481**: p. 129-36; discussion 137-41.

101. Rief, M., et al., *Reversible unfolding of individual titin immunoglobulin domains by AFM.* Science, 1997. **276**(5315): p. 1109-12.

102. Rief, M., et al., *The mechanical stability of immunoglobulin and fibronectin III domains in the muscle protein titin measured by atomic force microscopy.* Biophys J, 1998. **75**(6): p. 3008-14.

103. Rief, M., et al., *Single Molecule Force Spectroscopy on Polysaccharides by Atomic Force Microscopy.* Science, 1997. **275**(5304): p. 1295-7.

104. Rief, M., et al., *Single molecule force spectroscopy of spectrin repeats: low unfolding forces in helix bundles.* J Mol Biol, 1999. **286**(2): p. 553-61.

105. Sechler, J.L., S.A. Corbett, and J.E. Schwarzbauer, *Modulatory roles for integrin activation and the synergy site of fibronectin during matrix assembly.* Mol Biol Cell, 1997. **8**(12): p. 2563-73.

106. Shimaoka, M. and T.A. Springer, *Therapeutic antagonists and conformational regulation of integrin function.* Nat Rev Drug Discov, 2003. **2**(9): p. 703-16.

107. Smith, J.C., et al., *Mesoderm induction and the control of gastrulation in Xenopus laevis: the roles of fibronectin and integrins.* Development, 1990. **108**(2): p. 229-38.

108. Springer, T.A., H. Jing, and J. Takagi, *A novel Ca2+ binding beta hairpin loop better resembles integrin sequence motifs than the EF hand.* Cell, 2000. **102**(3): p. 275-7.

109. Strause, L., P. Saltman, and J. Glowacki, *The effect of deficiencies of manganese and copper on osteoinduction and on resorption of bone particles in rats.* Calcif Tissue Int, 1987. **41**(3): p. 145-50.

110. Takagi, J., H.P. Erickson, and T.A. Springer, *C-terminal opening mimics 'inside-out' activation of integrin alpha5beta1.* Nat Struct Biol, 2001. **8**(5): p. 412-6.

111. Tan, M.H., et al., *Deletion of the alternatively spliced fibronectin EIIIA domain in mice reduces atherosclerosis.* Blood, 2004. **104**(1): p. 11-18.

112. Tanaka, T., et al., *Paxillin association in vitro with integrin cytoplasmic domain peptides.* FEBS Lett, 1996. **399**(1-2): p. 53-8.

113. Taverna, D. and R.O. Hynes, *Reduced blood vessel formation and tumor growth in alpha5-integrin-negative teratocarcinomas and embryoid bodies.* Cancer Res, 2001. **61**(13): p. 5255-61.

114. Tees, D.F., R.E. Waugh, and D.A. Hammer, *A microcantilever device to assess the effect of force on the lifetime of selectin-carbohydrate bonds.* Biophys J, 2001. **80**(2): p. 668-82.

115. Towbin, H., T. Staehelin, and J. Gordon, *Electrophoretic transfer of proteins from polyacrylamide gels to nitrocellulose sheets: procedure and some applications.* Proc Natl Acad Sci U S A, 1979. **76**(9): p. 4350-4.

116. Tsuchida, J., et al., *The 'ligand-induced conformational change' of alpha 5 beta 1 integrin. Relocation of alpha 5 subunit to uncover the beta 1 stalk region.* J Cell Sci, 1998. **111 (Pt 12)**: p. 1759-66.

117. Tuckwell, D.S. and M.J. Humphries, *A structure prediction for the ligand-binding region of the integrin beta subunit: evidence for the presence of a von Willebrand factor A domain.* FEBS Lett, 1997. **400**(3): p. 297-303.

118. Wagner, P., et al., *Covalent immobilization of native biomolecules onto Au(111) via N-hydroxysuccinimide ester functionalized self-assembled monolayers for scanning probe microscopy.* Biophys J, 1996. **70**(5): p. 2052-66.

119. Wangsa-Wirawan, N.D., et al., *Measuring the interaction forces between protein inclusion bodies and an air bubble using an atomic force microscope.* Biotechnol Prog, 2001. **17**(5): p. 963-9.

120. Weisenhorn, A.L., et al., *Measuring adhesion, attraction, and repulsion between surfaces in liquids with an atomic-force microscope.* Physical Review. B. Condensed Matter., 1992. **45**(19): p. 11226-11232.

121. Whittaker, C.A. and R.O. Hynes, *Distribution and evolution of von Willebrand/integrin A domains: widely dispersed domains with roles in cell adhesion and elsewhere.* Mol Biol Cell, 2002. **13**(10): p. 3369-87.

122. Wu, Y., et al., *Recombinant fibronectin polypeptide antagonizes hepatic failure induced by endotoxin in mice.* Acta Pharmacol Sin, 2004. **25**(6): p. 783-8.

123. Xiong, J.P., et al., *Crystal structure of the extracellular segment of integrin alpha Vbeta3.* Science, 2001. **294**(5541): p. 339-45.

124. Xiong, J.P., et al., *Crystal structure of the extracellular segment of integrin alpha Vbeta3 in complex with an Arg-Gly-Asp ligand.* Science, 2002. **296**(5565): p. 151-5.

125. Yamada, K.M. and D.W. Kennedy, *Peptide inhibitors of fibronectin, laminin, and other adhesion molecules: unique and shared features.* J Cell Physiol, 1987. **130**(1): p. 21-8.

126. Yamada, K.M. and S. Miyamoto, *Integrin transmembrane signaling and cytoskeletal control.* Curr Opin Cell Biol, 1995. **7**(5): p. 681-9.

127. Yang, J.T., H. Rayburn, and R.O. Hynes, *Embryonic mesodermal defects in alpha 5 integrin-deficient mice.* Development, 1993. **119**(4): p. 1093-105.

128. Zhang, B., G. Xu, and J.S. Evans, *A kinetic molecular model of the reversible unfolding and refolding of titin under force extension.* Biophys J, 1999. **77**(3): p. 1306-15.

129. Zhong, C., et al., *Rho-mediated contractility exposes a cryptic site in fibronectin and induces fibronectin matrix assembly*. J Cell Biol, 1998. **141**(2): p. 539-51.